1. General

René 41, introduced in 1960, is widely used as a high temperature turbine alloy. It is a heat treatable nickel-base alloy, high in chromium, cobalt, and molybdenum. Its high strength is derived from the precipitation of a gamma-prime phase of $Ni_3(Al,Ti)$, and from the solid solution effects of cobalt and molybdenum. The cobalt addition also retards recrystallization, promotes improved hot corrosion resistance, and reduces titanium and aluminum solubilities in the gamma matrix, thereby increasing gamma-prime precipitation and strength. Heat treatment usually consists of solution annealing at 1950 to 2150F followed by water quenching and aging at 1400 to 1800F to precipitate the coherent ordered face-centered-cubic gamma-prime phase. The mechanical properties of René 41 can be custom tailored to some extent for specific applications by using various combinations of solution treating and aging. High solution treating and aging temperatures produce better stress-rupture properties, while lower heat treating temperatures increase short-time tensile properties. The alloy is forgeable, formable, and weldable following recommended procedures. Oxidation resistance is good up to about 1800F. René 41 has been used successfully for critical aircraft and spacecraft components subjected to high temperatures, such as after-burner parts, nozzle partitions, turbine blades and wheels, torque rings, combustion chamber liners, and structural hardware (Refs. 111-113).

1.1 Commercial Designation

René 41.

1.2 Alternate Designations

R41, J1610, AISI 683, UNS N07041.

1.3 Specifications

1.3.1 *[Table]* AMS specifications.

1.4 Composition

1.4.1 *[Table]* AMS specified compositions.

1.5 Heat Treatment

The standard heat treatment consists of solution annealing at 1975F followed by a water quench or rapid air cool. The material is then aged at 1400F for 16 hours and air cooled. Recommended heating and quenching times for various thicknesses are given in Table 1.5.1.

1.5.1 *[Table]* Time recommendations for heating and quenching various thicknesses of René 41.

For optimum stress rupture strength, the alloy can be solution treated at 2050F and aged at 1650F.

For maximum tensile and yield strength at temperatures up to 1800F, solution treat for 4 hours at 1950F and age for 16 hours at 1400F (see Figures 3.2.1.3 and 3.2.1.5 for effects of solution annealing and aging conditions on tensile properties).

Weld strain-age cracking can be minimized by solution annealing at 1975F with a 40F per minute cool to 1200F prior to welding (Ref. 78).

The typical heat treatment for cast René 41 is 1950F for 3 hours, air cool, plus 2050F for 0.5 hour, air cool, plus 1650F for 4 hours, air cool (Ref. 114).

Ni
19 Cr
11 Co
9.8 Mo
3.2 Ti
1.5 Al
0.006 B

René 41, like other nickel-base alloys, is subject to intergranular attack when heated in the presence of sulfur or sulfur compounds. Exposure to sulfurous atmospheres at elevated temperatures must be avoided. Parts must be free of all sulfur-base cutting oils or lubricants prior to welding or heat treatment (Refs. 111, 144).

Carbide distribution is affected by the solution annealing temperature. Heat treatment at 2150F causes solutioning of the M_6C phase. Subsequent exposure in the temperature range 1400 to 1600F produces a grain boundary film of $M_{23}C_6$, with deleterious effects on mechanical properties. A lower solution treatment temperature of about 1970F can be used to preserve the fine-grained as-worked structure with well dispersed M_6C and avoid subsequent reprecipitation as $M_{23}C_6$ (Refs. 115, 145).

1.6 Hardness

1.6.1 *[Figure]* Effect of solution treating temperature and cooling method on hardness of bar.

1.6.2 *[Figure]* Effect of delay before quenching on hardness of sheet.

1.6.3 *[Figure]* Effect of high temperature exposure on room temperature hardness.

1.6.4 *[Figure]* Hardness at room and elevated temperatures for various exposure times.

1.6.5 *[Figure]* Relation between hardness and tensile or yield strength at room temperature after high temperature exposure.

1.7 Forms and Conditions Available

The alloy is available in the full commercial range of sizes for sheet, strip, plate, bar, forgings, rings, wire, and investment castings (Refs. 5, 111, 146).

1.8 Melting and Casting Practice

The alloy is produced by vacuum induction melting plus either vacuum arc consumable electrode remelting or electroslag remelting.

1.9 Special Considerations

1.9.1 René 41 is subject to strain-age cracking during heat treatment after fusion welding. This problem can be

© 1994 by Purdue Research Foundation, West Lafayette, Indiana 47907. All Rights Reserved. U.S. Government License. This material may be used, duplicated or disclosed by United States Government agencies without the payment of any royalty.

alleviated by solution annealing with a rapid heat-up after welding or by using starting alloy in the solution annealed or solution annealed plus overaged condition (see Section 4.3.1).

1.9.2 René 41 should be cooled rapidly or quenched after solution annealing to prevent embrittlement, probably due to precipitation of the gamma-prime phase (see Sections 3.2.3 and 3.3.3 and Figure 3.4.7).

1.9.3 The solution annealing temperature should be kept below 2000F to prevent formation of an embrittling network of $M_{23}C_6$ phase during subsequent long time exposure at lower temperatures (see Sections 1.5, 2.1.2, and 4.3.1).

1.9.4 Long time thermal exposures at 1400F and higher cause strength reductions (see Figures 3.2.1.11, 3.2.1.12, 3.3.1.20, 3.3.1.21, 3.3.2.3, 3.3.5.1, and 3.3.6.4).

1.9.5 René 41, like other nickel-based alloys, is embrittled by exposure to high pressure hydrogen at room and elevated temperatures. The embrittlement is accentuated in the presence of notches (see Sections 2.3.3 and 3.2.7.1).

1.9.6 René 41 is sensitive to sharp notches in the solution annealed plus aged, solution annealed plus cold rolled plus aged, and cold rolled plus aged conditions (see Sections 3.2.7.1 and 3.3.7.1 and Figures 3.4.9 and 3.5.1.3 to 3.5.1.6).

1.9.7 The tensile properties of René 41 are degraded by thermal exposure in air after being coated with salt (see Section 2.3.1).

1.9.8 Sulfur contaminated work surfaces and sulfur-bearing furnace atmospheres cause intergranular attack and should be avoided (see Section 1.5.1).

2. Physical Properties and Environmental Effects

2.1 Thermal Properties

2.1.1 Melting Range. 2250 to 2535F (Refs. 111, 115).

2.1.2 Phase Changes.

Time-temperature-transformation diagrams. The gamma-prime solvus temperature is 1950 +/- 50F (Ref. 116).

Carbide phases which have been identified in René 41 include MC, M_6C, and $M_{23}C_6$. René 41 can be solution heat treated to generate MC and M_6C initially, as shown in Figure 2.1.2.1. A typical formula for M_6C is $(Ni,Co)_3Mo_3C$. The M_6C carbide phase is important as a grain boundary precipitate for controlling grain size during processing of wrought material. The MC and M_6C carbides are not stable at all temperatures, but decompose slowly in the temperature range 1400 to 1900F to form $M_{23}C_6$, as shown in Figure 2.1.2.2. The metal radical in $M_{23}C_6$ is primarily chromium with small amounts of molybdenum or tungsten. This phase may form as discrete particles along grain boundaries with a beneficial effect on stress-rupture life, or as continuous films, acicular particles, or as a cellular precipitate, all of which may cause embrittlement. The conditions determining the form of this precipitate have not been reported for René 41 (Refs. 61, 109, 115, 117).

2.1.2.1 *[Figure]* Minor phase concentration for alloy after heating for various times and temperatures.

2.1.2.2 *[Figure]* Minor phase concentration for alloy after 5000 hour exposure at 1400 to 2200F.

The carbide-forming tendency in superalloys such as René 41 is determined by the relative amounts of chromium, molybdenum, and tungsten. René 41 tends to form M_6C (as well as lesser amounts of MC and $M_{23}C_6$), as shown in Figure 2.1.2.3.

2.1.2.3 *[Figure]* Complex carbide-forming tendency in nickel-base alloys.

René 41 is borderline with regard to formation of embrittling intermetallic compounds such as mu and sigma. Sigma phase has been observed to form in some heats after long-time exposure at 1600F (see Figures 2.1.2.1 and 2.1.2.2) (Ref. 118).

The temperature dependence of hydrogen diffusivity is expressed by an Arrhenius-type equation as:

$$D = D_o \exp(-Q_D/RT)$$

where D_o is the frequency factor and Q_D is the activation energy of diffusion. Values of D_o and Q_D have been determined as 0.39 cm^2/sec and 8,668 cal/g. atom, respectively, for the diffusivity of hydrogen in René 41 over the temperature range 77 to 302F (Ref. 119).

2.1.3 Thermal Conductivity.

2.1.3.1 *[Figure]* Thermal conductivity.

2.1.4 Thermal Expansion.

2.1.4.1 *[Figure]* Mean coefficient of linear thermal expansion.

2.1.5 Specific Heat.

2.1.5.1 *[Figure]* Specific heat.

2.1.6 Thermal Diffusivity.

2.2 Other Physical Properties

2.2.1 Density, 0.298 lb/cu inch, 8.19 g/cc (Ref. 6).

2.2.2 Electrical Properties.

2.2.2.1 *[Figure]* Low temperature resistivity.

2.2.2.2 *[Table]* Effect of heat treatment on electrical resistivity.

2.2.3 Magnetic Properties. Relative magnetic permeability is less than 1.002 at 200 oersteds at room temperature (Ref. 18).

2.2.4 Emittance. Oxidized René 41 has a substantially higher emittance than clean alloy, as shown in Figure 2.2.4.1. The moderately higher emittance values for oxidized alloy in Figure 2.2.4.2 may reflect experimental scatter or differences in experimental technique.

2.2.4.1 *[Figure]* Total hemispherical emittance of clean and oxidized René 41.

2.2.4.2 *[Figure]* Total hemispherical emittance of oxidized René 41.

2.2.5 Damping Capacity.

2.3 Chemical Environments

2.3.1 General Corrosion. Welded René 41 has excellent resistance to corrosion by seawater. Experiments showed that after a 1-year exposure, all specimens were still bright and showed original machining marks. No stress-corrosion failures were observed (Ref. 113).

The tensile properties of René 41 are severely degraded by thermal exposure in air after being coated with salt. Such conditions would be pertinent to a space vehicle which had been exposed to sea air or sea salt conditions prior to launch. As shown in Tables 2.3.1.1 and 2.3.1.2, thermal exposure alone for 48 hours at 1400 or 1600F has very little effect on tensile properties of material initially in the solution annealed plus aged condition. However, salted specimens show greatly reduced tensile strength and ductility after exposure at 1600F and moderately reduced properties after exposure at 1400F as compared to the exposed conditions without salt. Salt has only a minor effect on the tensile properties of material exposed at 1100 and 800F. Stress loading during 1600F exposure with or without salt has little effect on residual properties, indicating that the degradation is due to sodium chloride exposure rather than to stress-corrosion cracking (Refs. 120, 121).

2.3.1.1 *[Table]* Effects of salt and thermal exposure on tensile properties.

2.3.1.2 *[Table]* Effect of salt on post-exposure tensile properties at room temperature.

René 41 exhibits a high corrosion rate in molten NaCl at 1508F. The weight loss rate when exposed in a quartz crucible is 253 mg/dm^2/day, while that in a platinum crucible is 4760 mg/dm^2/day. The latter rate is higher because of the effect of galvanic coupling with a more noble metal (platinum). The corrosion product consists of NiO, spinels, and Fe_2O_3-type oxides. Additional results on several other superalloys indicate that the corrosion rates of superalloys in molten NaCl at 1508F are highly dependent on oxygen pressure and to some extent on water content of the melt. Alloy composition has little effect on corrosion rates (Ref. 122).

René 41 is resistant to degradation of properties when exposed to decomposition products of hydrazine, which is of interest as a storable fuel for air-borne and spacecraft auxiliary power units. Both tensile and fatigue properties are little affected in an $NH_3/N_2/H_2$ environment, as shown in Table 2.3.1.3 and Figure 2.3.1.4 (Ref. 123). Ammonia, which also effectively simulates the hydrazine decomposition environment, has been determined to be no more severe than high temperature air in causing sustained load crack growth in René 41 (Ref. 124).

2.3.1.3 *[Table]* Effects of hydrazine decomposition products on tensile properties at 1450F.

2.3.1.4 *[Figure]* Effects of hydrazine decomposition products on low-cycle fatigue properties at 1450F.

René 41 has moderately good resistance to cavitation damage in liquid sodium at 800F, as shown in Figures 2.3.1.5 and 2.3.1.6.

2.3.1.5 *[Figure]* Comparison of cavitation damage resistance with other high temperature alloys in liquid sodium at 800F.

2.3.1.6 *[Figure]* Surface damage due to high frequency vibration in sodium at 800F, and comparison with results for other alloys.

2.3.2 Stress Corrosion. René 41 is not susceptible to stress corrosion during exposure to seawater, based on an extensive investigation of cold rolled and aged material (20 percent cold rolled plus 1400F, 16 hours) in aqueous salt solutions.

Materials studied included parent metal, GTA welds, and parent metal given simulated braze heat treatments. Smooth specimens were subjected to sea atmosphere exposures (80-ft lot at Kure Beach), 5 percent NaCl spray and alternate immersion in synthetic sea water for 1000 hours at stresses up to 90 percent of yield. In addition, fatigue cracked specimens were subjected to alternate immersion in synthetic sea water for 500 hours at 80 percent of their crack strength in air. No failures were encountered in any of these salt stress corrosion tests, and the tensile properties were essentially unaffected (Refs. 66, 79). Corrosion fatigue tests in synthetic sea water using both smooth and mildly notched specimens in axial loading also showed no effect of the environment (Ref. 66).

In another investigation (Ref. 68), the susceptibility to hot (650F) solid salt corrosion was determined for material stressed at 70 percent of ultimate. Bend ductility was unaffected by exposure under these conditions.

2.3.3 Hydrogen Effects. René 41 is embrittled by high pressure hydrogen at room temperature. Along with high-strength steels and other high-strength nickel base alloys, René 41 exhibits a large decrease in notched strength and a moderate decrease in unnotched strength when tested in hydrogen, as shown in Table

2.3.3.1. Substantial decreases in elongation and reduction in area also occur in hydrogen (Ref. 125).

2.3.3.1 *[Table]* Embrittlement of René 41 and other selected alloys by hydrogen at room temperature.

René 41 is also embrittled by exposure to hydrogen at 1200F. The degree of embrittlement (loss in elongation) varies with the initial condition and heat treatment of the alloy as reflected in the average particle size of the gamma-prime precipitate. As shown in Table 2.3.3.2, the ductility loss after exposure for 1000 hours in hydrogen is least for heat treatment no. 1, with a gamma-prime particle size of 0.005 micron, and greatest for heat treatment no. 3, with a particle size of 0.2 micron. It is suggested that the gamma-prime particles act as a sink for hydrogen, with the finest particle size being most effective and the largest size the least effective in trapping and removing hydrogen from the matrix lattice. The untrapped hydrogen, which is diffusible in the matrix, is that which is responsible for embrittlement. The effects are consistent with the mechanism termed Internal Reversible Hydrogen Embrittlement (Ref. 126).

2.3.3.2 *[Table]* Effects of heat treatment and exposure at 1200F in air or hydrogen on room temperature tensile properties.

2.3.4 Oxidation. René 41 has good oxidation resistance in air at temperatures up to about 1800F but is susceptible to internal oxidation (Ref. 111).

The oxidation weight gain behavior of sheet in static air is linear at short times but parabolic at longer times, as shown in Figure 2.3.4.1. The parabolic weight gain relationship indicates formation of an adherent, protective scale. As shown in Figure 2.3.4.2, the surface scale consists of alumina, chromia, and a mixed alumina-chromia oxide. The internal oxide is alumina. Nickel and titanium also enter into the reaction products at longer times and higher temperatures, as indicated.

2.3.4.1 *[Figure]* Oxidation behavior of sheet at 1600 to 2000F.

2.3.4.2 *[Figure]* Major reaction products after air oxidation at 1600 to 2000F.

The oxidation behavior of fine wire at 1500 to 2000F is also parabolic, as shown in Figure 2.3.4.3. However, oxidation of sheet at 2000F under dynamic flow conditions results in oxide flaking and weight losses, seen in Figure 2.3.4.4.

2.3.4.3 *[Figure]* Weight gain during furnace oxidation of wire at 1500 to 2000F.

2.3.4.4 *[Figure]* Weight change during dynamic oxidation of sheet at 1600 and 2000F.

The depth of internal oxidation is diffusion controlled and increases parabolically with time during exposure at 1600 to 2000F, as shown in Figure 2.3.4.5.

2.3.4.5 *[Figure]* Internal oxidation of sheet at 1600 to 2000F.

René 41 has good to excellent long term oxidation resistance at 1500F. As shown in Figure 2.3.4.6, René 41 shows a metal consumption by oxidation of about 5 mg/cm^2 after 10,000 hours cyclic exposure in air at 1500F, comparable to the metal consumption amounts for other oxidation-resistant superalloys. The scales are quite adherent and protective for alloys such as René 41 which show metal consumptions of less than 7 mg/cm^2 in Figure 2.3.4.6 (Ref. 127).

2.3.4.6 *[Figure]* Metal loss due to oxidation after 10,000 hours exposure in air at 1500F for René 41 and other nickel-base superalloys.

Oxide volatilization occurs during exposure of René 41 in air at 2192F. Analyses of condensed deposits indicated that chromium and titanium are lost from the alloy by oxide volatilization during the first few 8-hour exposure cycles, but the amount of these elements lost decreases sharply with continuing exposure. In contrast, the amount of molybdenum in the condensed deposit increases with increasing exposure cycles, indicating that the molybdenum loss rate by oxide volatization increases with time. The oxidized specimen also exhibited subsurface porosity to a depth of 0.02 inch and considerable grain growth after exposure for five 8-hour cycles at 2192F. These data indicate a significant effect of oxide volatilization on the oxidation behavior of René 41 at elevated temperatures. The retained scale after air exposure at 2192F consisted primarily of Cr_2O_3 with smaller amounts of spinel and rutile (Ref. 128).

Ceramic coatings are attractive for extending the life of turbine components by reducing metal temperature. However, frequent temperature cycling of zirconia-yttria thermal barrier coatings over NiCrAlY on René 41 from 1900F to room temperature sharply reduces coating life as compared to that observed for sustained operation at constant temperature (Ref. 129).

René 41 suffers oxidation during exposures in low pressure air such as would be experienced by a thermal protection system during Shuttle reentry or hypersonic flight. The effective thickness loss, which includes metal reacted or degraded by surface oxidation, internal oxidation, or diffusional loss of strengthening precipitates, is shown in Figure 2.3.4.7 for exposures in 8 torr air at 1400 and 1800F. Sheet of 10 mils thickness is satisfactory for service up to 5000 hours at 1400F but is completely degraded in less than 3500 hours at 1800F. For applications requiring low pressure oxidation resistance for long times at 1800F, René 41 is less attractive than other superalloys such as Haynes 188 or TD NiCr (Ref. 130).

2.3.4.7 *[Figure]* Effect of oxidation exposure in low pressure air on effective thickness loss on thin-gage alloy at 1400 and 1800F.

2.4 Nuclear Environments

3. Mechanical Properties

3.1 Specified Mechanical Properties

3.1.1 *[Table]* AMS specified properties for castings, bars, forgings, and rings.

3.1.2 *[Table]* AMS specified properties for sheet, strip, and plate.

3.2 Mechanical Properties at Room Temperature

3.2.1 Tension Stress-strain Diagrams and Tensile Properties. Carbon content has little effect on the yield strength of solution annealed and aged alloy, as shown in Figure 3.2.1.1. Tensile elongation, however, decreases with decreasing carbon below about 0.08 percent C. Specified carbon content for René 41 is 0.12 percent maximum.

3.2.1.1 *[Figure]* Effect of carbon content on room temperature yield strength and elongation.

Tensile strength in the solution annealed condition decreases and ductility increases as the annealing temperature is increased in the rage 1900 to 2150F for both wire and sheet, as shown in Figures 3.2.1.2 and 3.2.1.3, respectively. Aging to precipitate the strengthening gamma-prime phase causes a substantial increase in yield strength of sheet but also reduces ductility, shown in Figure 3.2.1.3. Similar effects are noted for cast alloy, shown in Table 3.2.1.4. The yield strength of solution annealed and aged sheet is highly dependent on aging time and temperature, as shown in Figure 3.2.1.5. Highest yield strength is obtained after aging for 16 hours at 1400F. Aging also increases the strength and hardness of melt spun fibers, as seen in Figure 3.2.1.6.

3.2.1.2 *[Figure]* Effect of annealing temperature on room temperature tensile properties for 0.002-inch diameter fiber.

3.2.1.3 *[Figure]* Effect of solution anneal time and temperature with and without double age on tensile properties of sheet at room temperature.

3.2.1.4 *[Table]* Effect of heat treatment on tensile properties of casting.

3.2.1.5 *[Figure]* Effect of aging time and temperature on room temperature yield strength of sheet.

3.2.1.6 *[Figure]* Effects of aging time in helium at 1436F on tensile strength and microhardness of melt spun René 41 fibers.

The yield and ultimate tensile strengths of solution annealed sheet are increased significantly and ductility is decreased by cold reduction, as shown in Figure 3.2.1.7. Aging after cold reduction has a minor, inconsistent effect on strength. However, solution annealing and aging essentially erases the effects of prior cold reduction.

3.2.1.7 *[Figure]* Effect of cold reduction by shear forming on room temperature tensile properties.

The strength properties of wire and bar are also increased by cold work, shown in Figure 3.2.1.8 and Table 3.2.1.9, respectively.

3.2.1.8 *[Figure]* Effect of cold reduction on ultimate and yield strength of fiber initially 0.002-inch diameter.

3.2.1.9 *[Table]* Effect of cold reduction by fluid extrusion on tensile properties of bar tested under normal atmospheric temperature and pressure.

Exposure of heat treated sheet for up to 30,000 hours at 550 or 650F under various conditions of stress had no significant effect on subsequent tensile properties, as shown in Figure 3.2.1.10. However, exposure of sheet or wire for times of several minutes to 100 hours at temperatures of 1500 to 2000F resulted in reduced tensile properties, as shown in Figure 3.2.1.11 and 3.2.1.12, respectively.

3.2.1.10 *[Figure]* Effect of exposure time and temperature simulating supersonic transport conditions on room temperature tensile properties.

3.2.1.11 *[Figure]* Effect of high temperature exposure on room temperature tensile properties.

3.2.1.12 *[Figure]* Effect of temperature and exposure time on tensile strength and ductility of 1-mil wire.

3.2.2 Compression Stress-strain Diagrams and Compression Properties.

3.2.3 Impact. Impact energy is substantially higher for material water quenched after solution annealing than for material cooled at lower rates. Materials with carbon contents of 0.08 and 0.12 percent have higher impact energies than material with a carbon content of 0.02 percent, as shown in Figure 3.2.3.1

3.2.3.1 *[Figure]* Effect of cooling rate after solution treatment on room temperature impact energy for three heats of differing carbon content.

3.2.4 Bending.

3.2.5 Torsion and Shear. Thermal exposure for 10 to 1000 hours at temperatures of 1400 to 1900F reduces shear strength, as shown in Figure 3.2.5.1. Cold reductions up to 60 percent either before or after solution annealing have little effect on shear strength, seen in Figure 3.2.5.2.

3.2.5.1 *[Figure]* Effect of time and temperature of exposure on shear strength of sheet at room temperature.

3.2.5.2 *[Figure]* Effect of cold reduction by shear forming on room temperature shear strength.

3.2.6 Bearing. Thermal exposure for 10 to 1000 hours at 1200 to 1800F reduces bearing strength, as shown in Figure 3.2.6.1.

3.2.6.1 *[Figure]* Effect of time and temperature of exposure on bearing strength of sheet at room temperature.

3.2.7 Stress Concentration.

3.2.7.1 Notch properties. The notch strength ratios and ductilities for 20 percent and 35 percent cold rolled sheet are reduced moderately on heat treating at 1400F, as shown in Figures 3.2.7.1.1 and 3.2.7.1.2. The notch strength properties are greatly reduced on testing in 10 ksi hydrogen but not in hydrogen-contaminated helium, shown in Figure 3.2.7.1.3.

3.2.7.1.1 *[Figure]* Effect of heat treatment on room temperature smooth and sharp notch tensile properties of 20 percent cold rolled sheet.

3.2.7.1.2 *[Figure]* Effect of heat treatment on room temperature smooth and sharp notch tensile properties of 35 percent cold rolled sheet.

3.2.7.1.3 *[Table]* Effect of high pressure hydrogen and of hydrogen-contaminated helium on embrittlement of smooth and notched bars.

3.2.7.2 Fracture toughness.

3.2.8 Combined Loading.

3.3 Mechanical Properties at Various Temperatures

3.3.1 Tension Stress-strain Diagrams and Tensile Properties.

Tensile stress-strain diagrams for solution annealed and aged alloy are largely independent of strain rate at temperatures of 1200F and below but become increasingly rate-dependent with increasing temperature above 1200F. No yield points are exhibited at temperatures from -423 to 2000F, as shown in Figures 3.3.1.1 and 3.3.1.2.

3.3.1.1 *[Figure]* Stress-strain curves of bar at room and low temperatures.

3.3.1.2 *[Figure]* Stress-strain curves at room and elevated temperatures for various sheet thicknesses and strain rates.

The tensile properties of solution annealed and aged sheet and plate as determined at several different laboratories are shown in Figures 3.3.1.3 and 3.3.1.4. The strength properties are essentially identical up to 2000F for aging temperatures of 1400 and 1650F. A ductility minimum exists at 1400 to 1600F for the 1400F-aged material. The lack of any apparent effect of aging temperature is attributed to data scatter. More detailed data from a single study presented earlier (Figure 3.2.1.5) indicated rather strongly that 1400F aging produces material with higher strength properties than 1650F.

3.3.1.3 *[Figure]* Tensile properties from -420 to 2000F of sheet and plate aged at 1400F after solution treatment, showing scatterband for numerous lots tested at several laboratories.

3.3.1.4 *[Figure]* Tensile properties from 70 to 2200F of sheet and plate aged at 1650F after solution treatment, showing scatterband for numerous lots tested at several laboratories.

The low temperature longitudinal and transverse tensile properties of solution annealed and solution annealed plus aged sheet from several different studies are presented in Figures 3.3.1.5 through 3.3.1.11. Strength values increase continuously and substantially with reduction in test temperature. Elongations and reduction in area decrease particularly at temperatures below -100F. Ultimate strengths are higher and yield strengths are lower for the longitudinal than for the transverse direction for both heat treat conditions. Ductilities are similar in both directions. (Results presented later in Figure 3.3.1.19 indicate that both the tensile and yield strengths are higher in the longitudinal than in the transverse direction, slightly different from the data presented here.)

3.3.1.5 *[Figure]* Effect of low test temperature on longitudinal tensile strength of sheet and bar.

3.3.1.6 *[Figure]* Effect of low test temperature on longitudinal yield strength of sheet and bar.

3.3.1.7 *[Figure]* Effect of low test temperature on longitudinal elongation of sheet and bar.

3.3.1.8 *[Figure]* Effect of low test temperature on reduction in area of bar.

3.3.1.9 *[Figure]* Effect of low test temperature on transverse tensile strength of sheet.

3.3.1.10 *[Figure]* Effect of low test temperature on transverse yield strength of sheet.

3.3.1.11 *[Figure]* Effect of low test temperature on transverse elongation of sheet.

The yield strength of aged material increases with increasing prior cold work at room temperature but not at 1400F. Solution annealing and aging subsequent to cold rolling eliminates the effects of cold rolling, as shown in Figure 3.3.1.12. (Similar effects at room temperature are shown in Figure 3.2.1.8.)

3.3.1.12 *[Figure]* Effect of cold work and heat treatment on tensile properties of sheet at room temperature and 1400F.

The tensile properties of form-rolled material in the as-rolled condition at temperatures up to 1650F,

shown in Figure 3.3.1.13, are similar to those observed in solution annealed and aged material, shown in Figures 3.3.1.3 and 3.3.1.4.

3.3.1.13 *[Figure]* Tensile properties from room temperature to 1700F of specimens from form-rolled T-section.

The strength level of cast alloy at 1200F, shown in Figure 3.3.1.14, is at the lower edge of the scatter band or less than that of solution annealed and aged material, seen in Figures 3.3.1.3 and 3.3.1.4, and decreases with increasing grain size.

Ductilities are also lower for cast alloy than for wrought heat treated alloy.

3.3.1.14 *[Figure]* Effect of grain size on tensile properties of as-cast alloy at 1200F.

Sheet fabricated from powder metallurgy bar has good tensile strength properties at room temperature and 1400F, shown in Table 3.3.1.15. These strengths are comparable to or higher than those shown in Figures 3.3.1.3 and 3.3.1.4 for melted and wrought alloy.

3.3.1.15 *[Table]* Properties at room temperature and 1400F of sheet produced from powder bar.

The effect of strain rate on tensile properties of heat treated alloy at temperatures up to 2000F is shown in Figure 3.3.1.16. No effect of strain rate is apparent at temperatures below 1400 to 1600F. Above this temperature range, strength decreases with decreasing strain rate as temperature-dependent deformation processes become rate-controlling. A minimum in ductility is apparent at 1600F, as also noted above in Figure 3.3.1.3.

3.3.1.16 *[Figure]* Effect of strain rate and test temperature on tensile properties of sheet.

Prior thermal exposure at temperatures up to 1500F has no significant effect on tensile properties, but exposure at higher temperatures is weakening. For cold rolled and annealed sheet, exposures for times as long as 30,000 hours at 550 or 650F under various stress conditions has no significant effect on tensile properties at the exposure temperature, as shown in Figures 3.3.1.17 and 3.3.1.18. Similarly, no significant effect of 1000-hour exposures at 650 or 1000F is apparent on tensile properties at temperatures up to 1200F, seen in Figure 3.3.1.19. Short-time exposures of up to 8 minutes at 1500F have no effect on tensile strength of wire at that temperature, but similar exposures at 1800 and 2000F significantly reduce the subsequent tensile strengths, shown in Figure 3.3.1.20. Stressed cyclic exposures at 1600 and 1800F under conditions simulating Shuttle operating conditions reduce the tensile strengths at temperatures from room temperature to 1800F, as shown in Figure 3.3.1.21.

3.3.1.17 *[Figure]* Tensile properties at 550F after exposure to stress and temperature or to temperature alone at 550F.

3.3.1.18 *[Figure]* Tensile properties at 650F after exposure to stress and temperature or to temperature alone at 650F.

3.3.1.19 *[Figure]* Effect of test temperature on tensile properties of cold worked and aged sheet with and without prior exposure to stress and temperature.

3.3.1.20 *[Figure]* Effect of exposure time prior to loading on tensile strength and elongation of 0.5- and 1-mil wire at 1500 to 2000F.

3.3.1.21 *[Figure]* Effect of exposure to 100 cycles at simulated space shuttle conditions on tensile strength at temperatures to 1800F.

3.3.2 Compression Stress-strain Diagrams and Compression Properties. Strain rate affects the compressive stress-strain diagrams, shown in Figure 3.3.2.1 for heat treated alloy, in similar manner as for tensile stress-strain diagrams (Figure 3.3.1.2). Strain rate has little effect at 1200F and below. However, at 1600 to 2000F, the flow stress decreases with decreasing strain rate. Compressive yield stresses, shown in Figure 3.3.2.2, vary similarly with strain rate and temperature.

3.3.2.1 *[Figure]* Compressive stress-strain curves at room and elevated temperatures at several strain rates.

3.3.2.2 *[Figure]* Effect of strain rate on compressive yield strength of sheet at room and elevated temperatures.

Prior exposure at 1400 or 1600F reduces the compressive yield strength of heat treated alloy at the same temperature, as shown in Figure 3.3.2.3. However, no effect of prior exposure at the test temperature is noted at room temperature to 1200F.

3.3.2.3 *[Figure]* Effect of exposure time at test temperature on compressive yield strength at room and elevated temperatures.

3.3.3 Impact. The data shown in Figures 3.3.3.1 and 3.3.3.2 indicate a substantial difference in impact energy at the common test temperature of 70F. This difference may reflect variations in heat treatment conditions or in specimen configuration (V-notch Charpy versus pre-cracked Charpy). A maximum in impact energy is observed at about 1000F.

3.3.3.1 *[Figure]* Effect of low test temperature on Charpy-V impact energy of bar.

3.3.3.2 *[Figure]* Effect of cooling rate from solution temperature on impact energy at room and elevated temperatures.

3.3.4 Bending.

3.3.5 Torsion and Shear. In similar fashion to the compressive yield strength (Figure 3.3.2.3), the shear strength at room temperature to 1200F is essentially unaffected by prior exposure at the test temperature. However,

at test temperatures of 1400 and 1600F, prior exposures of 0.5 to 1000 hours progressively decrease the shear strength, as shown in Figure 3.3.5.1.

3.3.5.1 *[Figure]* Effect of exposure time at test temperature on shear strength of sheet at room and elevated temperature.

3.3.6 Bearing. The bearing strength of heat treated alloy sheet decreases gradually with increasing temperature up to about 1400F but more rapidly at higher temperatures, as shown in Figures 3.3.6.1 and 3.3.6.2. Test orientation with respect to rolling direction has no significant effect on bearing strength. Similar effects of test temperature are observed for heat treated plate, as shown in Figure 3.3.6.3.

3.3.6.1 *[Figure]* Effect of test temperature and test direction on bearing strength of 0.040-inch sheet for e/D = 1.5.

3.3.6.2 *[Figure]* Effect of test temperature and test direction on bearing strength of 0.040-inch sheet for e/D = 2.0.

3.3.6.3 *[Figure]* Effect of test temperature on bearing strength of plate for e/D = 1.5 and 2.0.

Prior exposure for 0.5 to 1000 hours at the test temperature decreases bearing yield and ultimate strengths of sheet at temperatures above 1200F, as shown in Figure 3.3.6.4. This behavior is similar to that shown above for compressive strength (Figure 3.3.2.3) and shear strength (Figure 3.3.5.1).

3.3.6.4 *[Figure]* Effect of test temperature and exposure time at test temperature on bearing strength of 0.040-inch sheet.

3.3.7 Stress Concentration.

3.3.7.1 Notch properties. The notch strength of René 41 is highly dependent on notch acuity. The notch strength is also affected by but less dependent on temperature, strain rate, and metallurgical condition of the material. As shown in Figure 3.3.7.1.1, the notch strength ratio for cold rolled and aged sheet tends to increase slightly as the stress concentration factor is increased to about 3 but decreases significantly with further increases in notch sharpness. This behavior occurs from at least room temperature to 1000F. Fully heat treated bar exhibits somewhat different behavior, with notch strength ratios at 1000F of well above unity for stress concentration factors of about 3 and 6, as shown in Figure 3.3.7.1.2. However, sharply notched sheet in the fully heat treated condition has a notch strength ratio of much less than 1, indicated by the low notch strength compared to the ultimate strength in Figure 3.3.7.1.3.

3.3.7.1.1 *[Figure]* Effect of notch acuity on notch strength ratio of cold rolled and aged sheet at room and elevated temperatures.

3.3.7.1.2 *[Figure]* Effect of stress concentration on notch strength ratio at 1000F for forged bar.

3.3.7.1.3 *[Figure]* Effect of elevated test temperatures on sharp notch strength of sheet.

At low temperatures, strain rate has little effect on notch strength at stress concentration factors of less than about 3, as shown in Figure 3.3.7.1.4. However, the notch strength is significantly reduced at a fast loading rate of 8 ipm for more sharply notched configurations.

3.3.7.1.4 *[Figure]* Effect of low temperatures, loading rates and stress concentration factors on notch strength of 0.062-inch sheet in fully heat treated condition.

Prior exposure of notched sheet with a K_t of 3.1 has little effect on the notch strength ratio, as shown in Figure 3.3.7.1.5. However, sharply notched material ($K_t > 20$) is moderately degraded by prior 1000-hour exposures at 650 and 1000F, as shown in Figure 3.3.7.1.6.

3.3.7.1.5 *[Figure]* Effect of elevated temperatures and exposure time at test temperature on tensile strength and notch strength ratio of 0.05-inch sheet in fully heat treated condition.

3.3.7.1.6 *[Figure]* Effect of elevated temperature on notch strength and notch strength ratio of cold worked and aged sheet with and without exposure to stress and temperature.

The crack strength of center-cracked sheet decreases faster with increasing ratio of crack length to sheet width at -109F than at 550F, suggesting greater embrittlement at low temperatures, as shown in Figure 3.3.7.1.7. The crack strength is equal to or greater than that yield strength at room temperature to 1600F for solution annealed and aged sheet, as shown in Figure 3.3.7.1.8. However, for cold rolled and aged sheet, the crack strength is much lower than the yield strength up to 1200F, as shown in Figure 3.3.7.1.9. This comparison may indicated a greater crack sensitivity in the cold-rolled-plus-aged condition or may reflect the difference in specimen size.

3.3.7.1.7 *[Figure]* Crack strength of solution treated and aged sheet at -109, 70 and 550F.

3.3.7.1.8 *[Figure]* Effect of elevated temperatures on crack strength of fully heat treated 0.082-inch sheet.

3.3.7.1.9 *[Figure]* Effect of test temperature on crack strength and yield strength of 0.025-inch sheet in cold rolled and aged condition.

3.3.7.2 Fracture toughness.

3.3.8 Combined Loading.

3.4 Creep and Creep Rupture Properties

The creep rupture properties at 1200 to 1800F for solution annealed and aged sheet, bar, and forgings are shown in Figures 3.4.1, 3.4.2, and 3.4.3, respectively. These data show relatively good agreement for the rupture behavior among the various product forms, particularly considering that several different laboratories are represented.

3.4.1 *[Figure]* Creep rupture properties from 1200 to 1800F of a wide range of thicknesses of sheet and plate, tested at several laboratories.

3.4.2 *[Figure]* Creep rupture properties for bar from 1200 to 1650F.

3.4.3 *[Figure]* Creep rupture properties from 1000 to 1800F of bars, forgings, and billet tested at several laboratories.

The creep rate and rupture life behavior of sheet at 800 to 1200F, shown in Figures 3.4.4, 3.4.5, and 3.4.6, indicates a modest strength advantage for the solution treated plus cold rolled plus aged condition over the solution treated plus aged condition at 800 and 1000F but not at 1200F.

3.4.4 *[Figure]* Effects of stress and temperature on minimum creep rate of cold rolled and aged sheet.

3.4.5 *[Figure]* Effects of stress and temperature on minimum creep rate of fully heat treated sheet.

3.4.6 *[Figure]* Creep rupture curves at 1000 and 1200 for sheet in two conditions.

Cooling rate after solution annealing affects the short time rupture strength of solution annealed and aged plate, as shown in Figure 3.4.7. A high cooling rate of 150F/minute results in higher rupture strength at 1400F than slower cooling rates of 20 or 75F/minute.

3.4.7 *[Figure]* Effect of cooling rate from solution treatment temperature on creep rupture properties of plate at 1400F.

A size effect is observed in the short time rupture behavior of wire at 1500 to 2000F, as shown in Figure 3.4.8. Higher rupture strengths are obtained with larger wire diameters in the range 0.5 to 10 mil.

3.4.8 *[Figure]* Short time creep rupture curves of 0.5- to 10-mil wire from 1500 to 2000F.

The rupture strength at 1000 and 1200F is less for sharp notched sheet, shown in Figure 3.4.9, than for smooth sheet, shown above in Figure 3.4.6.

3.4.9 *[Figure]* Creep-rupture curves for sharp notched sheet in annealed and in cold rolled and aged conditions.

3.5 Fatigue Properties

3.5.1 Conventional High-cycle Fatigue. The axial high-cycle fatigue (HCF) behavior of sheet at room temperature to 1600F and rotating beam fatigue behavior of bar at room temperature are shown in Figures 3.5.1.1 and 3.5.1.2.

3.5.1.1 *[Figure]* Axial fatigue behavior of sheet at room and elevated temperatures.

3.5.1.2 *[Figure]* Rotating beam bending fatigue behavior of bar at room temperature.

The effects of R ratio and notch acuity on axial HCF at room temperature, 1200, and 1600F are shown in Figures 3.5.1.3, 3.5.1.4, and 3.5.1.5, respectively. The fatigue strength decreases with decreasing R ratio (from 1/3 to -1) and with increasing notch acuity (K_t from 1 to 5) at all 3 temperatures. The fatigue strength for a given notch sharpness and R ratio also decreases with increasing temperature in similar manner as shown above for unnotched sheet in Figure 3.5.1.1. Data from another study also illustrate the decrease in fatigue strength with increasing notch acuity at room temperature, seen in Figure 3.5.1.6.

3.5.1.3 *[Figure]* Effects of notches and R ratio on axial fatigue behavior of bar at room temperature.

3.5.1.4 *[Figure]* Effects of notches and R ratio on axial fatigue behavior of bar at 1200F.

3.5.1.5 *[Figure]* Effects of notches and R ratio on axial fatigue behavior of bar at 1600F.

3.5.1.6 *[Figure]* Effect of stress concentration factor on fatigue limit at 10^7 cycles for forged turbine wheel specimen at 1000F.

The rotating beam HCF behavior of electroslag remelted alloy is shown in Figures 3.5.1.7 and 3.5.1.8.

3.5.1.7 *[Figure]* Rotating beam fatigue behavior at room and elevated temperatures of plate fabricated from a DC electroslag remelted ingot.

3.5.1.8 *[Figure]* Rotating beam fatigue behavior at 1400F of plate fabricated from an AC electroslag remelted ingot.

Improving surface smoothness by chemical milling or electropolishing affects a modest increase in HCF strength, as shown in Figures 3.5.1.9 and 3.5.1.10.

3.5.1.9 *[Figure]* Effects of chemical milling on axial fatigue behavior of sheet at room temperature.

3.5.1.10 *[Figure]* Effect of electro-discharge machining and electropolishing on axial fatigue behavior of smooth and notched bar at room temperature.

Reduction in the HCF strength is observed for sheet when spot-welded as seen in Figure 3.5.1.11, and for foil when exposed to cyclic oxidation at 1800 and 2000F as shown in Figure 3.5.1.12.

3.5.1.11 *[Figure]* Effect of spot welds simulating weldable strain gages on axial fatigue behavior of sheet at 70 and 1500F.

3.5.1.12 *[Figure]* Axial fatigue properties of foil at room temperature after exposure to oxidation at 1800 or 2000F.

Strain range diagrams for axial fatigue of sheet and bar are shown in Figures 3.5.1.13 and 3.5.1.14, respectively.

3.5.1.13 *[Figure]* Stress range diagram for axial fatigue of sheet at room temperature and 1400F.

3.5.1.14 *[Figure]* Stress range diagrams for axial fatigue of bar at room and elevated temperatures.

Increases of as much as 50 percent in endurance limit (stress limit for fatigue life of at least 10^7 cycles) can be produced by grinding, milling, or turning operations under conditions which introduce a high surface compressive stress in the material (e.g., gentle grinding). In contrast, operations under conditions which cause a surface tensile stress (e.g., abusive grinding) produce lower endurance limits (Ref. 131).

3.5.2 Low-cycle Fatigue. Hold times of 1 to 24 minutes at the maximum strain progressively decrease the low-cycle fatigue life at 1400F, as shown in Figure 3.5.2.1

3.5.2.1 *[Figure]* Effect of hold-time at peak strain on low-cycle fatigue behavior at 1400F.

3.5.3 Fatigue Crack Propagation. Fatigue crack propagation rates at room temperature and 1100F are shown in Figure 3.5.3.1. The rates at 1100F are two-fold or more greater than those at room temperature. Increasing the stress ratio R also increases the crack growth rates, but frequency effects are not significant in the range 1 to 25 hertz (Ref. 124).

3.5.3.1 *[Figure]* Effects of temperature, stress ratio, and frequency on low-cycle fatigue crack growth rates of forged alloy in air.

3.6 Elastic Properties

3.6.1 Poisson's Ratio, 0.31 (Ref. 6).

3.6.2 Modulus of Elasticity.

3.6.2.1 *[Figure]* Tensile modulus of elasticity at room and elevated temperatures.

3.6.2.2 *[Figure]* Compressive modulus of elasticity at room and elevated temperatures.

3.6.3 Modulus of Rigidity.

3.6.3.1 *[Figure]* Modulus of rigidity at room and elevated temperatures.

3.6.4 Tangent Modulus.

3.6.4.1 *[Figure]* Tangent modulus curves in compression for various test temperatures and exposure times.

3.6.5 Secant Modulus.

4. Fabrication

4.1 Forming

René 41 can be forged with some difficulty using starting temperatures of 2125 to 2150F (maximum) and finishing at 1850 to 1950F. The alloy can be formed readily in the solution heated and rapid cooled condition (1950 to 1200F in 4 seconds or less). Slow cooling after solution treating results in some age hardening, which adversely affects formability (Ref. 111). High rolling temperatures (2150F) with light reductions (2 to 3 percent) can cause deleterious carbide precipitation and reduced formability. Rolling temperatures should be kept at 2100F or lower, with final reductions of at least 10 to 15 percent (Ref. 145).

4.2 Machining and Grinding

René 41 is difficult to machine. Low speeds and moderate to heavy depths of cut should be used. Material to be machined should be in the solution treated and fully aged condition (Ref. 111). Sawing and drilling are more difficult than Inconel 718 due to the high work-hardening rate of the material. However, grinding does not appear to be exceptionally difficult (Ref. 113).

4.3 Joining

4.3.1 Fusion welding. A primary problem in the weld fabrication of René 41 hardware is cracking in the heat affected zone and base metal during post-weld heat treatment. Cracks ranging in size from microscopic to several inches in length can develop during this heat treatment, which usually consists of a solution anneal followed by aging. This phenomenon is commonly referred to as strain-age cracking (SAC) and is related to precipitation of the gamma-prime phase. The precipitation reaction, which occurs at 1400 to 1650F, strengthens the matrix but reduces the overall ductility. Maximum thermal stresses also occur in this temperature range. These factors can combine to result in severe cracking when residual welding stresses are also present (Refs. 113, 132).

The susceptibility to weld cracking in gamma-prime strengthened superalloys is related to the combined titanium plus aluminum content, the elements which form the gamma-prime phase, as indicated in Figure 4.3.1.1. Alloys with low titanium plus aluminum content, shown below the dashed line, are readily weldable. However, as the combined titanium plus aluminum is increased, welding becomes more difficult. René 41 is seen to be borderline; it can be joined by fusion welding with relatively little difficulty but sometimes cracks during post-weld heat treatment (Ref. 133).

4.3.1.1 *[Figure]* Weldability of gamma-prime strengthened superalloys.

Different heats of René 41 vary in their susceptibility to SAC, probably due to minor chemistry differences (Refs. 75, 76, 78). A statistical study of cracking based on analyses of 30 heats indicated that silicon promotes SAC susceptibility, while carbon and, to a lesser extent, boron reduce SAC (Ref. 134).

In addition to chemistry, SAC is affected by the amount of weld restraint. Highly restrained welds are more likely to crack than unrestrained welds. For this reason, the use of René 41 is generally avoided in large, welded, highly restrained components.

Post-weld mechanical properties and the susceptibility to SAC are affected by heat treatment prior to welding. As shown in Figures 4.3.1.2 and 4.3.1.3, sheet which had been solution annealed only prior to GTA welding has lower strength but substantially better ductility than GTA-welded sheet which had been previously solution annealed plus aged. The former condition is better suited for welding, since the higher ductility reduces the possibility of SAC (Refs. 60, 111).

4.3.1.2 *[Figure]* Tensile properties at room and low temperature of solution treated sheet with and without GTA weld.

4.3.1.3 *[Figure]* Tensile properties at room and low temperature of solution treated and aged sheet with and without GTA weld.

Strain-age cracking in René 41 is highly dependent on the rate of heating through the temperature range 1100 to 1800F during post-weld heat treatment. Gamma-prime precipitation and associated cracking are promoted by slow heating rates. The time-temperature relationships for SAC as determined by heat treatment of circular weld patches in René 41 are shown in Figure 4.3.1.4. These high-restraint welds showed cracking in as short as 4 minutes for heats sensitive to SAC and as long as 45 minutes for crack-resistant heats (Ref. 133).

4.3.1.4 *[Figure]* Time-temperature relationships for isothermal strain-age weld cracking in crack-sensitive and crack-resistant heats of René 41.

Another effective means of reducing weld cracking is to overage after solution annealing before welding. This treatment also produces a ductile base material which is better able to absorb the residual welding stresses than standard solution annealed plus aged material. The overaging heat treatment consists of annealing at 1975F for 0.5 hour followed by slow cooling and holding for 4 hours at 1800 and 1600F and 16 hours at 1400F. This treatment shifts the nose of the "C" curve in Figure 4.3.1.4 (see discussion above) from about 4 to greater than 500 minutes (Refs. 133, 135).

Strain-age cracking can also be alleviated by a re-solution anneal followed by aging rather as opposed to only aging after welding. However, post-weld solution annealing temperatures should be kept below 2000F to prevent subsequent formation of a $M_{23}C_6$ carbide network which also reduces ductility (Ref. 145).

Other factors which are beneficial in reducing SAC of René 41 include thorough cleaning before welding and exclusion of oxygen from the heat treating atmosphere. However, except under marginal restraint conditions, the use of an oxygen-free furnace atmosphere is not by itself sufficient for completely eliminating post-weld heat treat cracking (Ref. 136). The weld area should also be kept cool by means of copper back-up bars or water cooled fixtures (Ref. 111). Following the torch with a water spray reduces the hardness and produces maximum ductility in the weld and weld affected zones. No preheat is used for welding.

A second problem, termed microfissuring, can also occur during welding of René 41. Microfissuring is due to partial liquefaction of the alloy during welding and occurs mainly at the weld root where shrinkage stresses are encountered. This problem can be avoided by using a more ductile material, such as Hastelloy W, for the root passes when joining the alloy with itself or other age hardenable nickel base alloys (Refs. 33, 34, 113).

René 41 can be successfully welded in heavy sections by electron beam welding (Ref. 74).

4.3.2 Brazing. Brazing is a feasible method for fabrication of René 41 into complex structures such as lightweight honeycomb sandwichs for space transportation systems and advanced high speed aircraft. A modified braze alloy based on AMI 930 (Ni - 22.5Mn - 7.5Si - 5.2Cu - 0.01Al) can be brazed while solution treating and aging René 41. Good mechanical properties are obtained in both the base and braze materials (Refs. 137, 138).

Several René 41/braze alloy combinations have excellent resistance to thermal fatigue. Brazes of AMI-100 (Ni - 19Cr - 10Si - 3Fe - 0.5Co - 0.5Mn - 0.15C), AMI-300 (Ni - 19.5Cr - 9.5Si - 9.5Mn - 2.3Fe - 0.10C), and

Palniro 1 (50Au - 25Ni - 25Pd) were applied as overlays onto the radius of single-edge-wedge thermal fatigue specimens and survived 7,000 cycles (4 minute heating in fluidized bed at 1364F plus 4 minute cooling in fluidized bed at 77F) with no cracking. Similar specimens with René 41 foil brazed onto the radii survived 11,000 cycles with no cracking. Specimens butt-brazed together at mid-section survived 11,000 cycles when brazed with AMI-100 or Palniro 1, but failed by separation after 3,000 cycles when brazed with AMI-300 (Ref. 139).

Other suitable alloys for vacuum brazing include Ni - 33Cr - 24Pd - 4Si and Ni - Mn - Si - Cu - Misch metal. Both of these alloys provide excellent wetting and flow characteristics on René 41 and can join 0.015-inch thick material without erosion or embrittling effects. The optimum brazing temperatures are 2150F for Ni - Cr - Pd - Si and 1975F for the Misch metal braze alloy (Ref. 140).

4.3.3 Resistance welding. René 41 can be joined by resistance welding (Ref. 111)

4.4 Surface Treating

René 41 is not subject to embrittlement by hydrogen from cleaning, pickling, or electroplating treatments (Ref. 95).

Table 1.3.1 AMS specifications (Refs. 1-4, 77)

Alloy	René 41
AMS Specification	**Product Form** [a]
5399C	Investment castings
5545C	Sheet, strip, plate (ST)
5712F	Bars, forgings, rings (ST)
5713F	Bars, forgings, rings (STA)
5800D	Welding wire

[a] ST — Solution treated at 1975F.
STA — Solution treated at 1975F + aged at 1400F for 16 hours.

Table 1.4.1 AMS specified compositions (Refs. 1-4, 77)

Alloy	René 41							
AMS Specification	5399B		5545C		5712F, 5713F		5800D	
Element	Percent		Percent		Percent		Percent	
	Min	Max	Min	Max	Min	Max	Min	Max
Chromium	18.00	20.00	18.00	20.00	18.00	20.00	18.00	20.00
Cobalt	10.00	12.00	10.00	12.00	10.00	12.00	10.00	12.00
Molybdenum	9.00	10.50	9.00	10.50	9.00	10.50	9.00	10.50
Iron	—	5.00	—	5.00	—	5.00	—	5.00
Titanium	3.00	3.30	3.00	3.30	3.00	3.30	3.00	3.30
Aluminum	1.40	1.80	1.40	1.60	1.40	1.80	1.40	1.60
Carbon	0.06	0.12	—	0.12	—	0.12	—	0.12
Boron	0.003	0.010	0.003	0.010	0.003	0.010	0.003	0.010
Silicon	—	0.50	—	0.50	—	0.50	—	0.50
Manganese	—	0.50	—	0.10	—	0.10	—	0.10
Sulfur	—	0.015	—	0.015	—	0.015	—	0.015
Phosphorus	—	0.015	—	—	—	—	—	—
Copper	—	—	—	0.50	—	—	—	—
Lead	—	—	—	—	—	0.0005	—	—
Bismuth	—	—	—	—	—	0.00003	—	—
Selenium	—	—	—	—	—	0.0003	—	—
Nickel	balance		balance		balance		balance	

Table 1.5.1 Time recommendations for heating and quenching various thicknesses of René 41 (Refs. 47, 49)

Form	All forms, thicknesses as indicated	
Material Thickness (In.)	**Hold Time (min.)**	**Maximum Quench Delay (sec.)**
Annealing 2025 ± 25F, WQ		
≤0.039	4 ± 1	5
0.040 - 0.099	6 ± 1	5
0.100 - 0.249	12 ± 2	5
0.250 - 0.499	20 ± 4	7
0.500 - 0.749	30 ± 5	7
0.750 - 1.000	40 ± 5	7
Solution Treatment 1975 ± 25F, WQ		
≤0.059	10 ± 2	5
0.060 - 0.249	15 ± 3	5
0.250 - 0.449	20 ± 4	7
0.500 - 0.999	30 ± 5	7
1.0 - 1.99	50 ± 5	7
2.0 - 3.0	70 ± 5	7

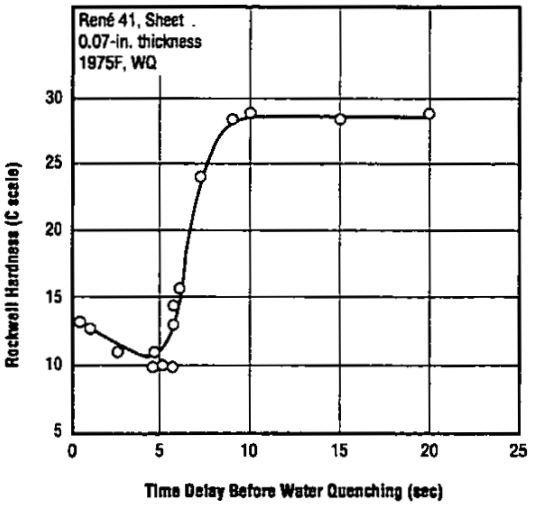

Fig. 1.6.2 Effect of delay before quenching on hardness of sheet (Ref. 47)

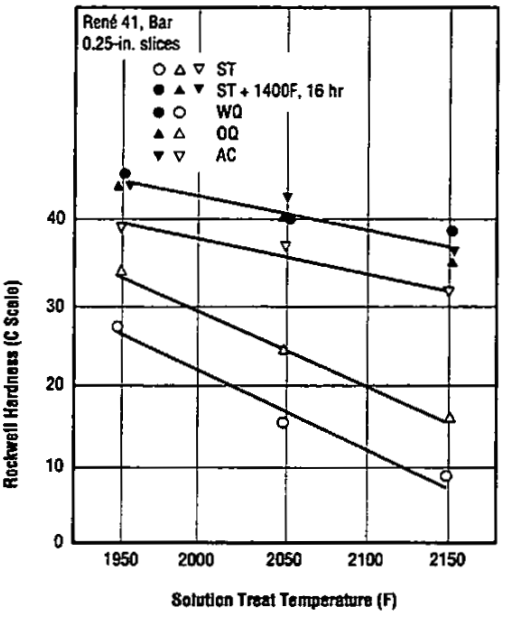

Fig. 1.6.1 Effect of solution treating temperature and cooling method on hardness of bar (Ref. 3)

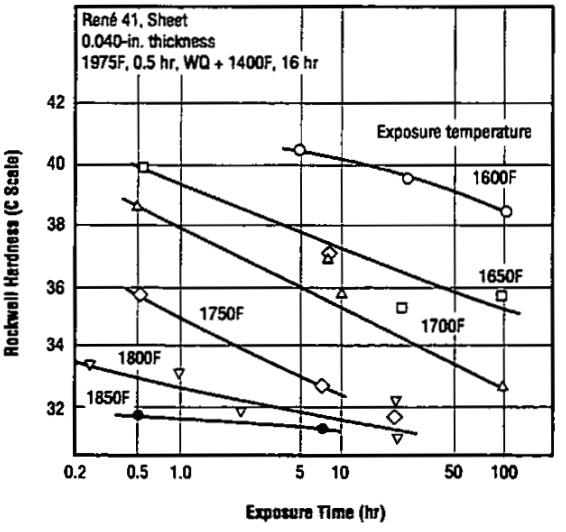

Fig. 1.6.3 Effect of high temperature exposure on room temperature hardness (Ref. 62)

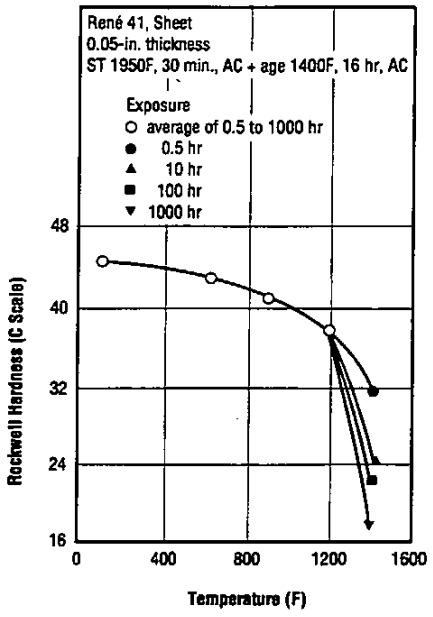

Fig. 1.6.4 Hardness at room and elevated temperatures for various exposure times (Refs. 29, 85-89)

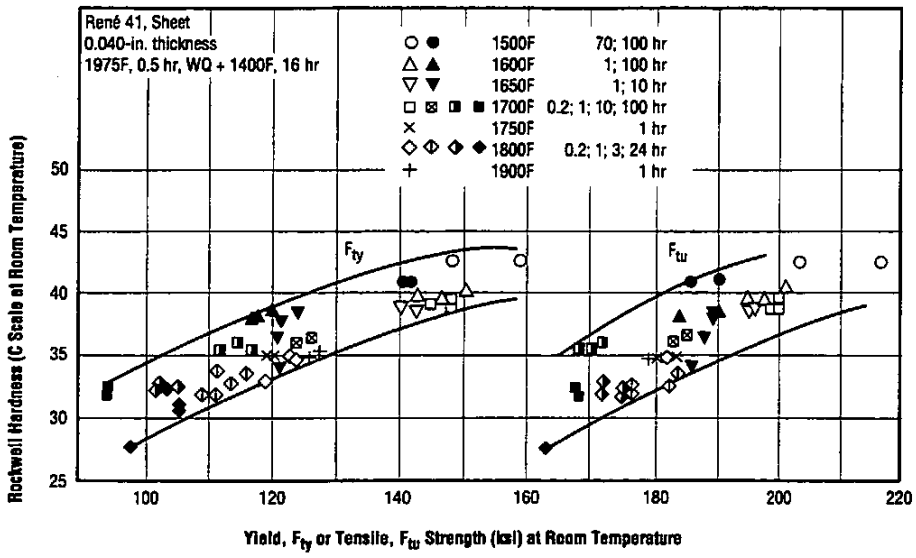

Fig. 1.6.5 Relation between hardness and tensile or yield strength at room temperature after high temperature exposure (Ref. 62)

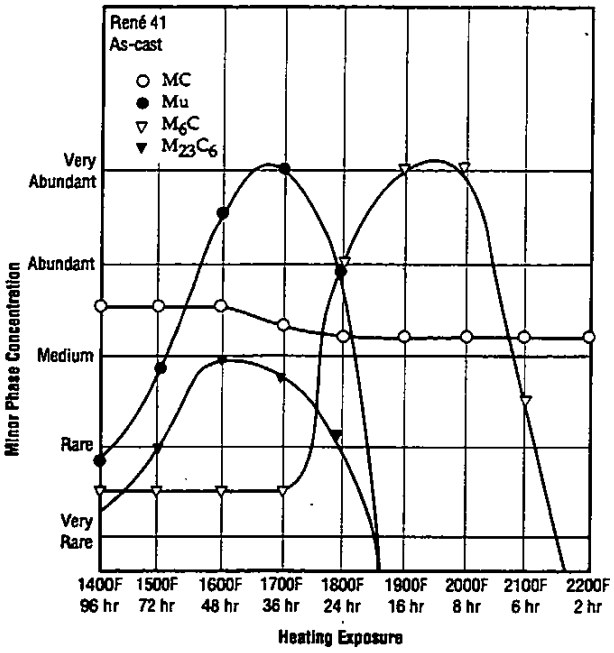

Fig. 2.1.2.1 Minor phase concentration for alloy after heating for various times and temperatures (Ref. 61)

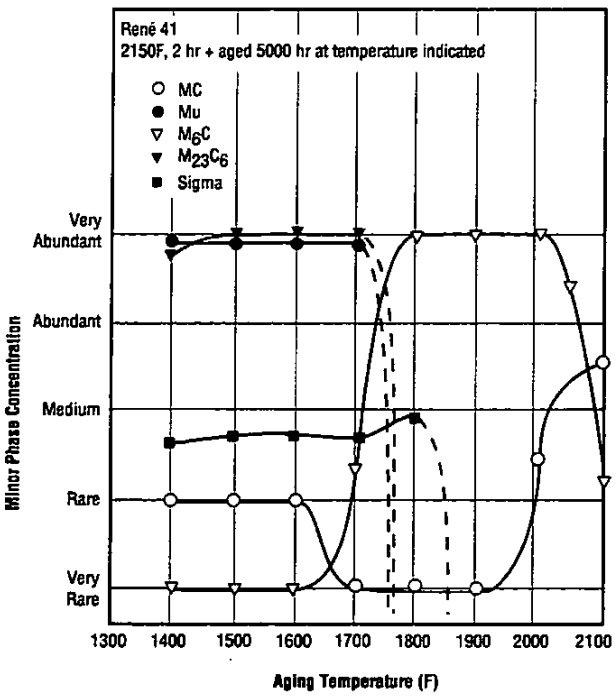

Fig. 2.1.2.2 Minor phase concentration for alloy after 5000 hour exposure at 1400 to 2200F (Ref. 109)

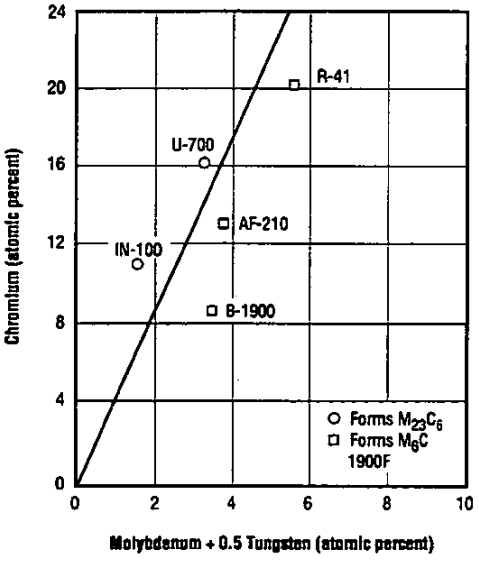

Fig. 2.1.2.3 Complex carbide-forming tendency in nickel-base alloys (Ref. 52)

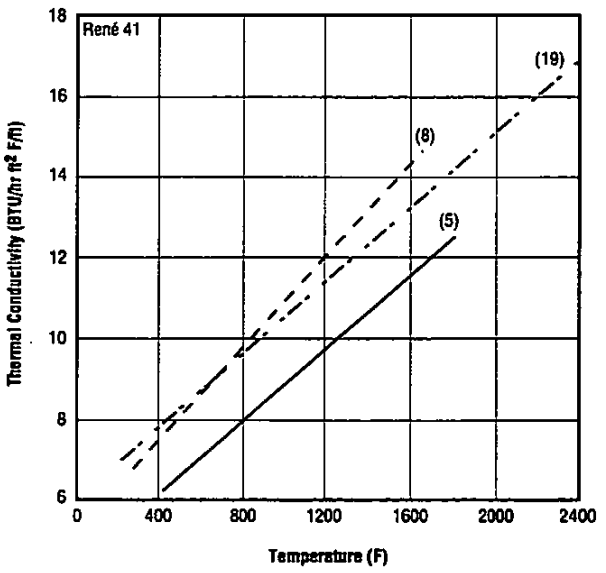

Fig. 2.1.3.1 Thermal conductivity (Refs. 5, 8, 19)

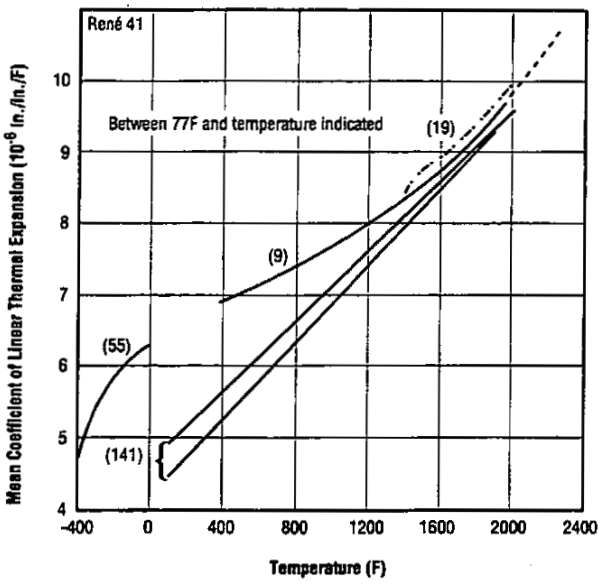

Fig. 2.1.4.1 Mean coefficient of linear thermal expansion (Refs. 9, 19, 55, 141)

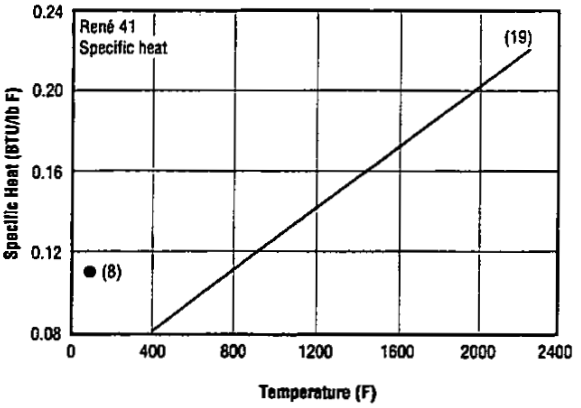

Fig. 2.1.5.1 Specific heat (Refs. 8, 19)

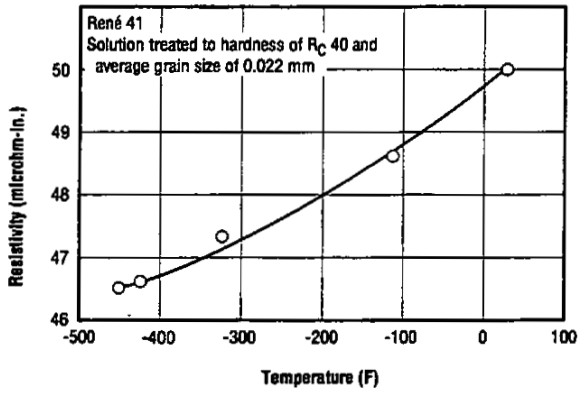

Fig. 2.2.2.1 Low temperature resistivity (Ref. 106)

Table 2.2.2.2 Effect of heat treatment on electrical resistivity (Ref. 18)

Alloy	René 41
Form	Sheet
Thickness (in.)	0.075
Condition	**Microhm-in. at RT**
Solution treat	51.5
Solution treat + 1950F, 4 hr, AC	49.2
1400F, 16 hr, AC	49.9
2150F, 30 min., AC	52.6
1650F, 4 hr, AC	52.8

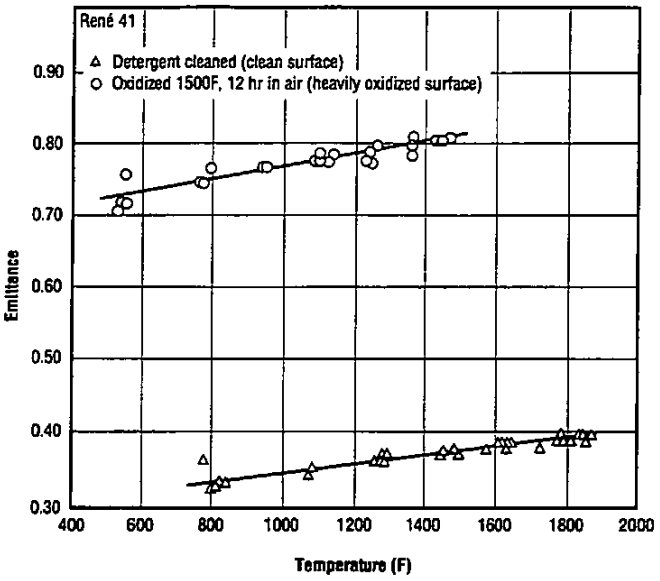

Fig. 2.2.4.1 Total hemispherical emittance of clean and oxidized René 41 (Ref. 142)

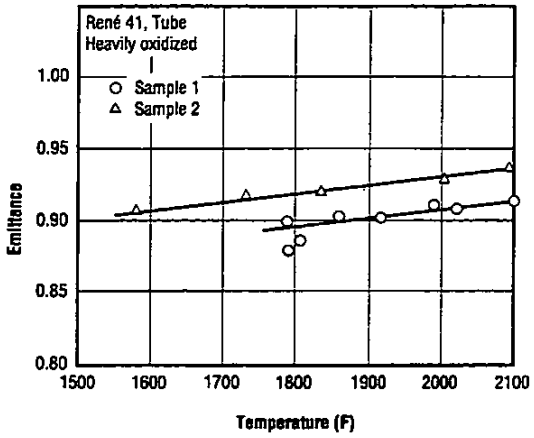

Fig. 2.2.4.2 Total hemispherical emittance of oxidized René 41 (Ref. 143)

Table 2.3.1.1 Effects of salt and thermal exposure on tensile properties (Ref. 120)

Alloy	René 41					
Initial Condition[a]	Exposure Conditions		Tensile Properties			
	Thermal	Salt (mg/cm^2)	F_{ty} (ksi)	F_{tu} (ksi)	e (percent)	Loss in F_{tu} (percent)
SA	none	none	63	137	47.5	—
SA + A	none	none	150	207	22.5	—
SA	1400F, 48 hr	none	150	209	21.0	—
SA + A	1400F, 48 hr	none	168	224	17.5	—
SA + A	1400F, 48 hr	0.17	155	192	9.3	14
SA + A	1100F, 48 hr	0.15	156	210	20.3	6
SA + A	800F, 48 hr	0.08	154	214	24.8	4

[a] SA — Solution annealed at 1950F.
A — Aged 1400F, 16 hours.

Table 2.3.1.2 Effect of salt on post-exposure tensile properties at room temperature (Ref. 121)

Alloy	René 41[a]					
	Exposure Conditions			Tensile Properties		
Salt[b]	Stress (ksi)	Time (hr)	Temperature (F)[c]	F_{ty} (ksi)	F_{tu} (ksi)	e (percent)
—	—	—	unexposed	92	160	23
no	3	48	1600	132	149	10
no	0	48	1600	128	155	23
yes	3	48	1600	70	95	2
yes	0	48	1600	66	90	3

a Heat treated 2150F, 2 hours, AC plus 1650F, 4 hours, AC.

b Slurry coated to thickness of 0.015-inch (equivalent to 150 mg/cm^2 of salt).

c Exposed in air.

Table 2.3.1.3 Effects of hydrazine decomposition products on tensile properties at 1450F (Ref. 123)

Alloy	René 41				
Test Environment	Hold Time Prior to Test (hr)	Tensile Properties			
		F_{ty} (ksi)	F_{tu} (ksi)	e (percent)	Reduction in Area (percent)
Argon	0	112.8	162.9	21.6	22.2
$NH_3/N_2/H_2$	0	129.7	175.7	15.7	20.7
$NH_3/N_2/H_2$	2	122.4	168.5	15.5	19.5

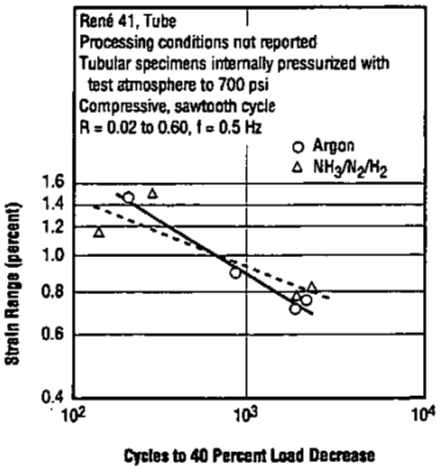

Fig. 2.3.1.4 Effects of hydrazine decomposition products on low-cycle fatigue properties at 1450F (Ref. 123)

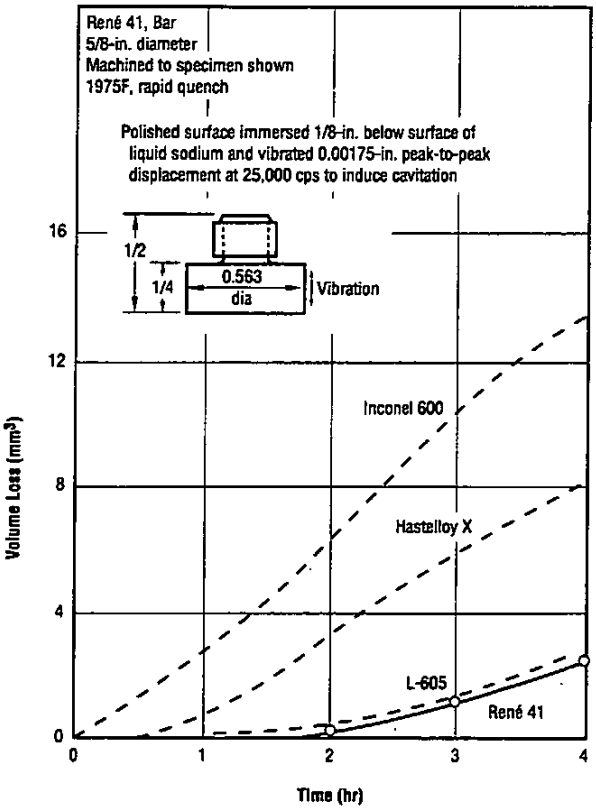

Fig. 2.3.1.5 Comparison of cavitation damage resistance with other high temperature alloys in liquid sodium at 800F (Ref. 91)

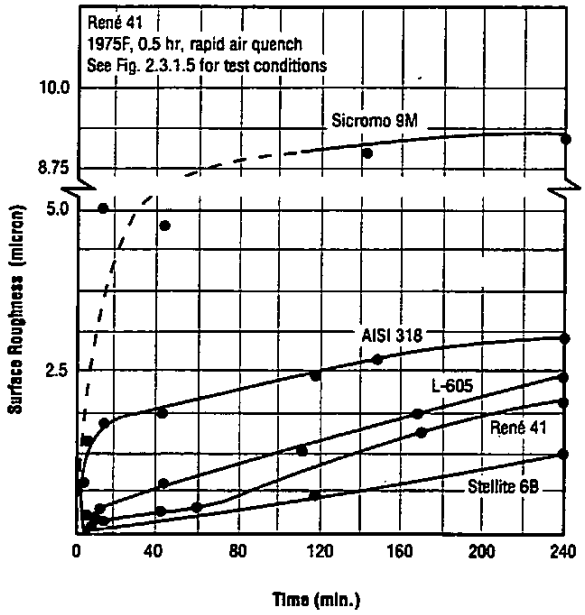

Fig. 2.3.1.6 Surface damage due to high frequency vibration in sodium at 800F, and comparison with results for other alloys (Ref. 97)

Table 2.3.3.1 Embrittlement of René 41 and other selected alloys by hydrogen at room temperature[a] (Ref. 125)

Alloy	René 41					
Alloy	Strength Ratio H_2/He		Unnotched Ductility			
	Notched[b]	Unnotched	Elongation (percent)		Reduction in Area (percent)	
			He	H_2	He	H_2
18 Ni Maraging (250 Grade)	0.12	0.68	8.2	0.2	55	2.5
Type 410 Stainless	0.22	0.79	15	1.3	60	12
17-7 PH	0.23	0.92	17	1.7	45	2.5
9Ni - 4Co	0.24	0.86	15	0.5	67	15
H-11	0.25	0.57	8.8	0	30	0
René 41	0.27	0.84	21	4.3	29	11
4140	0.40	0.96	14	2.6	48	9
Inconel 718	0.46	0.93	17	1.5	26	1
Ti - 6Al - 4V (STA)	0.58	—	—	—	—	—
Ti - 6Al - 4V (Annealed)	0.79	—	—	—	—	—
Ti - 5Al - 2.5Sn (ELI)	0.81	—	—	—	45	39
Type 304 ELC Stainless	0.87	—	—	—	78	71
Type 305 Stainless	0.89	—	—	—	78	75
Type 310 Stainless	0.93	—	—	—	64	62
A286	0.97	—	—	—	44	43
7075-T73 Al alloy	0.98	—	—	—	37	35
Type 316 Stainless	1.00	—	—	—	72	75
6061-T6 Al alloy	1.10	—	—	—	61	66

[a] Tested in high purity 10,000 psi hydrogen or helium.

[b] K_t = 8.4.

Table 2.3.3.2 Effects of heat treatment and exposure at 1200F in air or hydrogen on room temperature tensile properties (Ref. 126)

Alloy	René 41				
Initial Condition [a]	Exposure Time (hr)	Post-exposure Tensile Properties			
		Exposed in Air		Exposed in Hydrogen [b]	
		F_{tu} (ksi)	e (percent)	F_{tu} (ksi)	e (percent)
Cold Rolled	0	152	34	—	—
	20	168	12	151	7
	1000	174	7	171	3
Heat Treatment No. 1	0	131	50	—	—
	20	167	35	156	25
	1000	176	24	173	18
Heat Treatment No. 2	0	187	21	—	—
	20	193	18	185	12
	1000	186	16	187	9
Heat Treatment No. 3	0	181	20	—	—
	20	184	18	178	14
	1000	174	13	170	2

[a] Heat treatment No. 1: 1950F, 0.5 hour, WQ (average gamma-prime particle size 0.005 micron). Heat treatment No. 2: 1950F, 0.5 hour, WQ plus 1400F, 16 hours, WQ (average gamma-prime particle size 0.02 micron). Heat treatment No. 3: 1950F, 0.5 hour, FC plus 1400F, 16 hour, AC (average gamma-prime particle size 0.2 micron).

[b] Hydrogen pressure was 15 psi. Minimum purity of hydrogen was 99.0 percent.

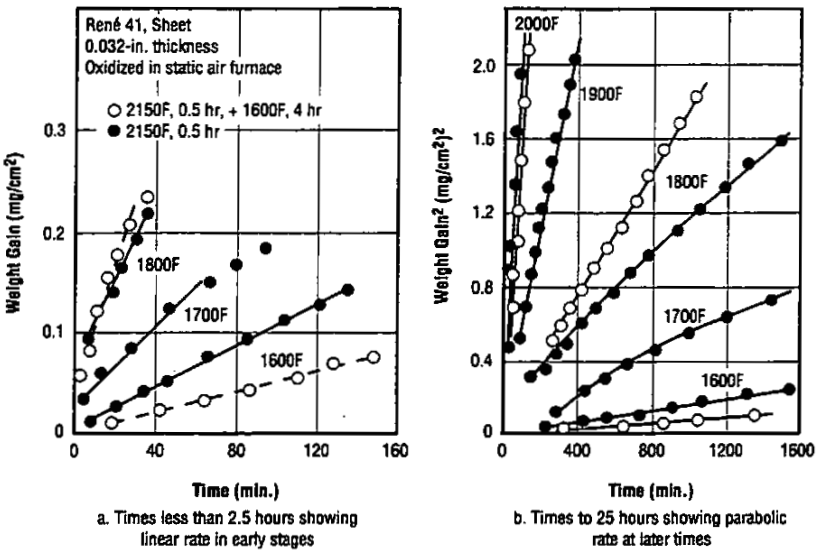

a. Times less than 2.5 hours showing linear rate in early stages

b. Times to 25 hours showing parabolic rate at later times

Fig. 2.3.4.1 Oxidation behavior of sheet at 1600 to 2000F (Ref. 105)

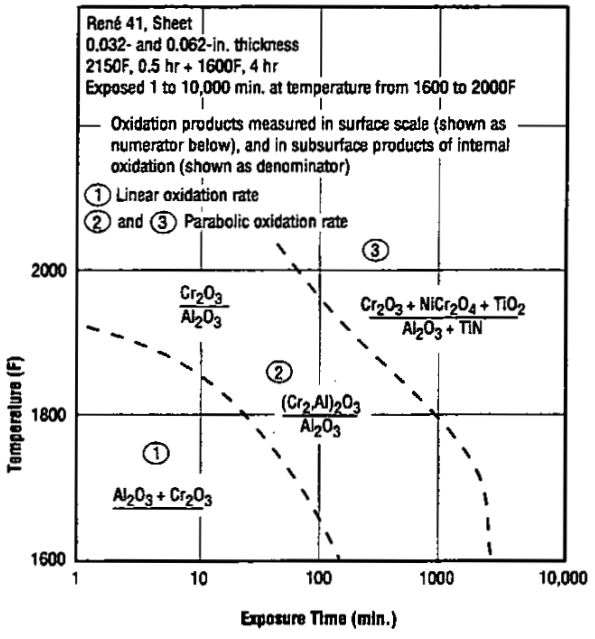

Fig. 2.3.4.2 Major reaction products after air oxidation at 1600 to 2000F (Ref. 105)

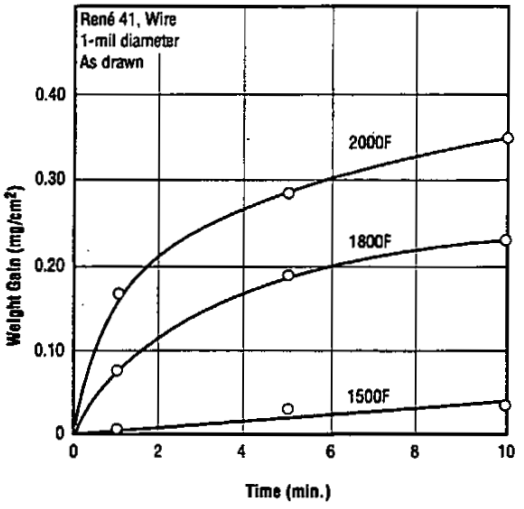

Fig. 2.3.4.3 Weight gain during furnace oxidation of wire at 1500 to 2000F (Ref. 83)

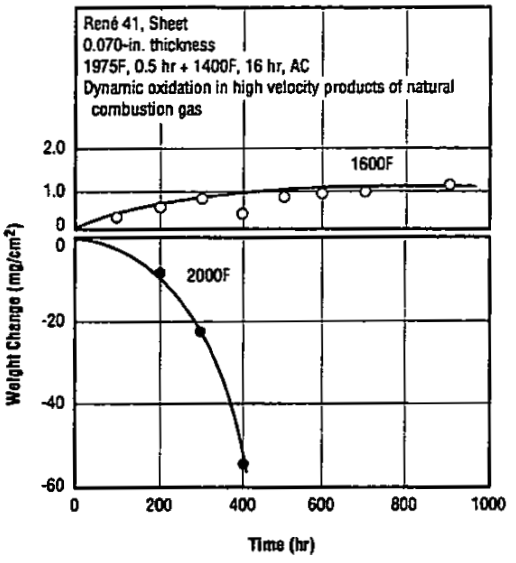

Fig. 2.3.4.4 Weight change during dynamic oxidation of sheet at 1600 and 2000F (Ref. 72)

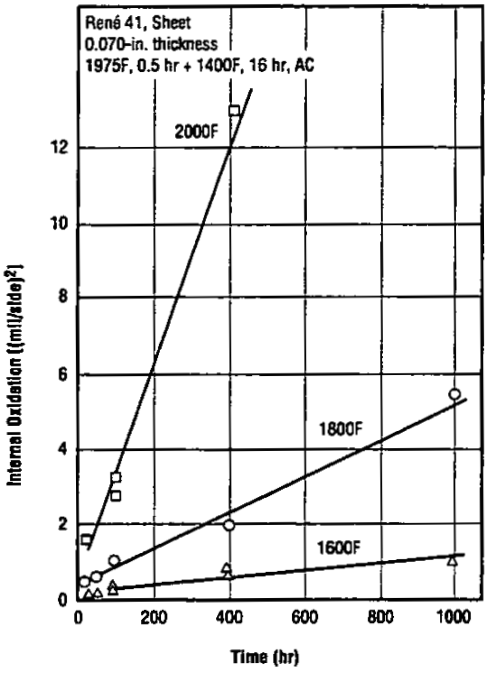

Fig. 2.3.4.5 Internal oxidation of sheet at 1600 to 2000F (Ref. 72)

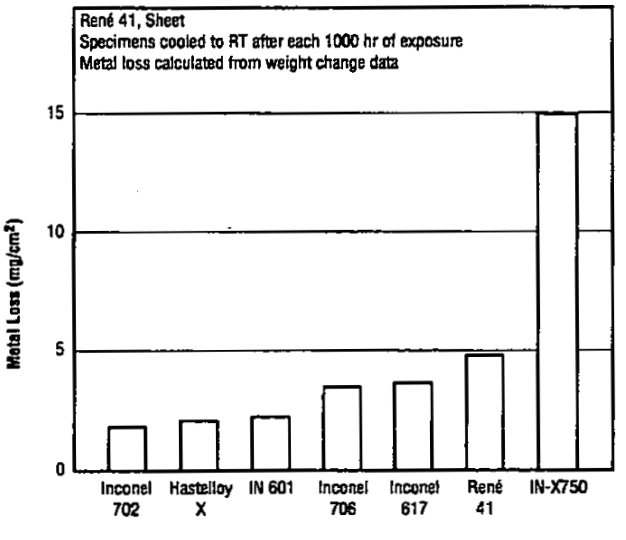

Fig. 2.3.4.6 Metal loss by oxidation after 10,000 hours exposure in air at 1500F for René 41 and other nickel-base superalloys (Ref. 127)

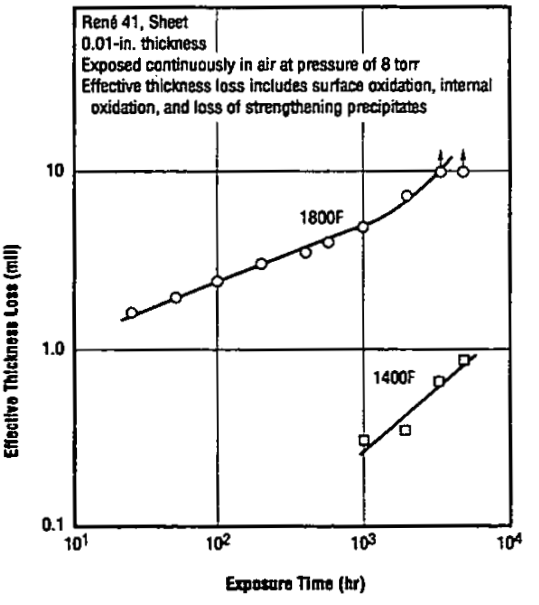

Fig. 2.3.4.7 Effect of oxidation exposure in low pressure air on effective thickness loss of thin-gage alloy at 1400 and 1800F (Ref. 130)

Table 3.1.1 AMS specified properties for castings, bars, forgings, and rings (Refs. 2, 3, 77)

Alloy	René 41												
AMS Specifications	Form	Heat Treatment[a]	Tensile Properties					Rupture Properties				Hardness	
			Temperature (F)	F_{ty} min (ksi)	F_{tu} min (ksi)	e, min (percent)[b]	RA, min (percent)	Temperature (F)	Stress (ksi)	Rupture Life, min (hr)	e, min (percent)	min	max
5399B	Casting	SHT + PHT	1200	90	110	3	5	1650	25	25	5	30 HRC	—
5712F, 5713F	Bars, forgings and rings	SHT	—	—	—	—	—	—	—	—	—	—	363 HB
		SHT + PHT	RT	130	170	8	10	1350	87.5	23	—	—	—
			1400	105	135	5	10	—	—	—	—	311 HB	

Note: The original AMS documents should be consulted for complete specification details.

[a] SHT — Solution heat treatment of 1950F, 0.5 hour, RAC (casting) or 1975F, time commensurate with thickness, suitable quench (bars, forgings, rings).
PHT — Precipitation heat treatment of 1400F, 16 hours, AC.

[b] Elongation in 4D.

Table 3.1.2 AMS specified properties for sheet, strip, and plate (Ref. 1)

Alloy	René 41								
AMS Specifications	Condition[a]	Thickness (in.)	Tensile Properties				Hardness		Bend Diameter, min (t)
			Temperature (F)	F_{ty}, min (ksi)	F_{tu}, min (ksi)	e, min (percent)[b]	min	max	
5545C	SHT	≤ 0.015	RT	100	170	20	—	—	—
		> 0.015 ≤ 0.115		100	170	30	—	—	—
		> 0.115 ≤ 0.187		115	180	30	—	—	—
		> 0.187		140	195	30	—	—	—
		≤ 0.040		—	—	—	—	75 HR15N	—
		> 0.040 ≤ 0.070		—	—	—	—	64 HRA	—
		> 0.070 ≤ 0.187		—	—	—	—	30 HRC	—
		≤ 0.062		—	—	—	—	—	2
		> 0.062 ≤ 0.125		—	—	—	—	—	2.5
		> 0.125 ≤ 0.187		—	—	—	—	—	3
	SHT + PHT	≤ 0.020	RT	120	160	6	—	—	—
		> 0.020		130	170	10	—	—	—
		≤ 0.020	1400	110	130	3	—	—	—
		> 0.020		110	140	3	—	—	—
		all		—	—	—	35 HRC	—	—

Note: The original AMS documents should be consulted for complete specification details.

[a] SHT — Solution heat treatment of 1975F, 1 hour per inch of thickness, RAC or faster.
PHT — Precipitation heat treatment of 1400F, 16 hours, AC.

[b] Elongation in 2 inch or 4D.

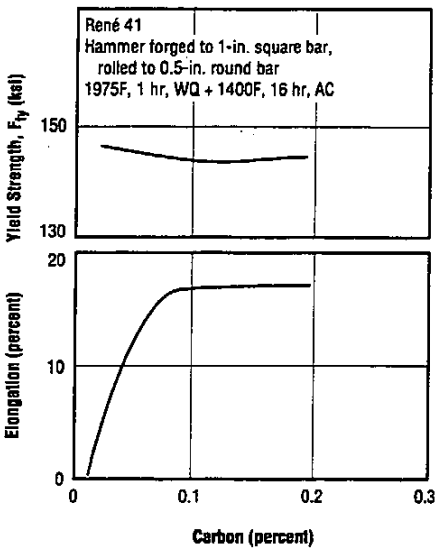

Fig. 3.2.1.1 Effect of carbon content on room temperature yield strength and elongation (Ref. 46)

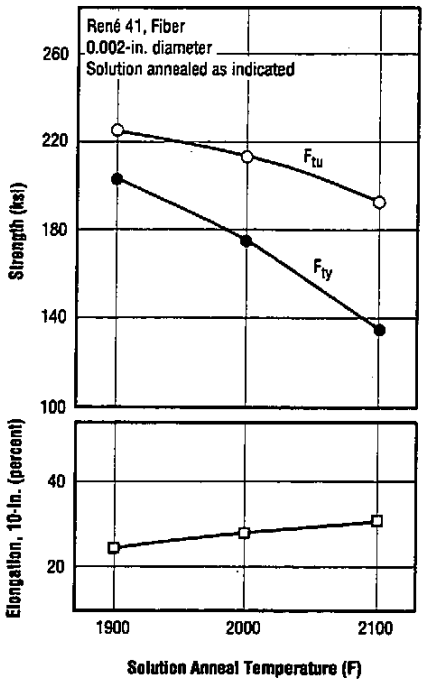

Fig. 3.2.1.2 Effect of annealing temperature on room temperature tensile properties for 0.002-inch diameter fiber (Ref. 82)

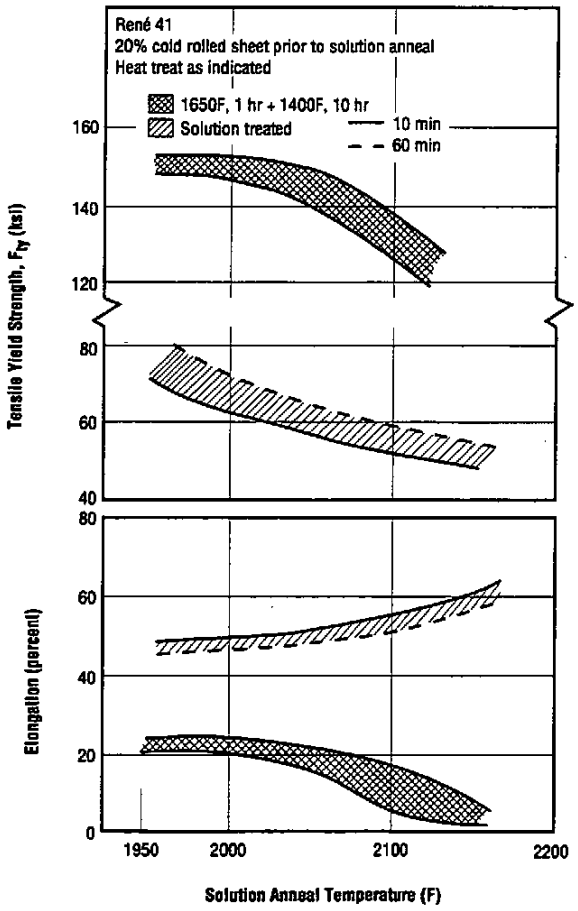

Fig. 3.2.1.3 Effect of solution anneal time and temperature with and without double age on tensile properties of sheet at room temperature (Refs. 47, 49)

Table 3.2.1.4 Effect of heat treatment on tensile properties of casting (Ref. 100)

Alloy	René 41			
Form	Casting			
Condition	**As Cast**	**1950F, 4 hr, AC**	**2150F, 2 hr, AC**	**1950F, 4 hr, AC + 1400F, 16 hr, AC**
F_{tu} (ksi)	124 - 128	106 - 112	126 - 130	112 - 114
F_{ty} (ksi)	78 - 80	82 - 84	82	98 - 101
e, 2-in. (percent)	16	11 - 17	33	3 - 5
RA (percent)	19 - 23	16 - 19	30 - 32	8 - 9

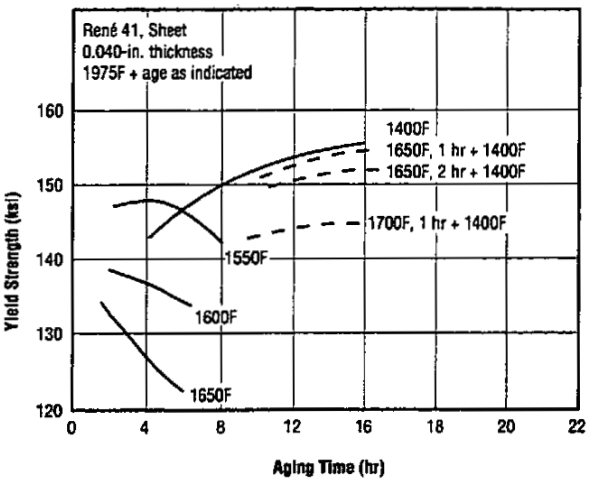

Fig. 3.2.1.5 Effect of aging time and temperature on room temperature yield strength of sheet (Refs. 47, 49)

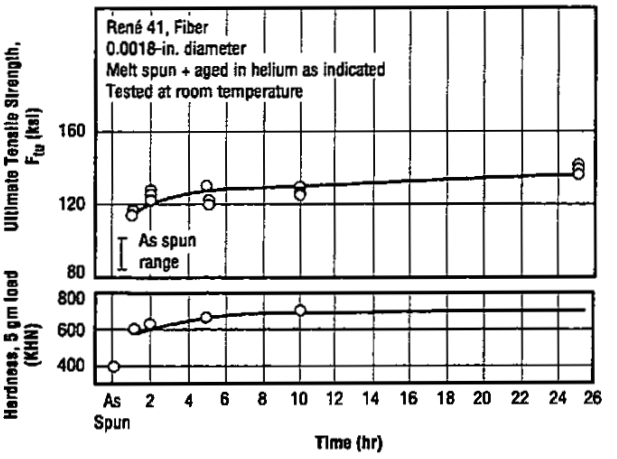

Fig. 3.2.1.6 Effects of aging time in helium at 1436F on tensile strength and microhardness of melt spun René 41 fibers (Ref. 87)

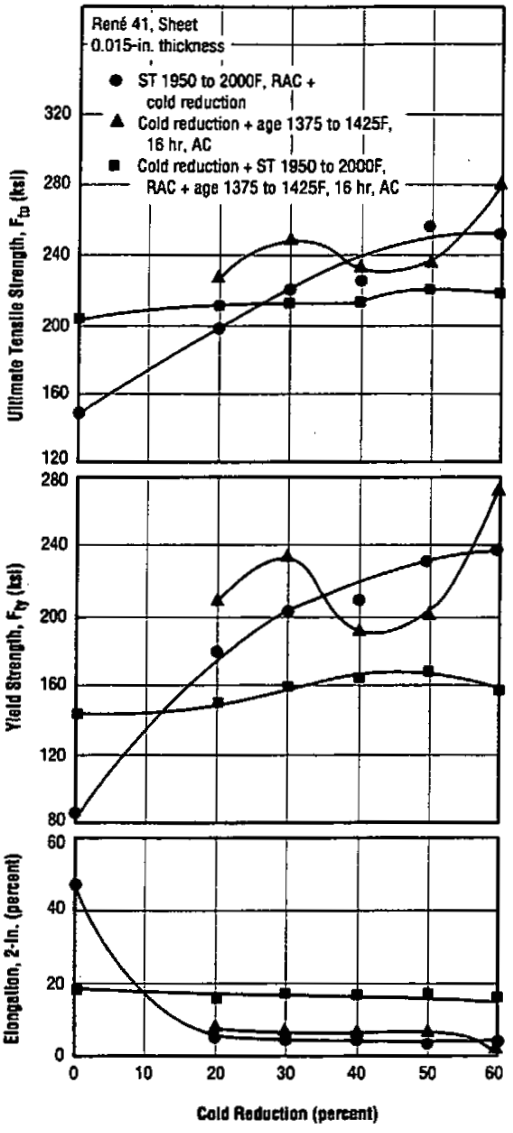

Fig. 3.2.1.7 Effect of cold reduction by shear forming on room temperature tensile properties (Ref. 32)

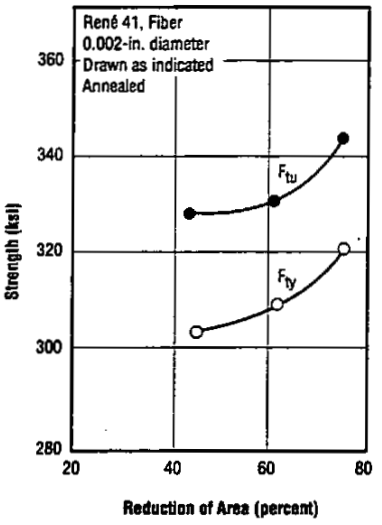

Fig. 3.2.1.8 Effect of cold reduction on ultimate and yield strength of fiber initially 0.002-inch diameter (Ref. 82)

Table 3.2.1.9 Effect of cold reduction by fluid extrusion on tensile properties of bar tested under normal atmospheric temperature and pressure (Ref. 96)

Alloy	René 41	
Form	Bar	
Condition	As Heat Treated	Heat treat + 50 percent cold reduction by fluid extrusion + re-age [a]
F_{ty} (ksi)	133.8	243.0
RA (percent)	12	11

[a] Fluid extrusion at 15.8 kilobars.

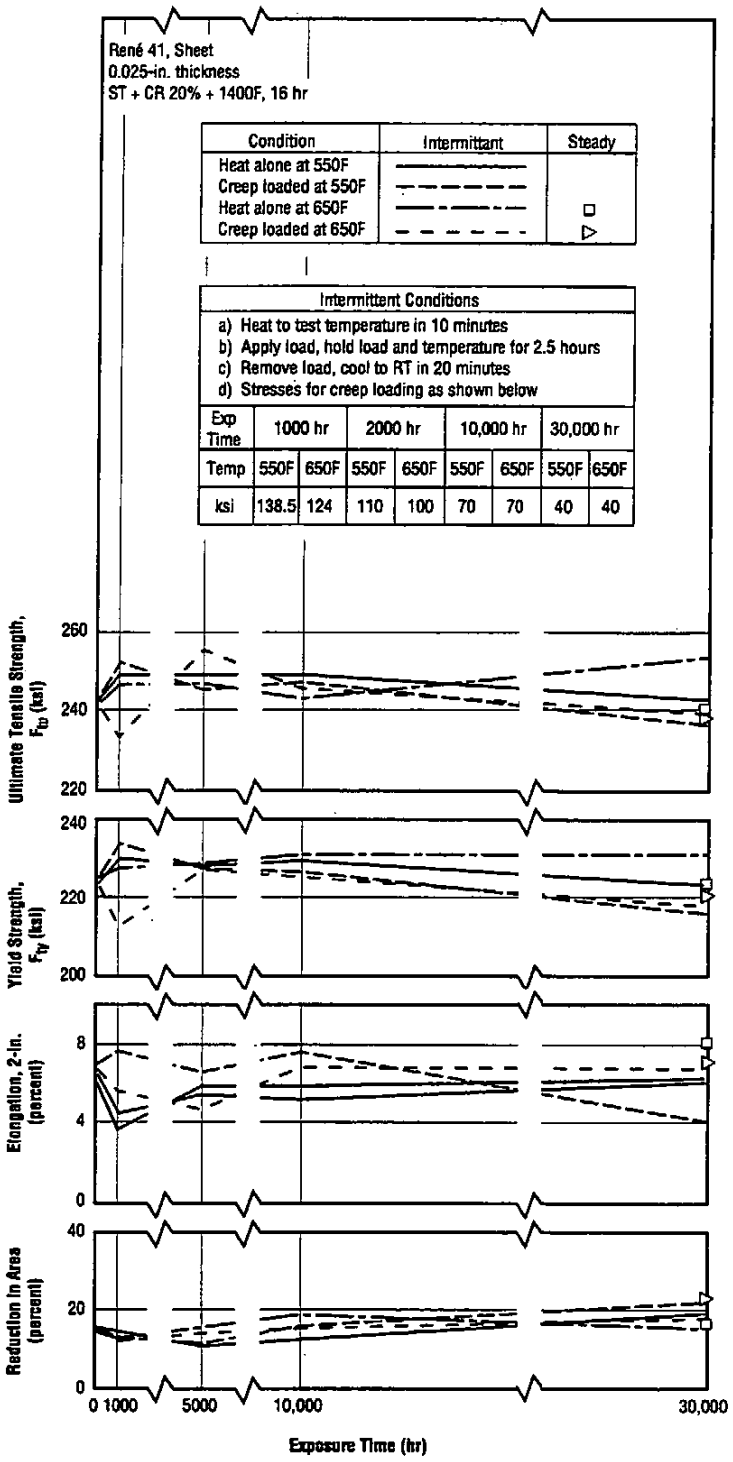

Fig. 3.2.1.10 Effect of exposure time and temperature simulating supersonic transport conditions on room temperature tensile properties (Refs. 62-65)

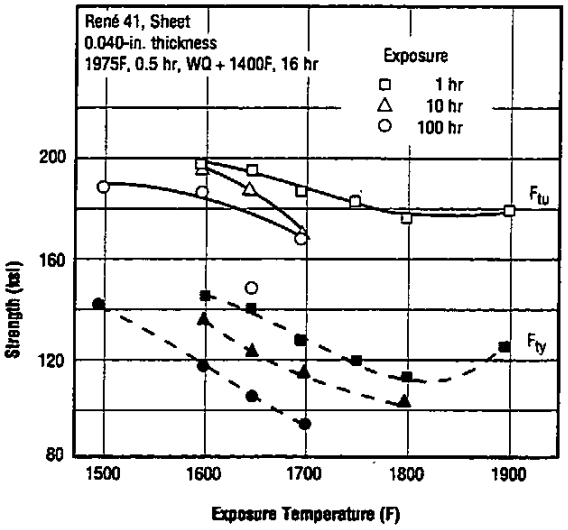

Fig. 3.2.1.11 Effect of high temperature exposure on room temperature tensile properties (Ref. 62)

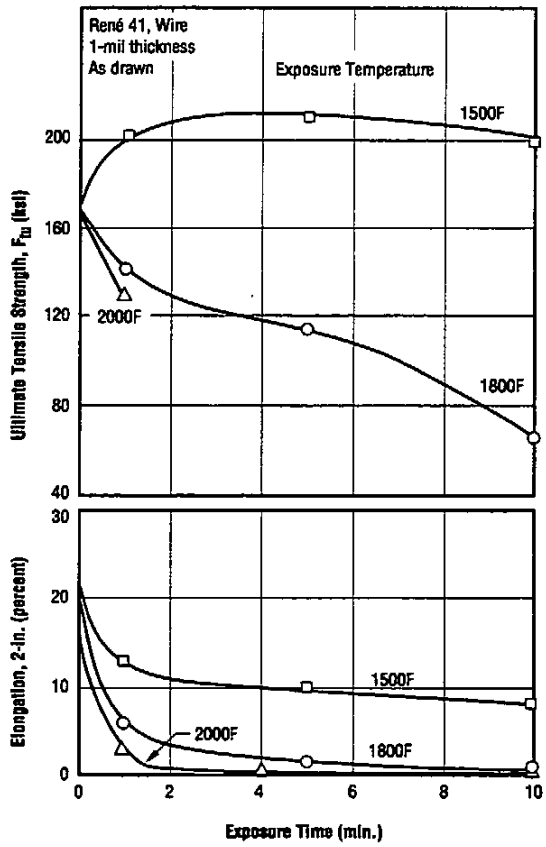

Fig. 3.2.1.12 Effect of temperature and exposure time on tensile strength and ductility of 1-mil wire (Ref. 83)

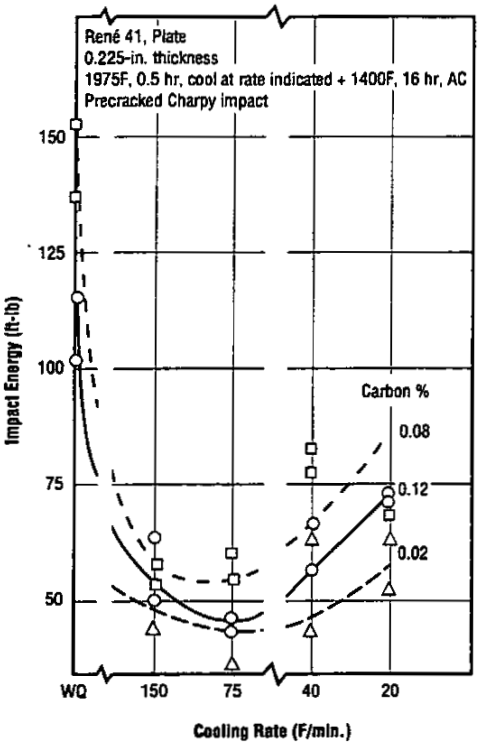

Fig. 3.2.3.1 Effect of cooling rate after solution treatment on room temperature impact energy for three heats of differing carbon content (Ref. 75)

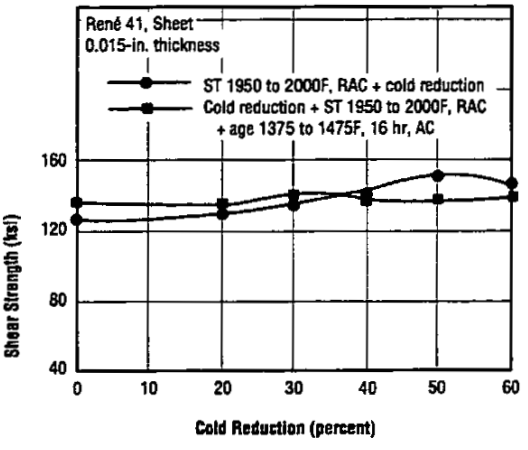

Fig. 3.2.5.2 Effect of cold reduction by shear forming on room temperature shear strength (Ref. 32)

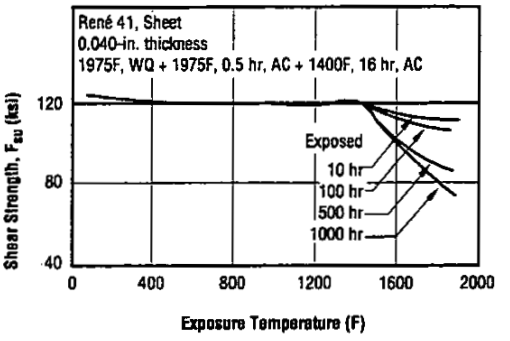

Fig. 3.2.5.1 Effect of time and temperature of exposure on shear strength of sheet at room temperature (Ref. 43)

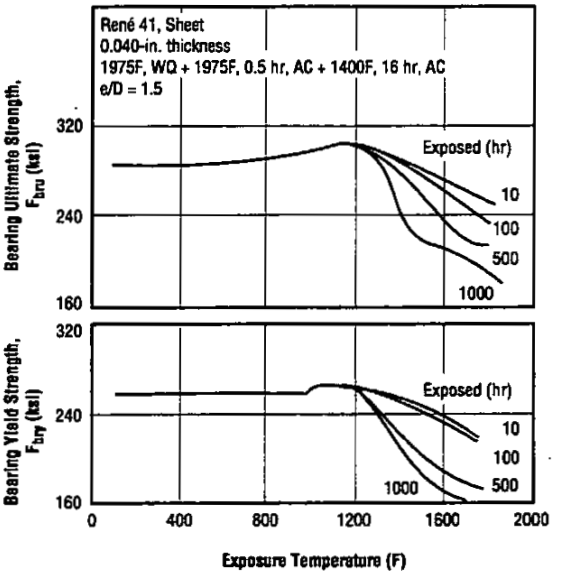

Fig. 3.2.6.1 Effect of time and temperature of exposure on bearing strength of sheet at room temperature (Ref. 43)

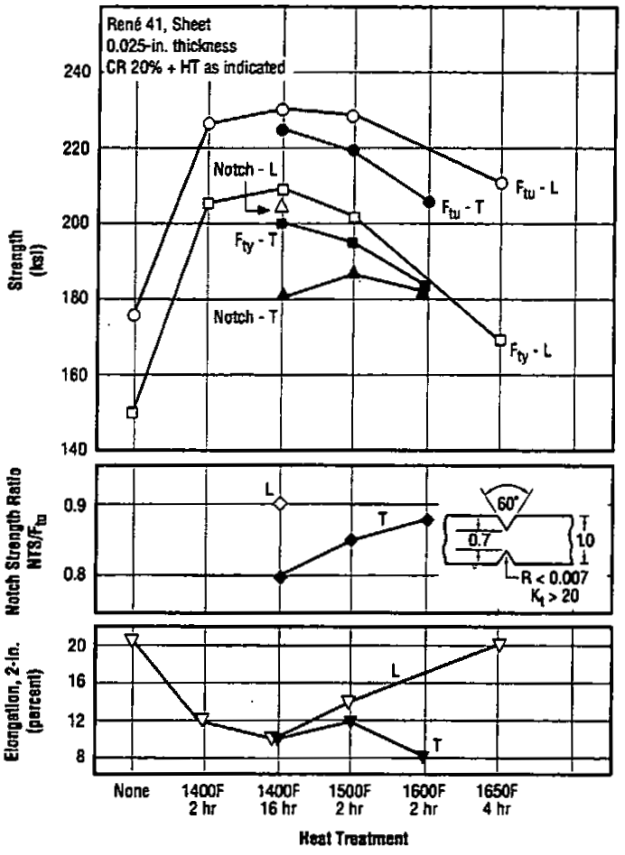

Fig. 3.2.7.1.1 Effect of heat treatment on room temperature smooth and sharp notch tensile properties of 20 percent cold rolled sheet (Ref. 71)

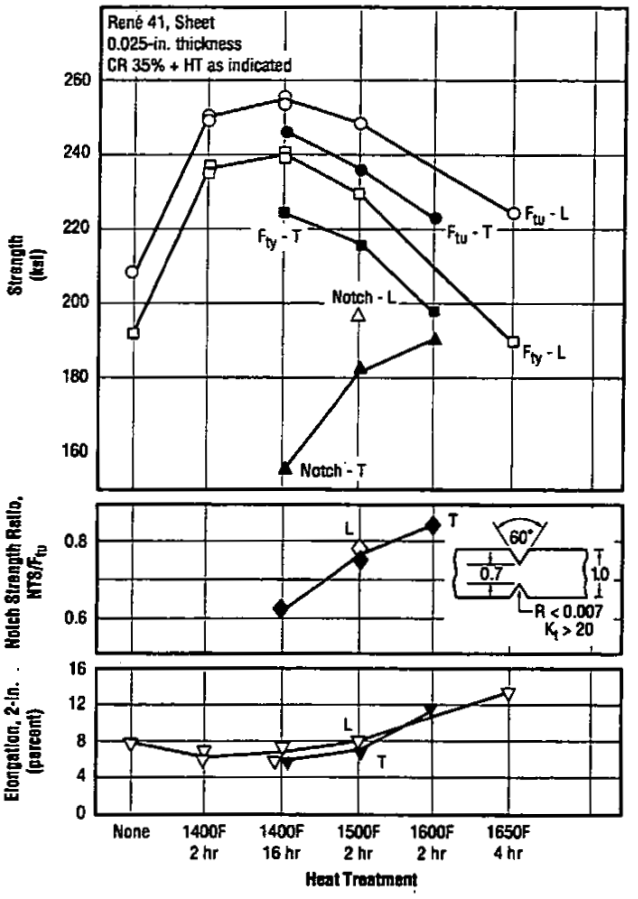

Fig. 3.2.7.1.2 Effect of heat treatment on room temperature smooth and sharp notch tensile properties of 35 percent cold rolled sheet (Ref. 71)

Table 3.2.7.1.3 Effect of high pressure hydrogen and of hydrogen-contaminated helium on embrittlement of smooth and notched bars (Ref. 94)

Alloy	René 41					
Form	Bar					
Condition	1975F, 1 hr, WQ + 1400F, 16 hr, AC					
Shape	Smooth D = 0.250 inch		Notched K_t = 8.4 60° 0.150 0.250 R = 0.00095			
Test Environment	**Air**	**10 ksi H_2**	**Air**	**He**	**10 ksi H_2**	**10 ksi He + 44 ppm H_2**
F_{ty} (ksi)	—	163	—	—	—	—
F_{tu} (ksi)	196	165	280	270	77	270
e (percent)	21	4.3	—	—	—	—
RA (percent)	29	11	3.4	2.0	0.2	2.0

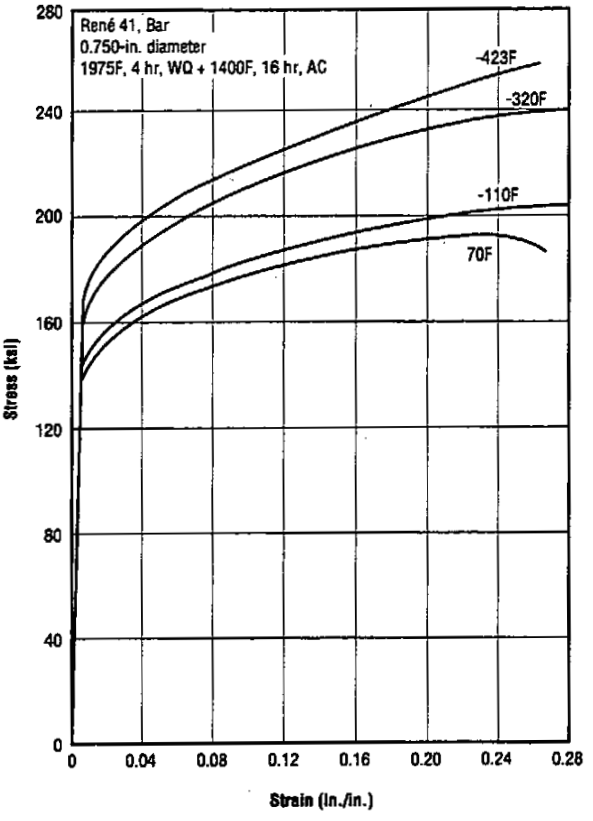

Fig. 3.3.1.1 Stress-strain curves of bar at room and low temperatures (Refs. 55, 56)

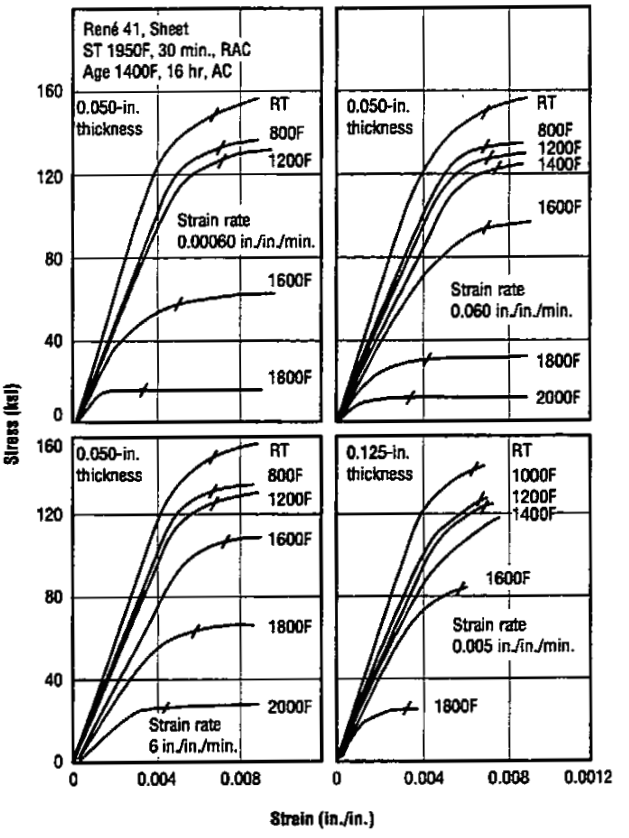

Fig. 3.3.1.2 Stress-strain curves at room and elevated temperatures for various sheet thicknesses and strain rates (Refs. 24, 25)

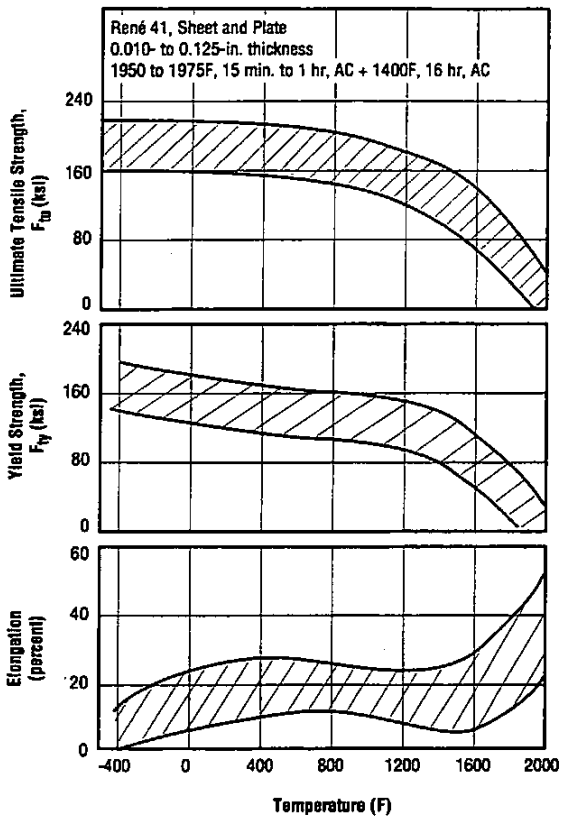

Fig. 3.3.1.3 Tensile properties from -420 to 2000F of sheet and plate aged at 1400F after solution treatment, showing scatterband for numerous lots tested at several laboratories (Ref. 80)

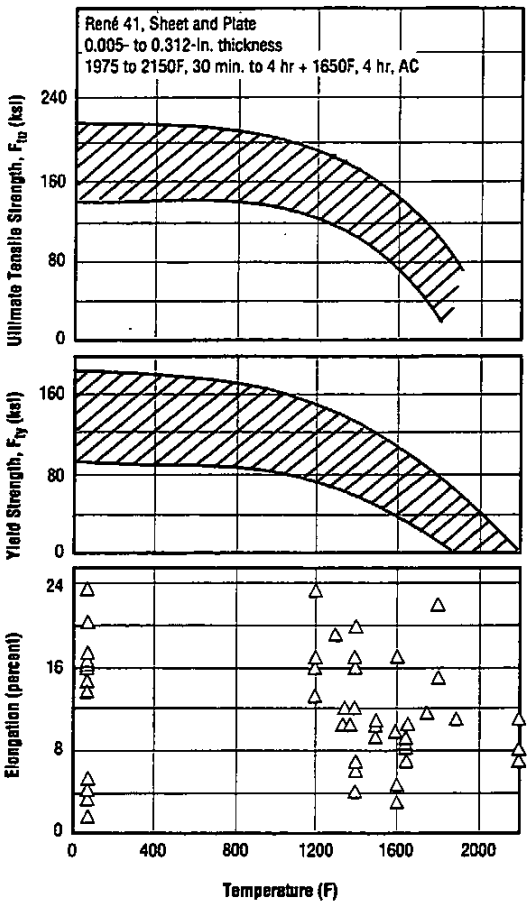

Fig. 3.3.1.4 Tensile properties from 70 to 2200F of sheet and plate aged at 1650F after solution treatment, showing scatterband for numerous lots tested at several laboratories (Ref. 80)

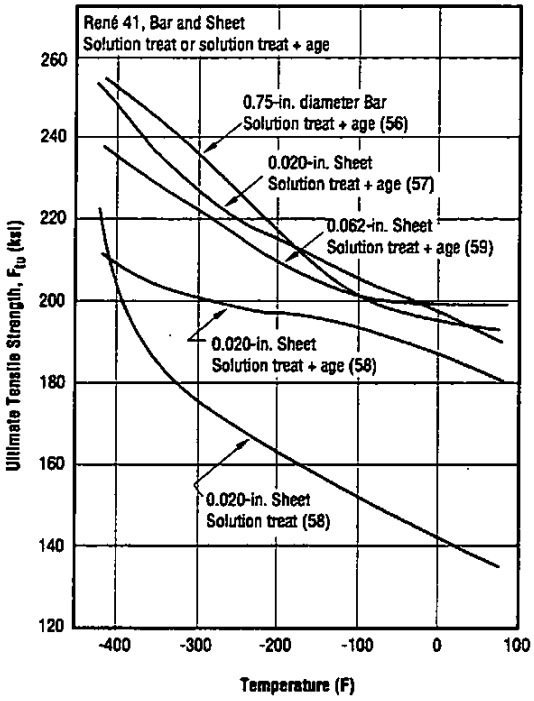

Fig. 3.3.1.5 Effect of low test temperature on longitudinal tensile strength of sheet and bar (Refs. 55-59)

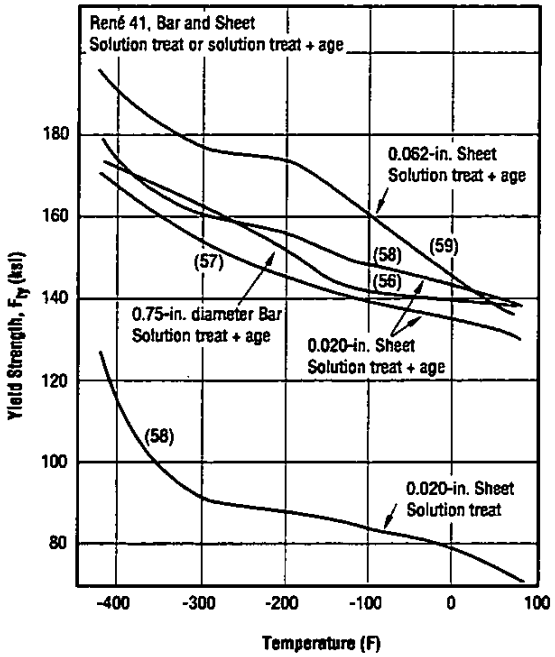

Fig. 3.3.1.6 Effect of low test temperature on longitudinal yield strength of sheet and bar (Refs. 55-59)

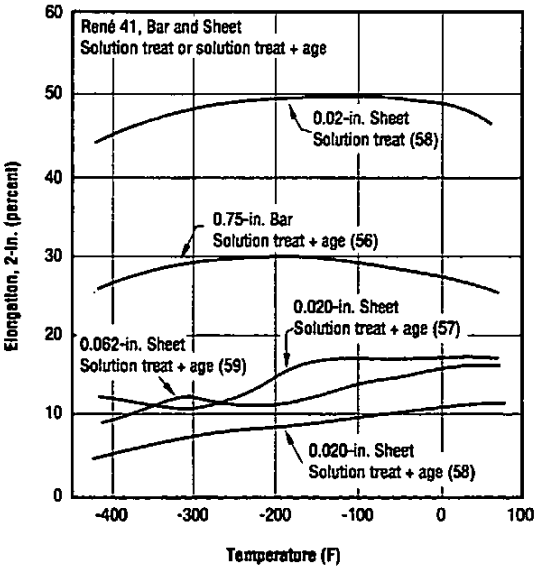

Fig. 3.3.1.7 Effect of low test temperature on longitudinal elongation of sheet and bar (Refs. 55-59)

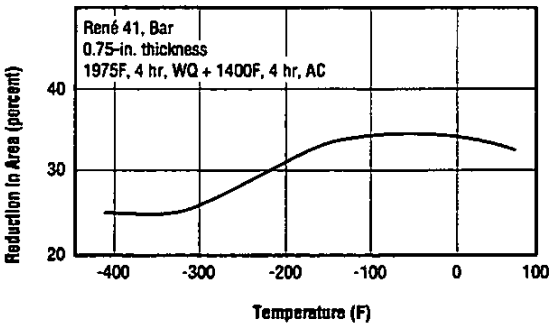

Fig. 3.3.1.8 Effect of low test temperature on reduction in area of bar (Refs. 55, 56)

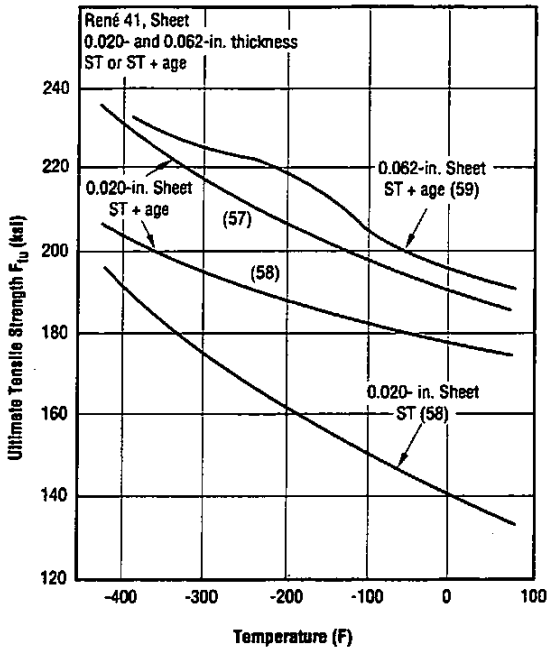

Fig. 3.3.1.9 Effect of low test temperature on transverse tensile strength of sheet (Refs. 55, 57-59)

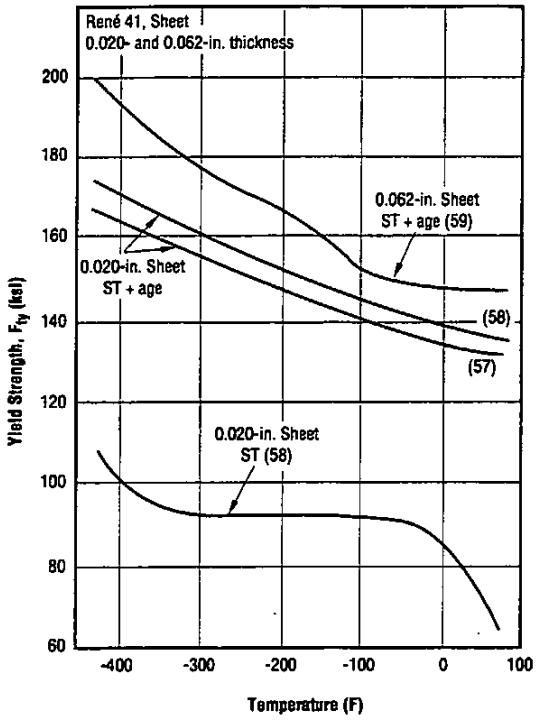

Fig. 3.3.1.10 Effect of low test temperature on transverse yield strength of sheet (Refs. 55, 57-59)

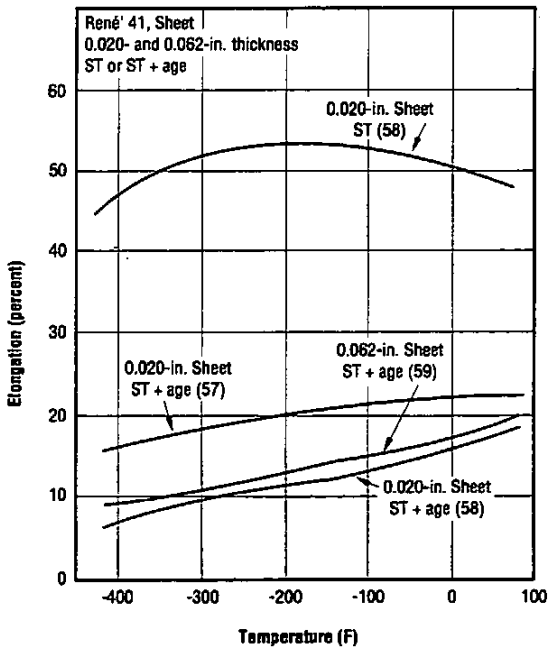

Fig. 3.3.1.11 Effect of low test temperature on transverse elongation of sheet (Refs. 55, 57-59)

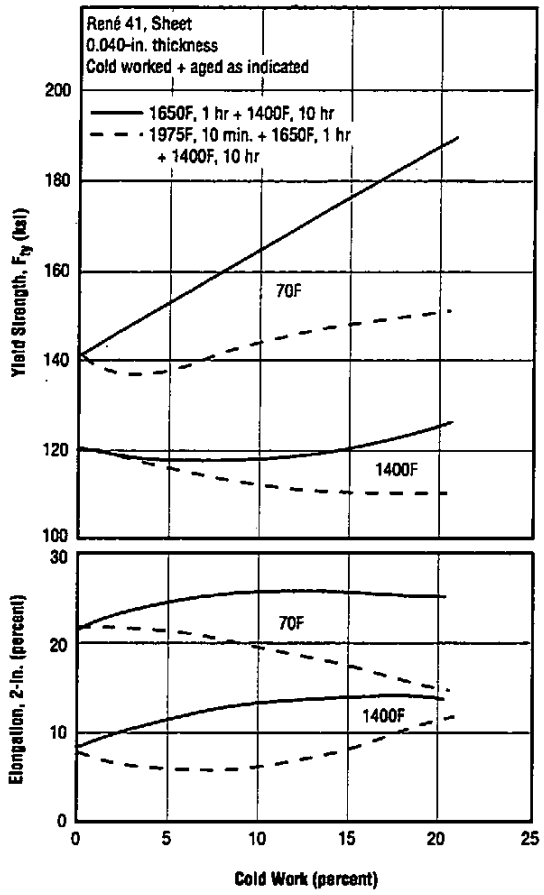

Fig. 3.3.1.12 Effect of cold work and heat treatment on tensile properties of sheet at room temperature and 1400F (Refs. 47, 49)

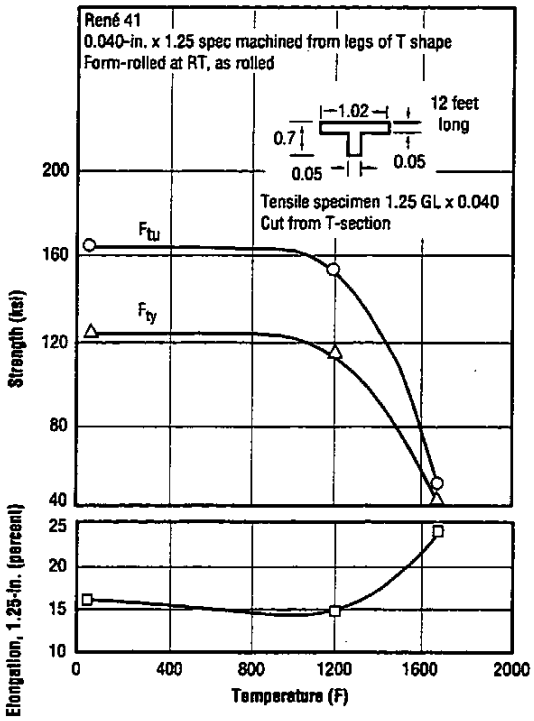

Fig. 3.3.1.13 Tensile properties from room temperature to 1700F of specimens from form-rolled T-section (Ref. 84)

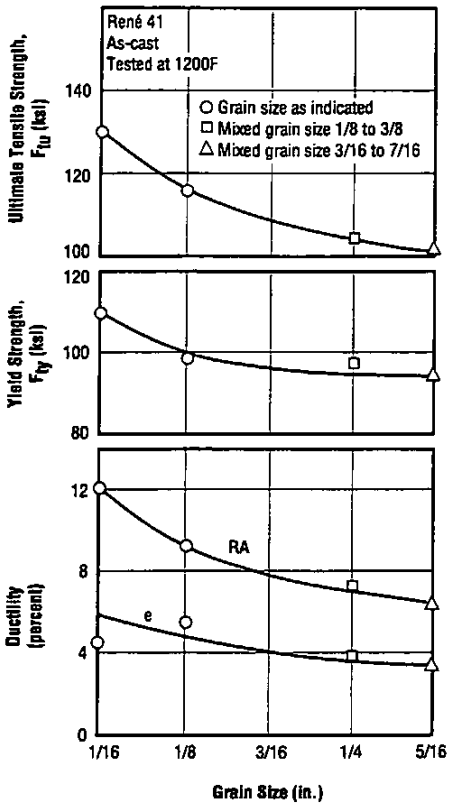

Fig. 3.3.1.14 Effect of grain size on tensile properties of as-cast alloy at 1200F (Refs. 44, 45)

Table 3.3.1.15 Properties at room temperature and 1400F of sheet produced from powder bar (Ref. 108)

Alloy	René 41	
Form	Sheet	
Thickness (in.)	0.064	
Condition [a]	1975F, 25 min., WQ	1975F, 25 min., WQ + 1400F, 16 hr
F_{tu} (ksi) at RT	154	238
F_{ty} (ksi) at RT	109	182
e (percent) at RT	30	14.5
F_{tu} (ksi) at 1400F	—	159
F_{ty} (ksi) at 1400F	—	136
e (percent) at 1400F	—	16
Rupture life (hr) [c]	—	37 [b]
Rupture e, 1-in. (percent)	—	9

[a] All test results shown are averages of four tests, except footnote b.

[b] Average of 3 tests.

[c] Tested at 63 ksi, 1400F.

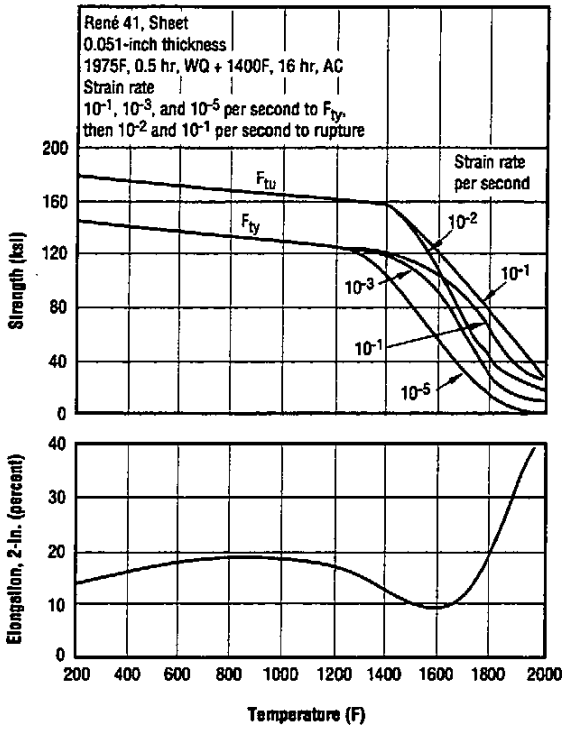

Fig. 3.3.1.16 Effect of strain rate and test temperature on tensile properties of sheet (Ref. 36)

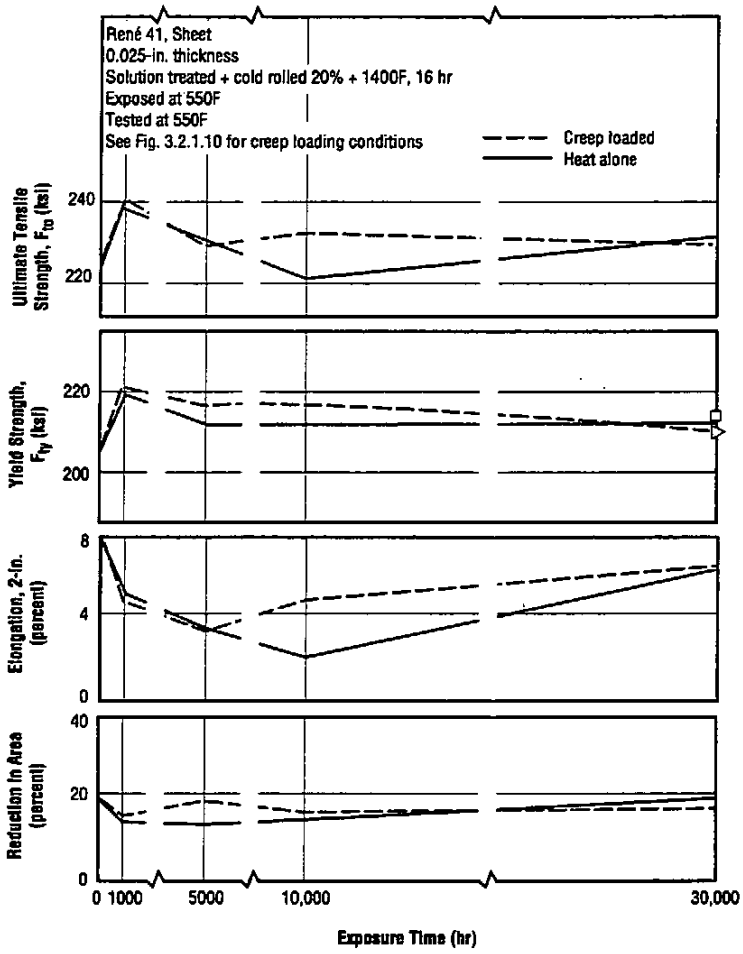

Fig. 3.3.1.17 Tensile properties at 550F after exposure to stress and temperature or to temperature alone at 550F (Ref. 63)

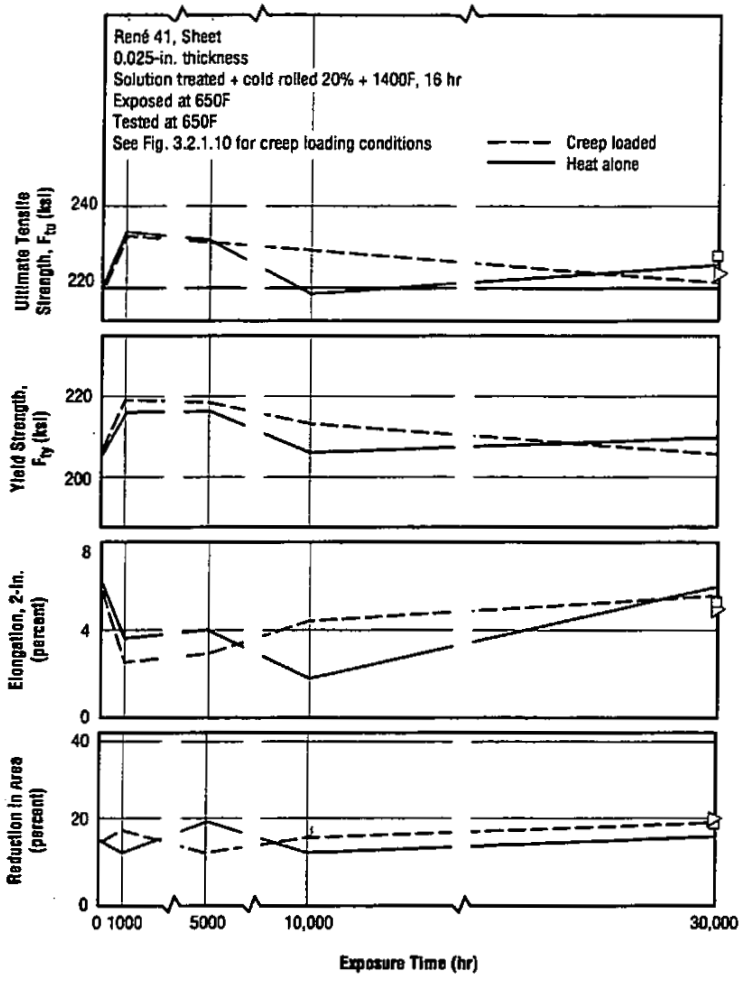

Fig. 3.3.1.18 Tensile properties at 650F after exposure to stress and temperature or to temperature alone at 650F (Ref. 63)

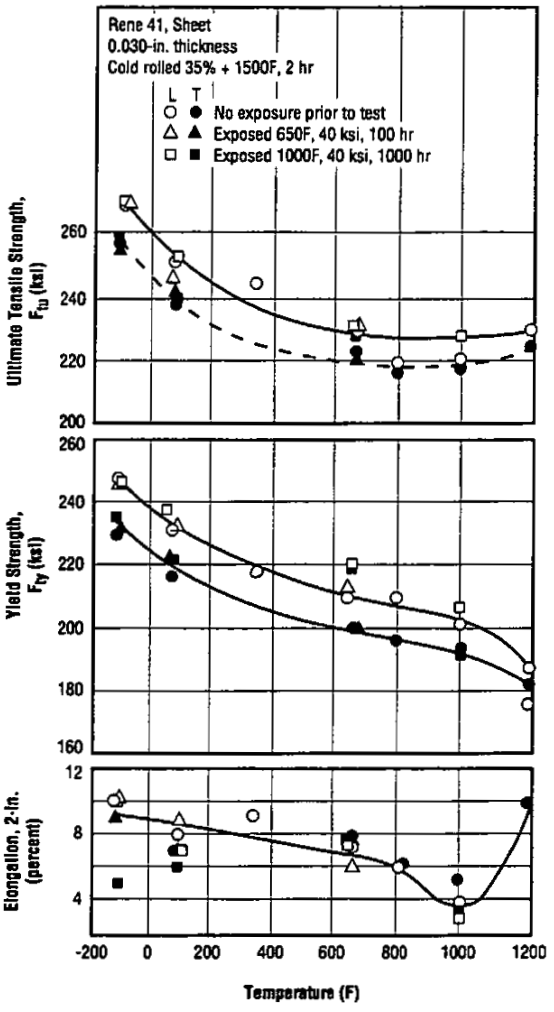

Fig. 3.3.1.19 Effect of test temperature on tensile properties of cold worked and aged sheet with and without prior exposure to stress and temperature (Ref. 54)

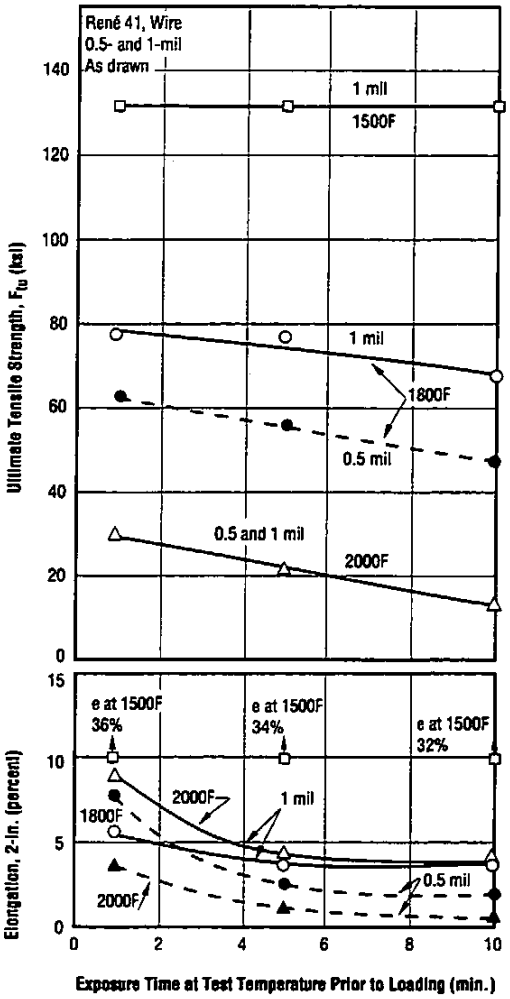

Fig. 3.3.1.20 Effect of exposure time prior to loading on tensile strength and elongation of 0.5- and 1-mil wire at 1500 to 2000F (Ref. 83)

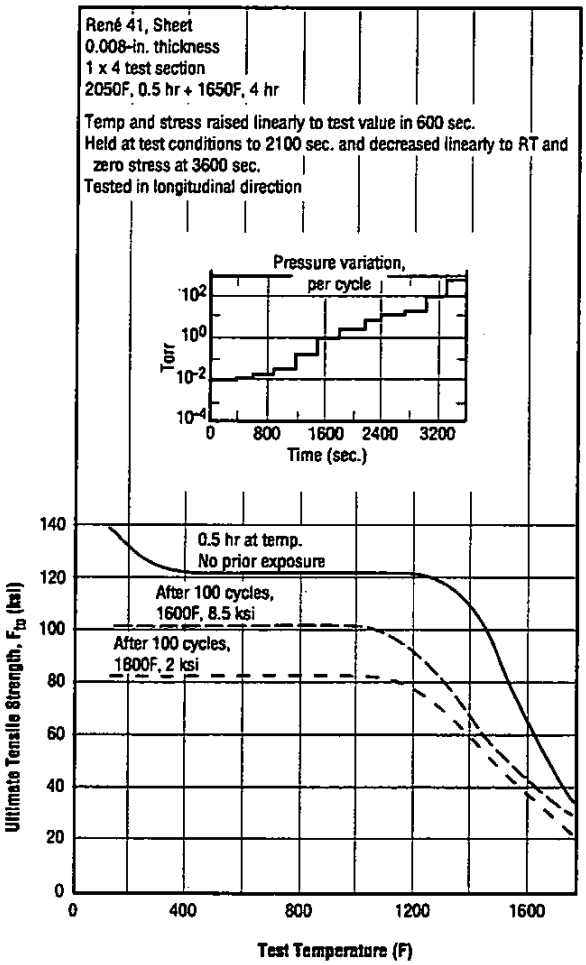

Fig. 3.3.1.21 Effect of exposure to 100 cycles at simulated space shuttle conditions on tensile strength at temperatures to 1800F (Ref. 93)

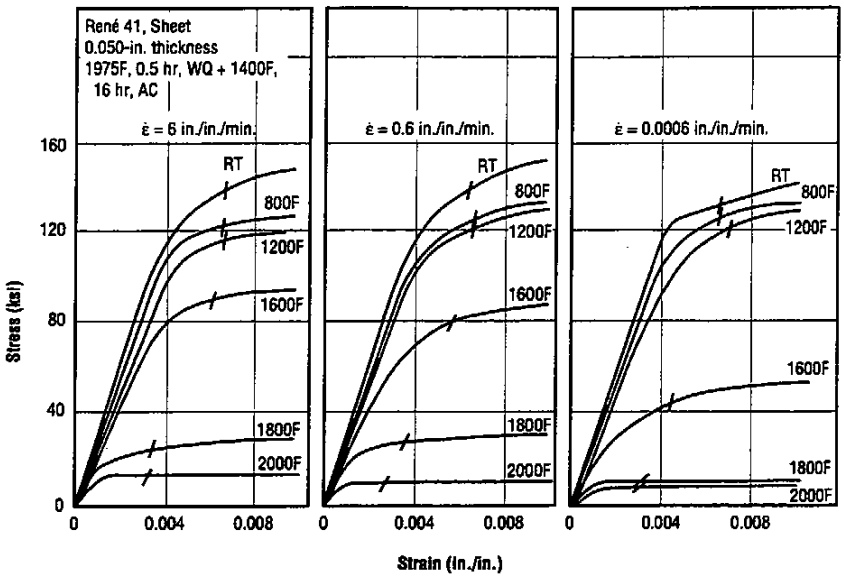

Fig. 3.3.2.1 Compressive stress-strain curves at room and elevated temperatures at several strain rates (Ref. 36)

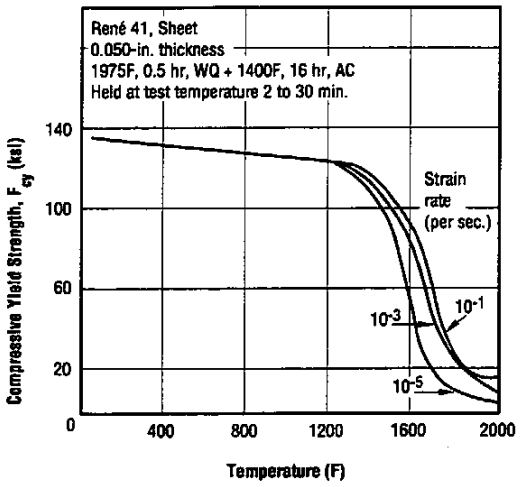

Fig. 3.3.2.2 Effect of strain rate on compressive yield strength of sheet at room and elevated temperatures (Ref. 36)

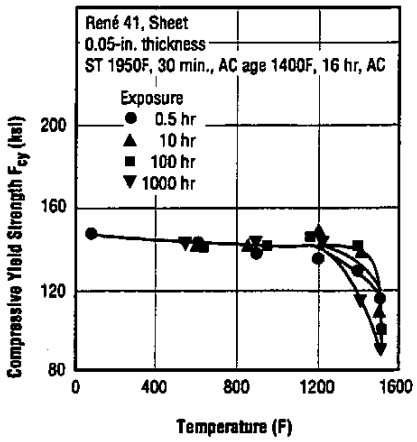

Fig. 3.3.2.3 Effect of exposure time at test temperature on compressive yield strength at room and elevated temperatures (Ref. 29)

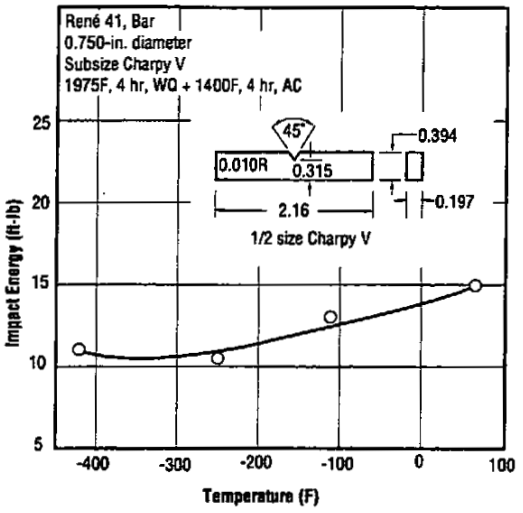

Fig. 3.3.3.1 Effect of low test temperature on Charpy-V impact energy of bar (Refs. 55, 56)

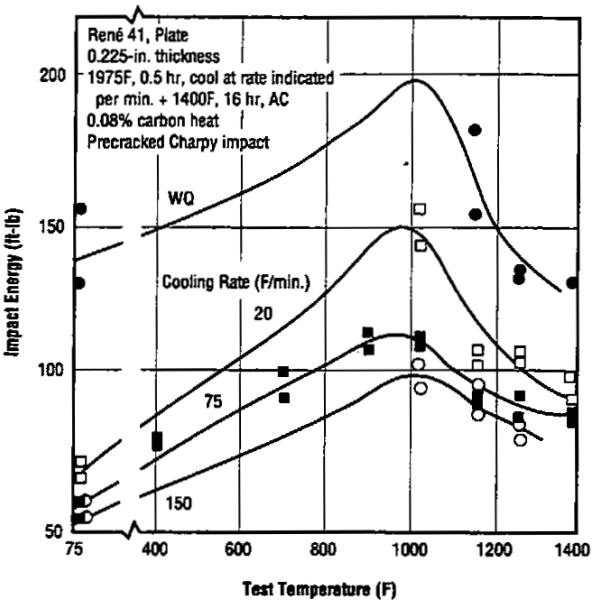

Fig. 3.3.3.2 Effect of cooling rate from solution temperature on impact energy at room and elevated temperatures (Ref. 75)

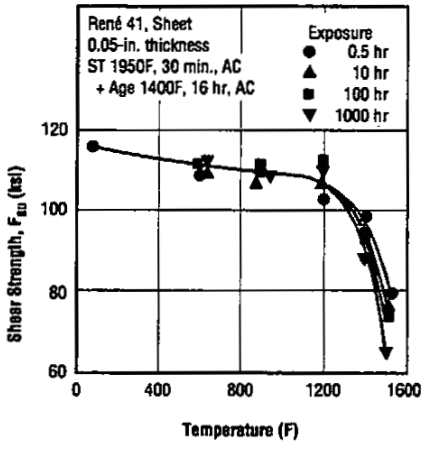

Fig. 3.3.5.1 Effect of exposure time at test temperature on shear strength of sheet at room and elevated temperature (Ref. 29)

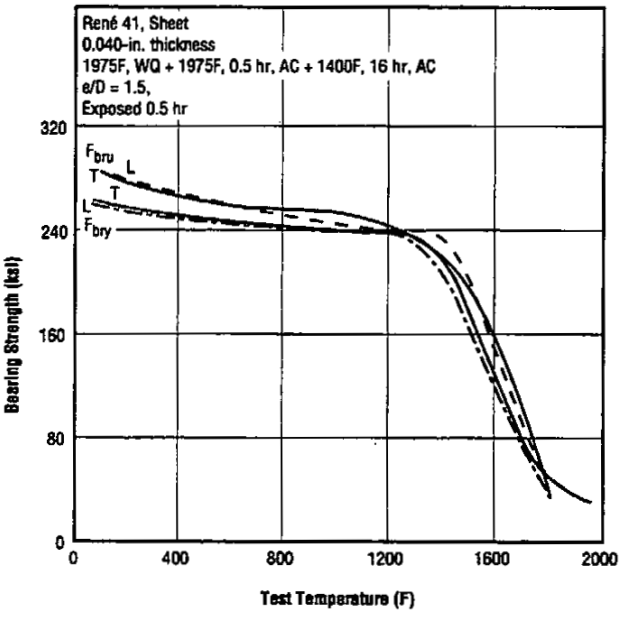

Fig. 3.3.6.1 Effect of test temperature and test direction on bearing strength of 0.040-inch sheet for e/D = 1.5 (Ref. 43)

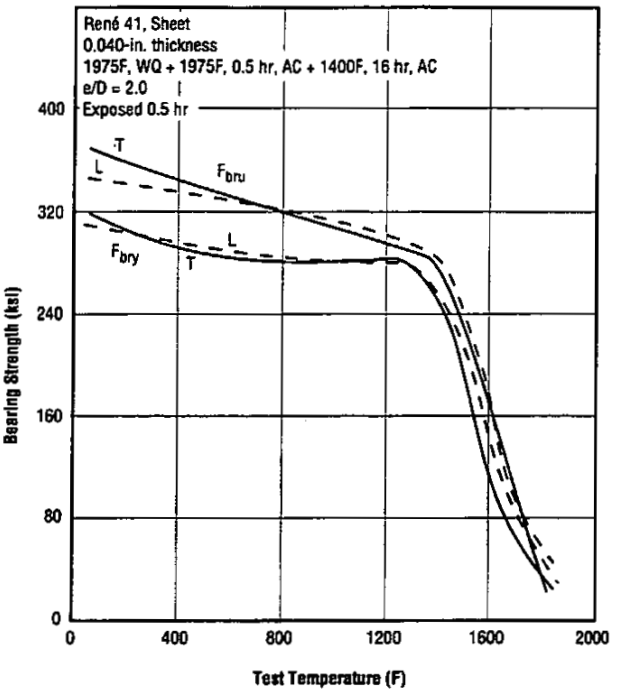

Fig. 3.3.6.2 Effect of test temperature and test direction on bearing strength of 0.040-inch sheet for e/D = 2.0 (Ref. 43)

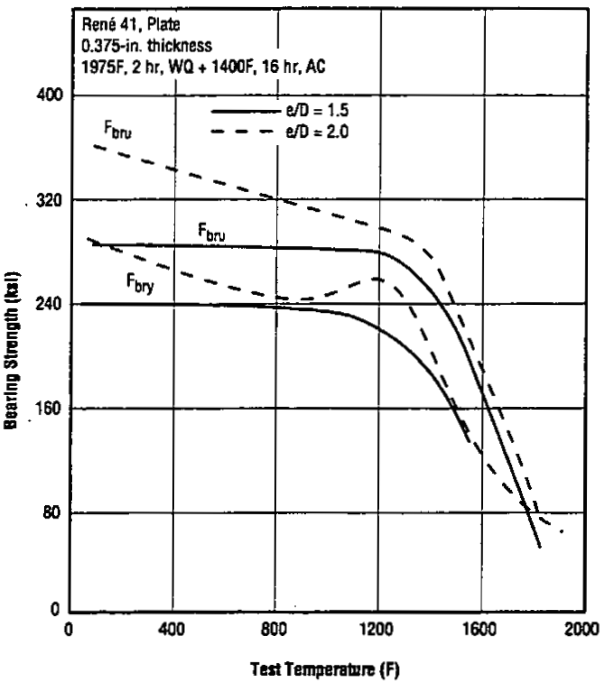

Fig. 3.3.6.3 Effect of test temperature on bearing strength of plate for e/D = 1.5 and 2.0 (Ref. 43)

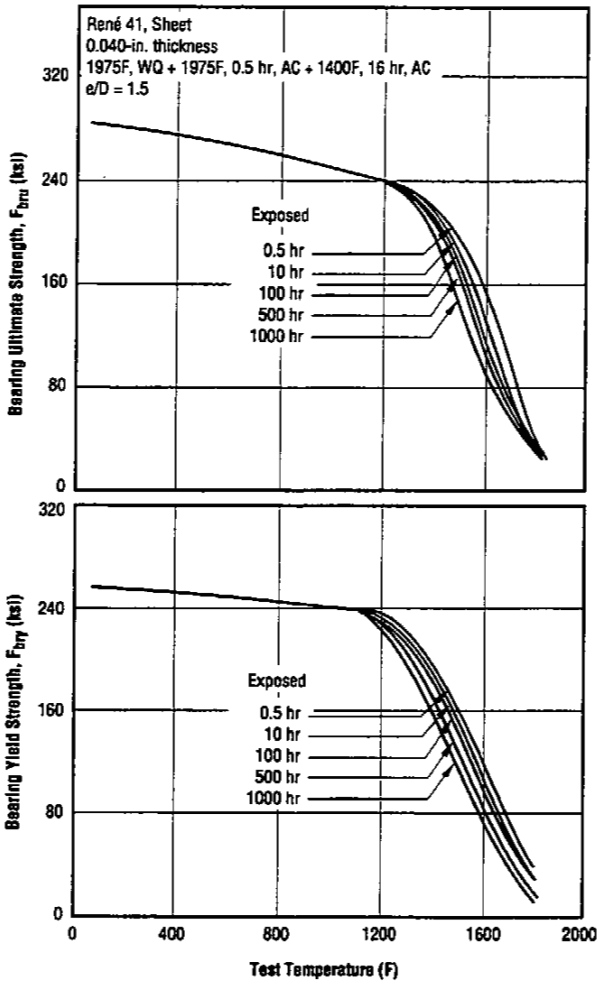

Fig. 3.3.6.4 Effect of test temperature and exposure time at test temperature on bearing strength of 0.040-inch sheet (Ref. 43)

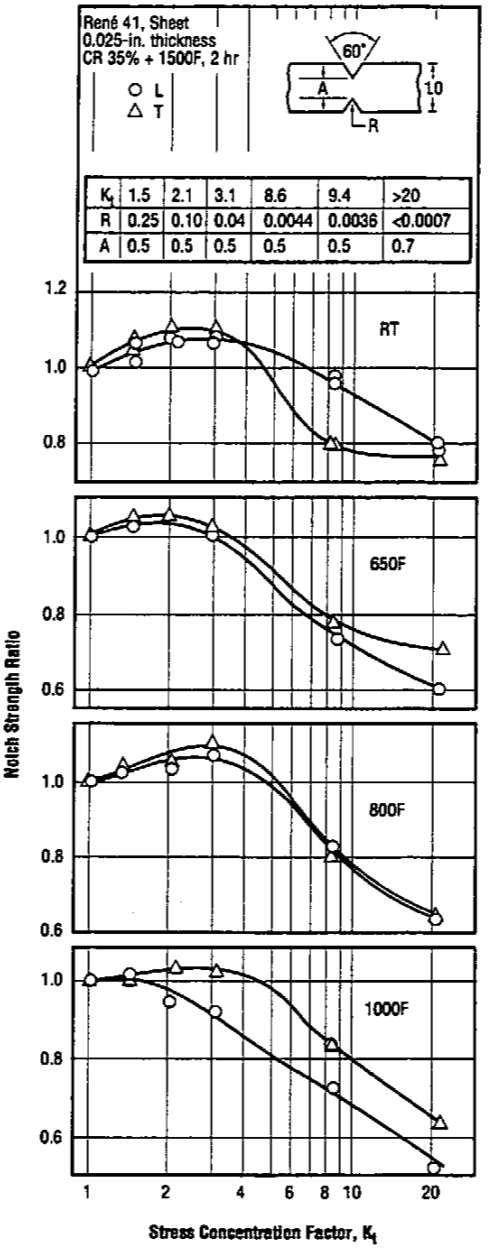

Fig. 3.3.7.1.1 Effect of notch acuity on notch strength ratio of cold rolled and aged sheet at room and elevated temperatures (Ref. 65)

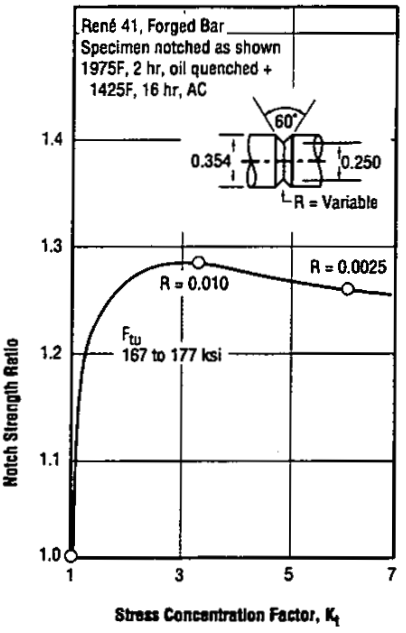

Fig. 3.3.7.1.2 Effect of stress concentration on notch strength ratio at 1000F for forged bar (Ref. 89)

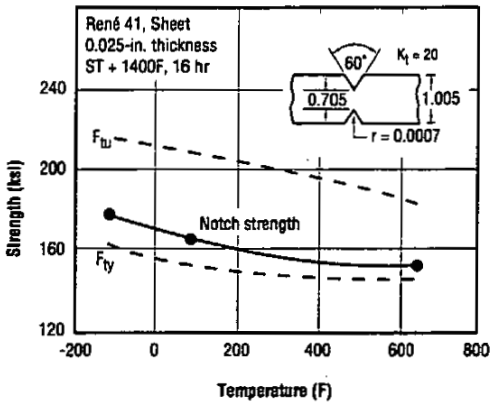

Fig. 3.3.7.1.3 Effect of elevated test temperatures on sharp notch strength of sheet (Ref. 27)

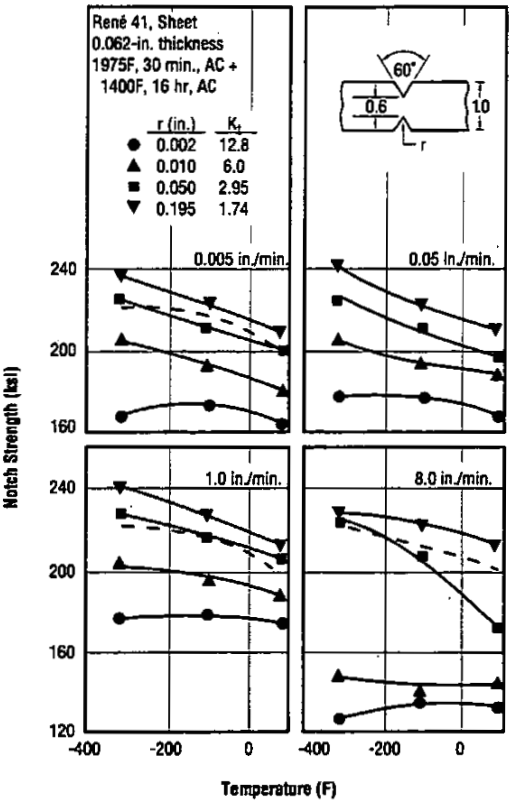

Fig. 3.3.7.1.4 Effect of low temperatures, loading rates and stress concentration factors on notch strength of 0.062-inch sheet in fully heat treated condition (Ref. 35)

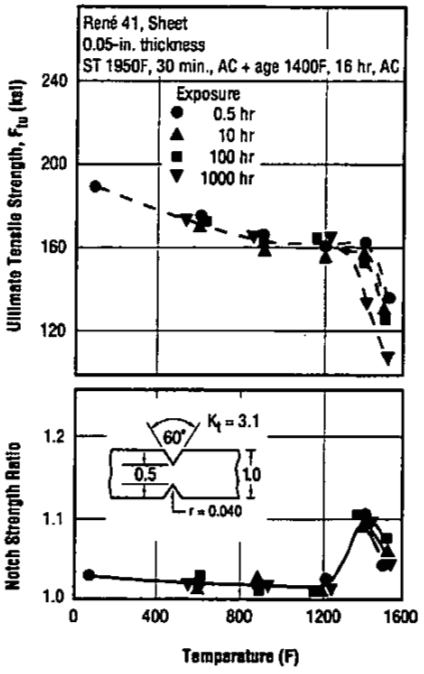

Fig. 3.3.7.1.5 Effect of elevated temperatures and exposure time at test temperature on tensile strength and notch strength ratio of 0.05-inch sheet in fully heat treated condition (Ref. 29)

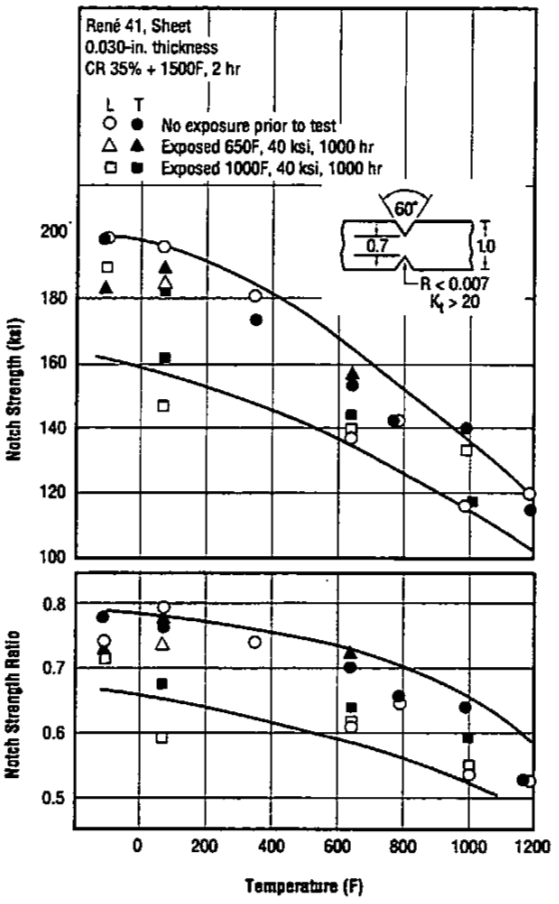

Fig. 3.3.7.1.6 Effect of elevated temperature on notch strength and notch strength ratio of cold worked and aged sheet with and without exposure to stress and temperature (Ref. 54)

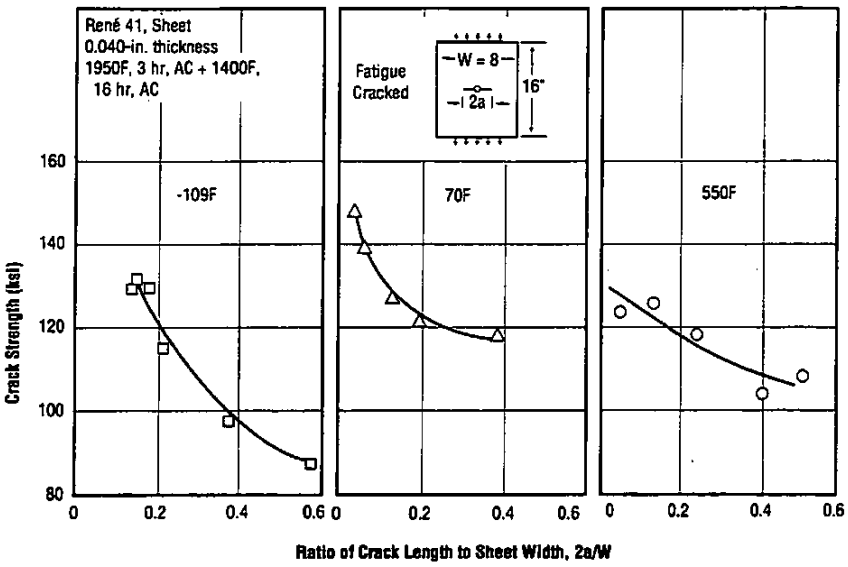

Fig. 3.3.7.1.7 Crack strength of solution treated and aged sheet at -109, 70 and 550F (Ref. 42)

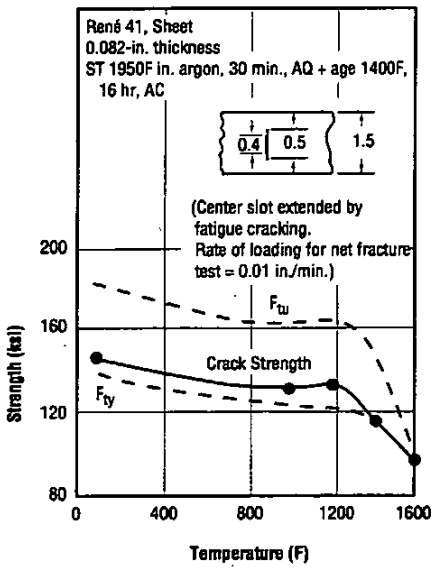

Fig. 3.3.7.1.8 Effect of elevated temperatures on crack strength of fully heat treated 0.082-inch sheet (Ref. 28)

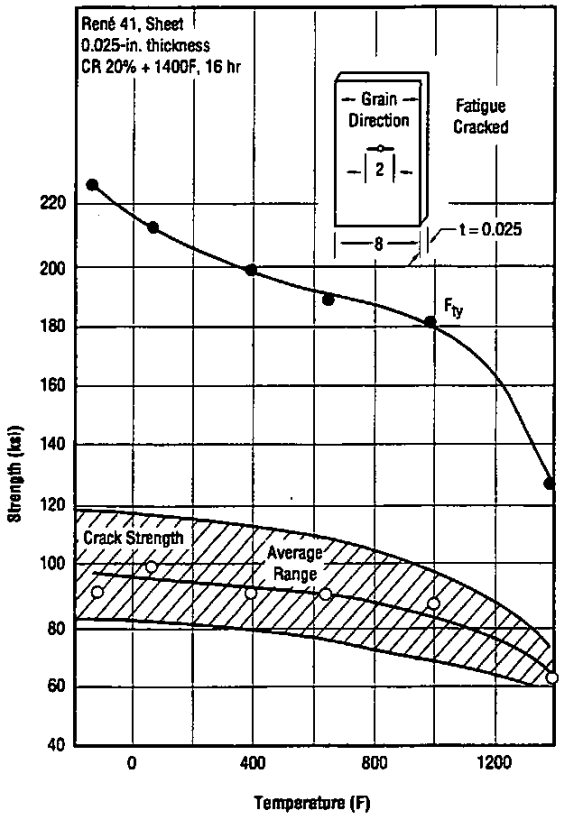

Fig. 3.3.7.1.9 Effect of test temperature on crack strength and yield strength of 0.025-inch sheet in cold rolled and aged condition (Ref. 5)

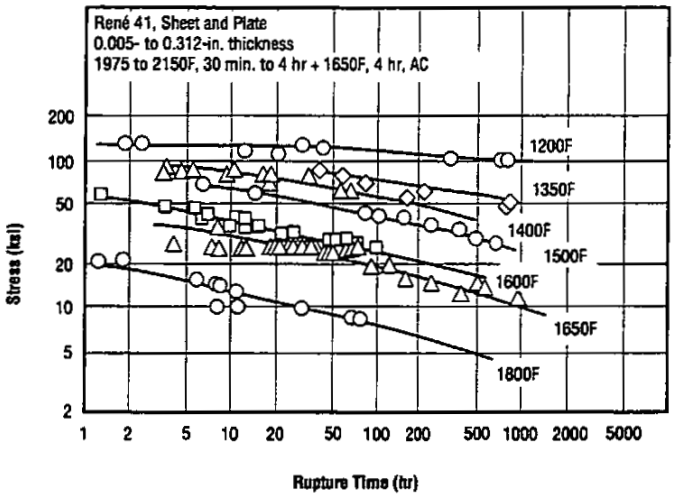

Fig. 3.4.1 Creep rupture properties from 1200 to 1800F of a wide range of thicknesses of sheet and plate tested at several laboratories (Ref. 80)

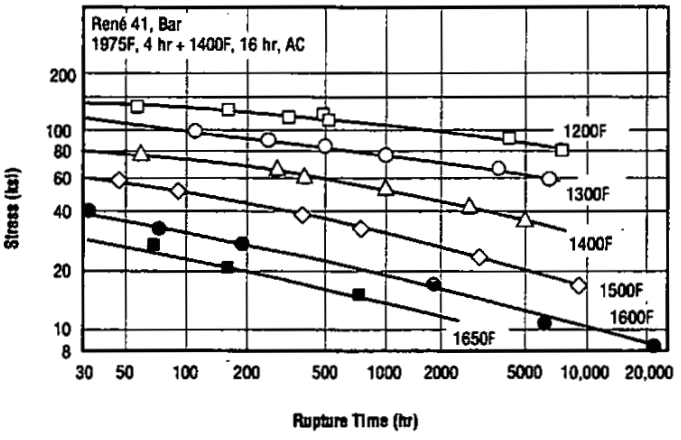

Fig. 3.4.2 Creep rupture properties for bar from 1200 to 1650F (Ref. 73)

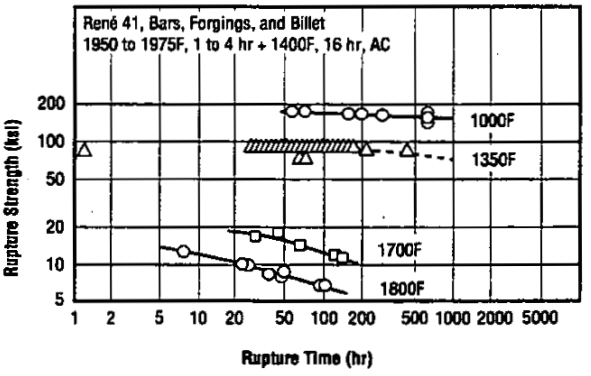

Fig. 3.4.3 Creep rupture properties from 1000 to 1800F of bars, forgings, and billet tested at several laboratories (Ref. 80)

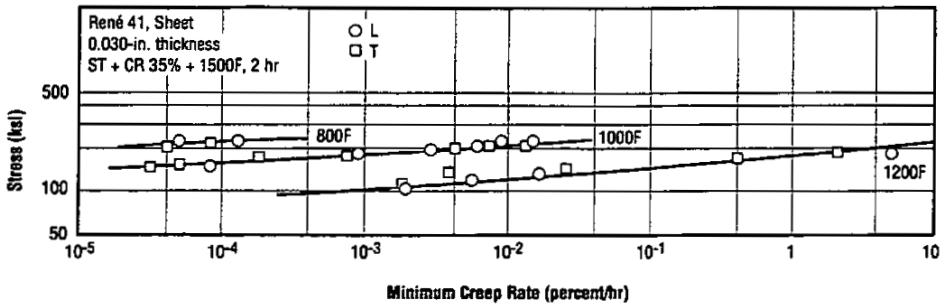

Fig. 3.4.4 Effect of stress and temperature on minimum creep rate of cold rolled and aged sheet (Ref. 69)

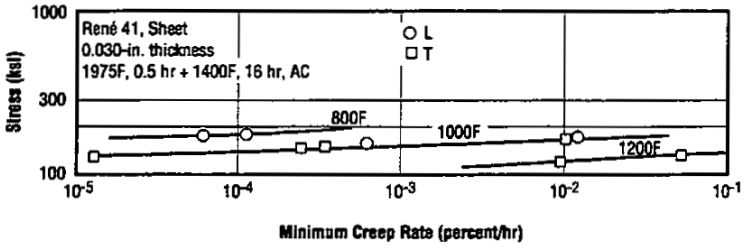

Fig. 3.4.5 Effects of stress and temperature on minimum creep rate of fully heat treated sheet (Ref. 69)

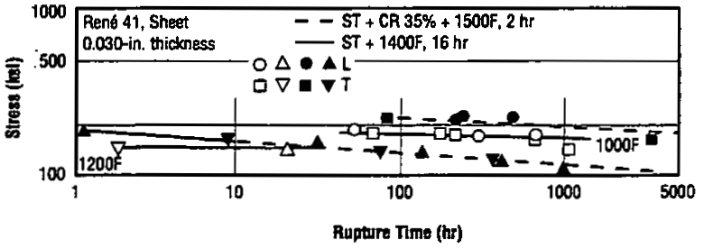

Fig. 3.4.6 Creep rupture curves at 1000 and 1200F for sheet in two conditions (Ref. 69)

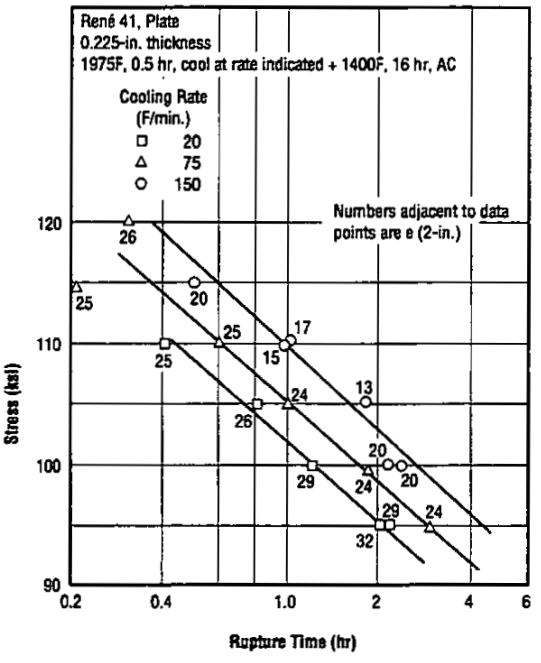

Fig. 3.4.7 Effect of cooling rate from solution treatment temperature on creep rupture properties of plate at 1400F (Ref. 75)

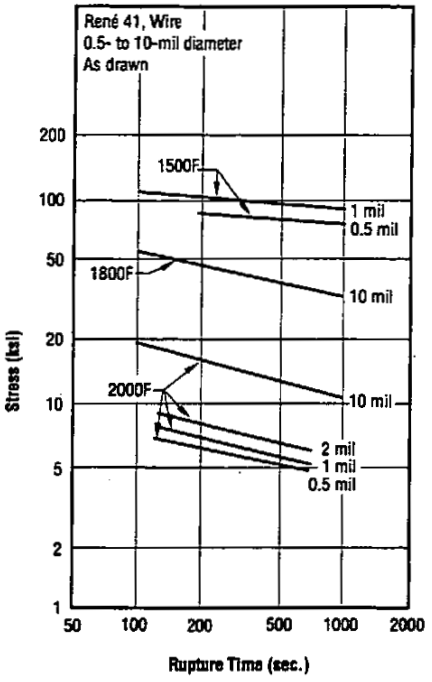

Fig. 3.4.8 Short time creep rupture curves of 0.5- to 10-mil wire from 1500 to 2000F (Ref. 83)

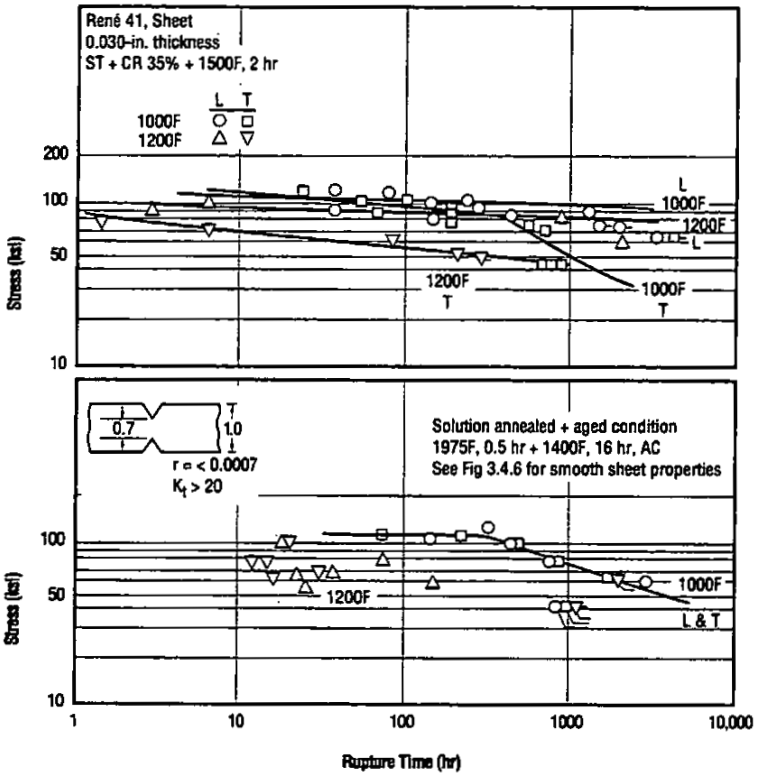

Fig. 3.4.9 Creep-rupture curves for sharp notched sheet in annealed and in cold rolled and aged conditions (Ref. 69)

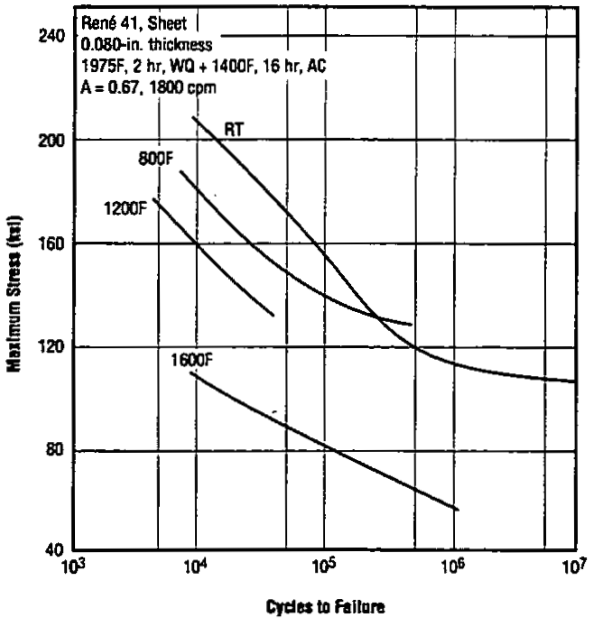

Fig. 3.5.1.1 Axial fatigue behavior of sheet at room and elevated temperatures (Ref. 43)

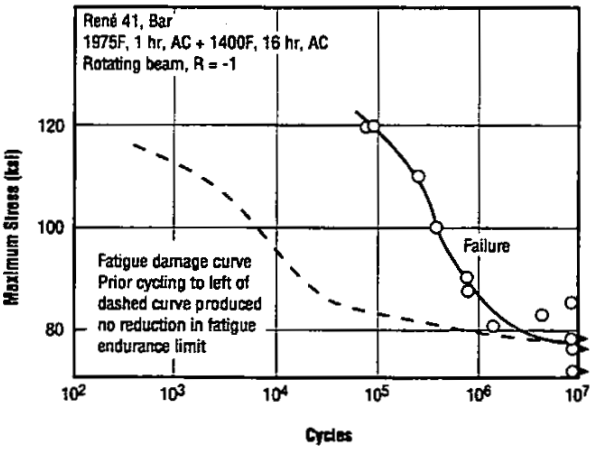

Fig. 3.5.1.2 Rotating beam bending fatigue behavior of bar at room temperature (Ref. 64)

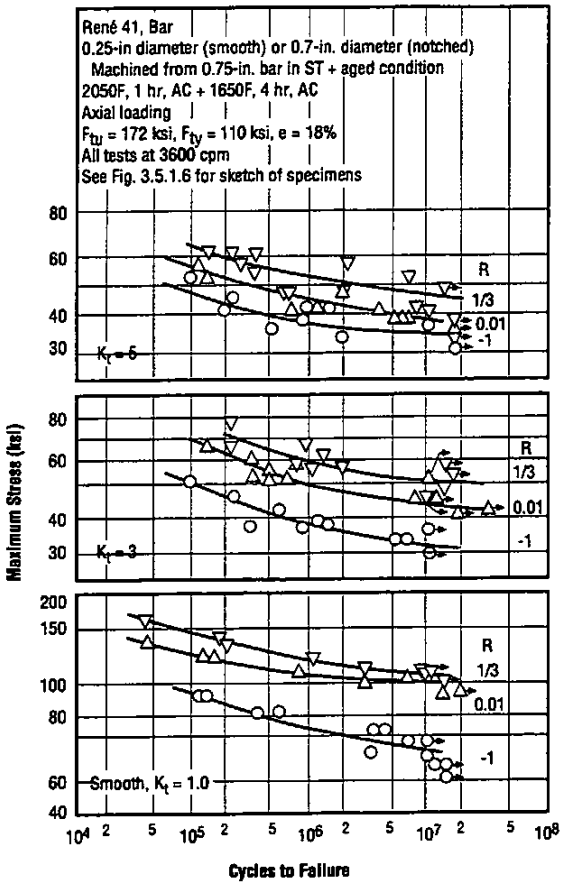

Fig. 3.5.1.3 Effects of notches and R ratio on axial fatigue behavior of bar at room temperature (Ref. 81)

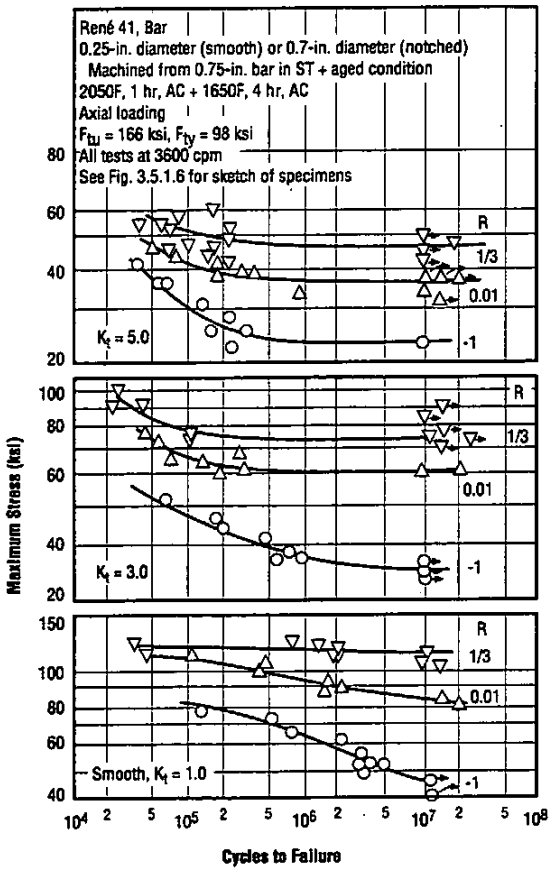

Fig. 3.5.1.4 Effects of notches and R ratio on axial fatigue behavior of bar at 1200F (Ref. 81)

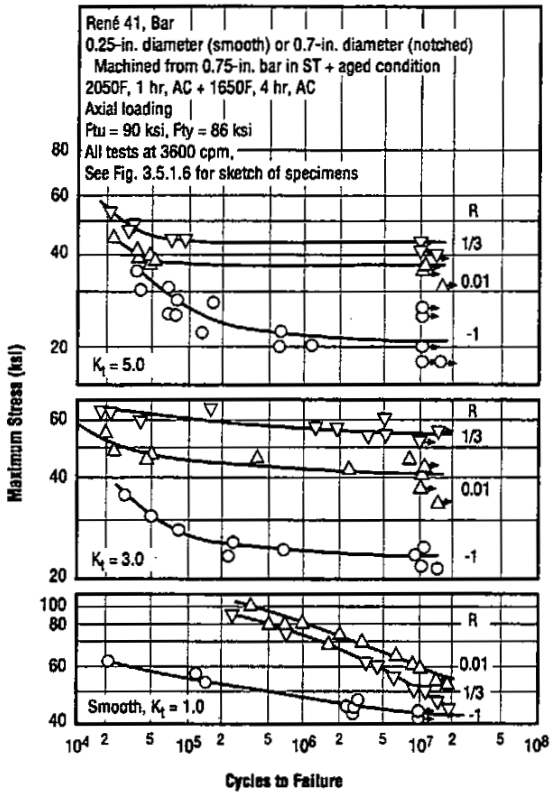

Fig. 3.5.1.5 Effects of notches and R ratio on axial fatigue behavior of bar at 1600F (Ref. 81)

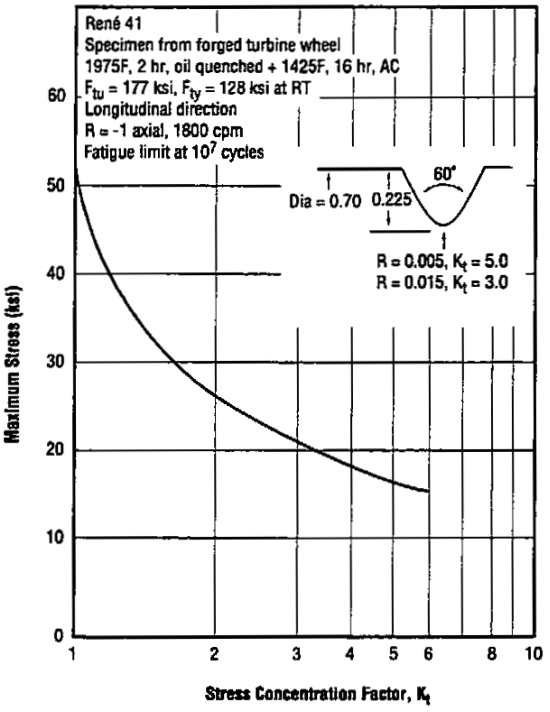

Fig. 3.5.1.6 Effect of stress concentration factor on fatigue limit at 10^7 cycles for forged turbine wheel specimen (Ref. 89)

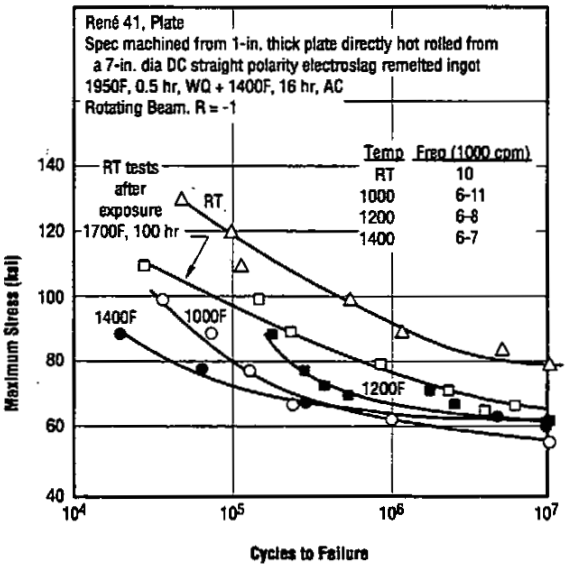

Fig. 3.5.1.7 Rotating beam fatigue behavior at room and elevated temperatures of plate fabricated from a DC electroslag remelted ingot (Ref. 104)

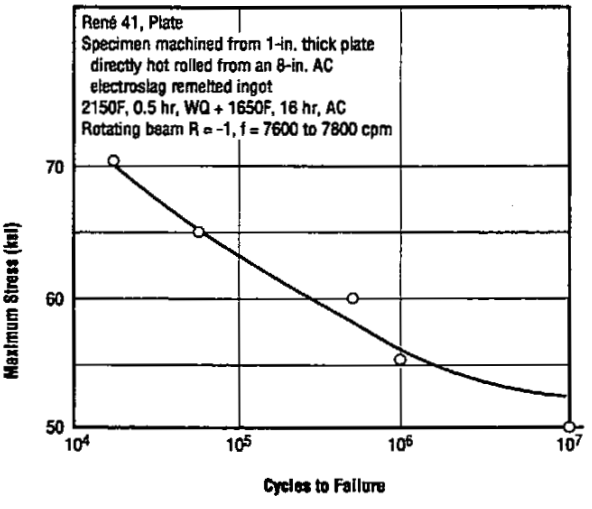

Fig. 3.5.1.8 Rotating beam fatigue behavior at 1400F of plate fabricated from an AC electroslag remelted ingot (Ref. 104)

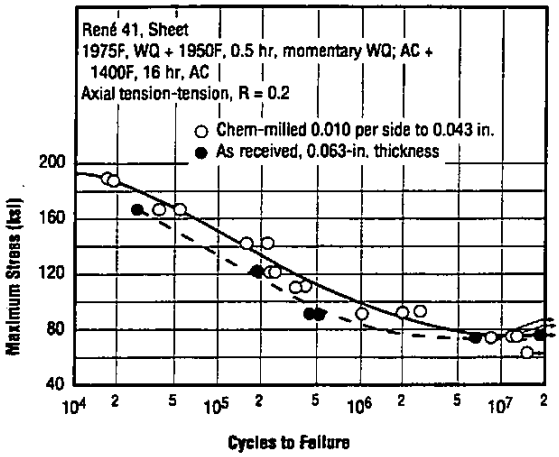

Fig. 3.5.1.9 Effects of chemical milling on axial fatigue behavior of sheet at room temperature (Ref. 85)

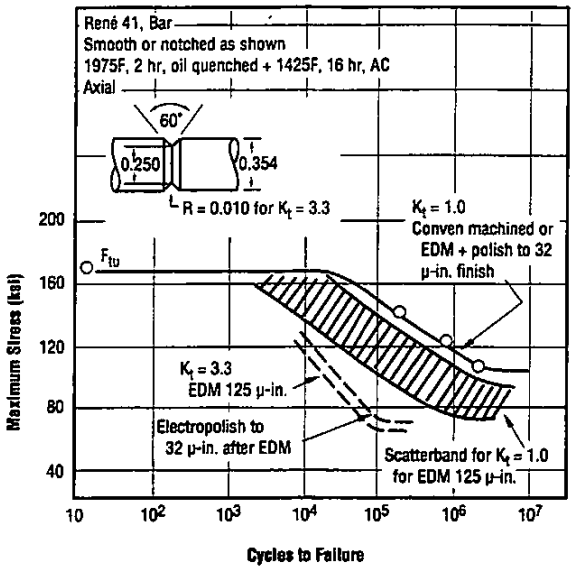

Fig. 3.5.1.10 Effect of electro-discharge machining and electro-polishing on axial fatigue behavior of smooth and notched bar at room temperature (Ref. 89)

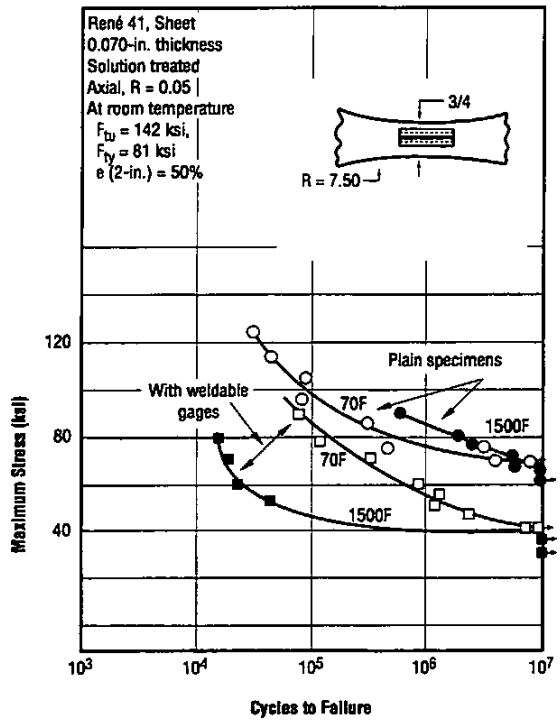

Fig. 3.5.1.11 Effect of spot welds simulating weldable strain gages on axial fatigue behavior of sheet at 70 and 1500F (Ref. 110)

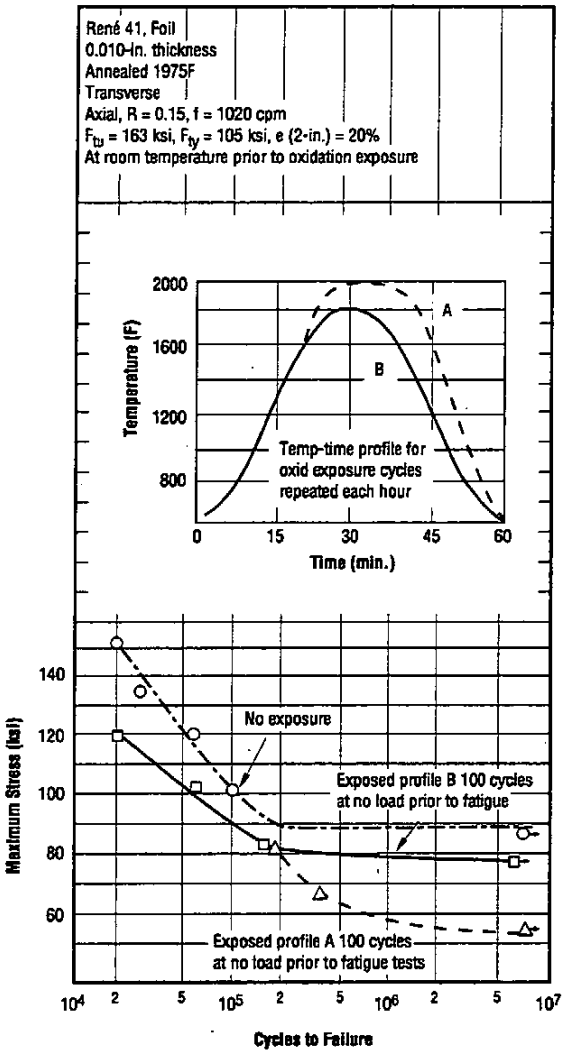

Fig. 3.5.1.12 Axial fatigue properties of foil at room temperature after exposure to oxidation at 1800 or 2000F (Ref. 86)

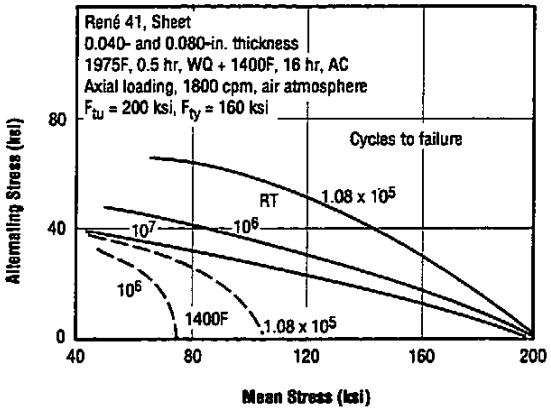

Fig. 3.5.1.13 Stress range diagram for axial fatigue of sheet at room temperature and 1400F (Ref. 43)

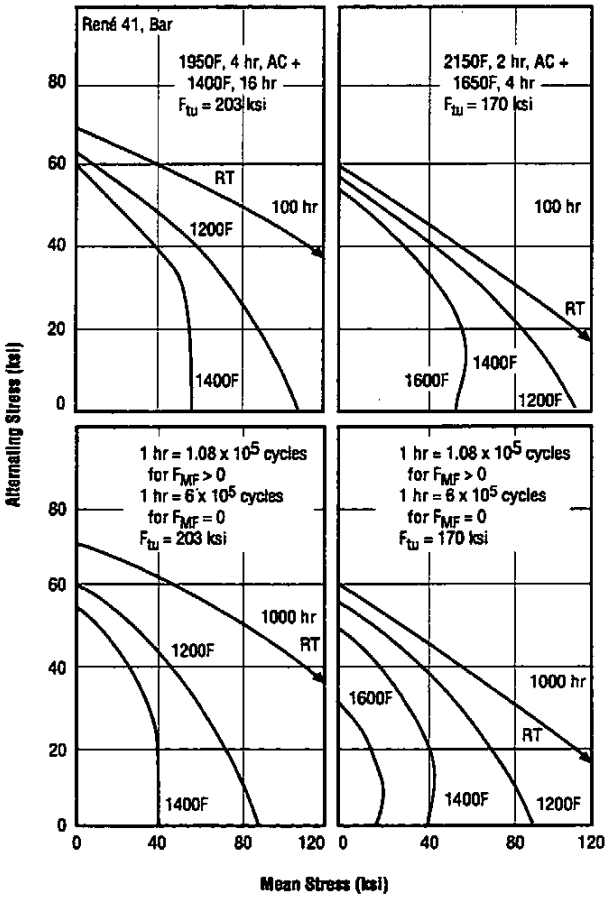

Fig. 3.5.1.14 Stress range diagrams for axial fatigue of bar at room and elevated temperatures (Ref. 8)

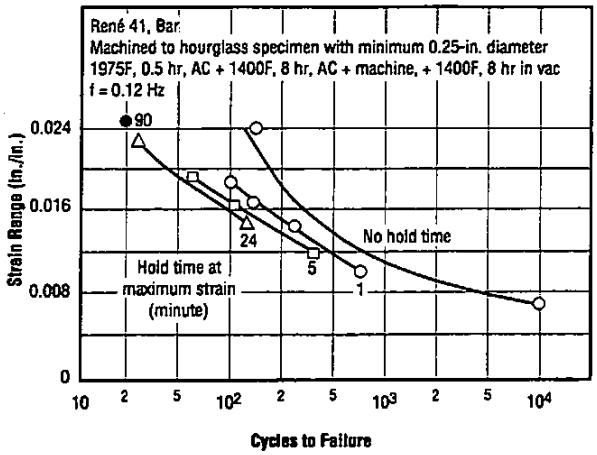

Fig. 3.5.2.1 Effect of hold-time at peak strain on low cycle fatigue behavior at 1400F (Ref. 88)

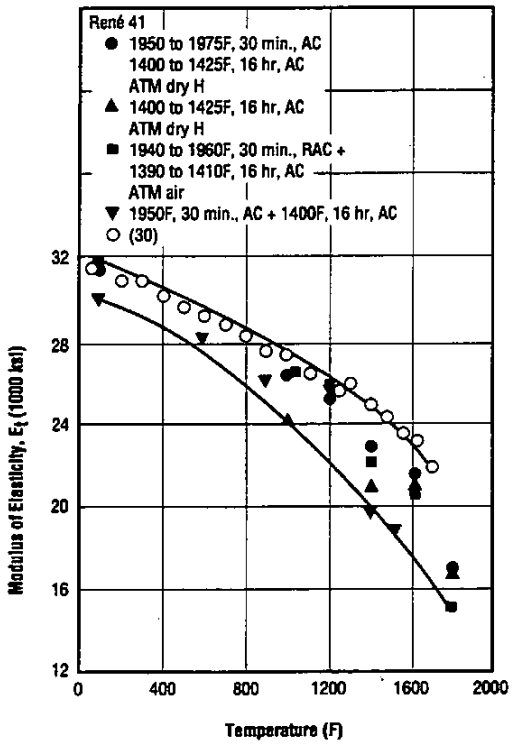

Fig. 3.6.2.1 Tensile modulus of elasticity at room and elevated temperatures (Refs. 24, 29, 30)

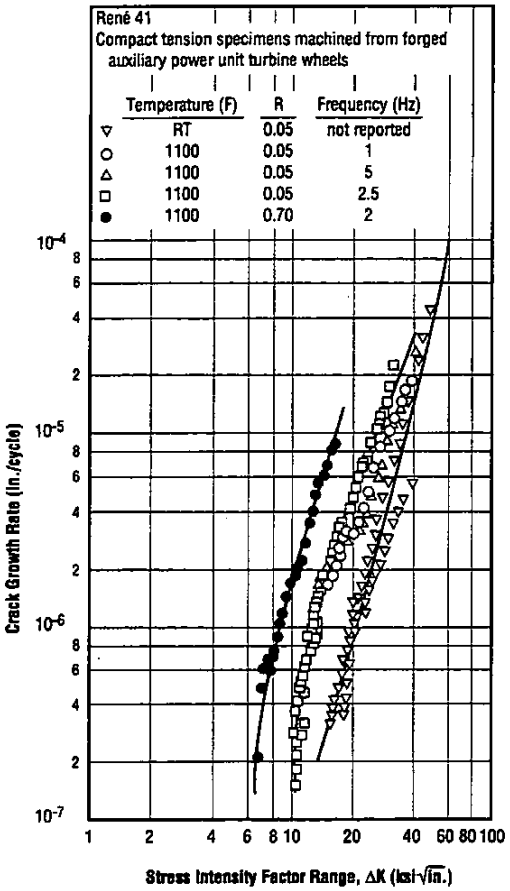

Fig. 3.5.3.1 Effects of temperature, stress ratio, and frequency on low-cycle fatigue crack growth rates of forged alloy in air (Ref. 124)

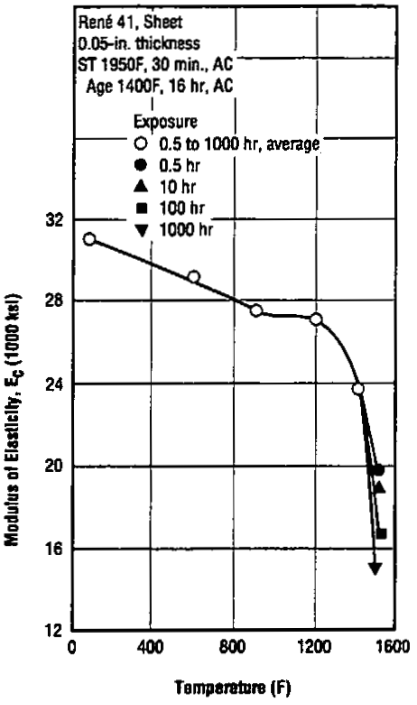

Fig. 3.6.2.2 Compressive modulus of elasticity at room and elevated temperatures (Ref. 29)

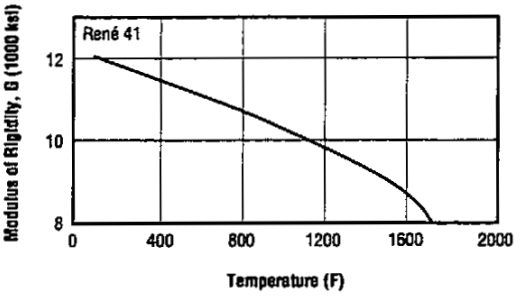

Fig. 3.6.3.1 Modulus of rigidity at room and elevated temperatures (Ref. 9)

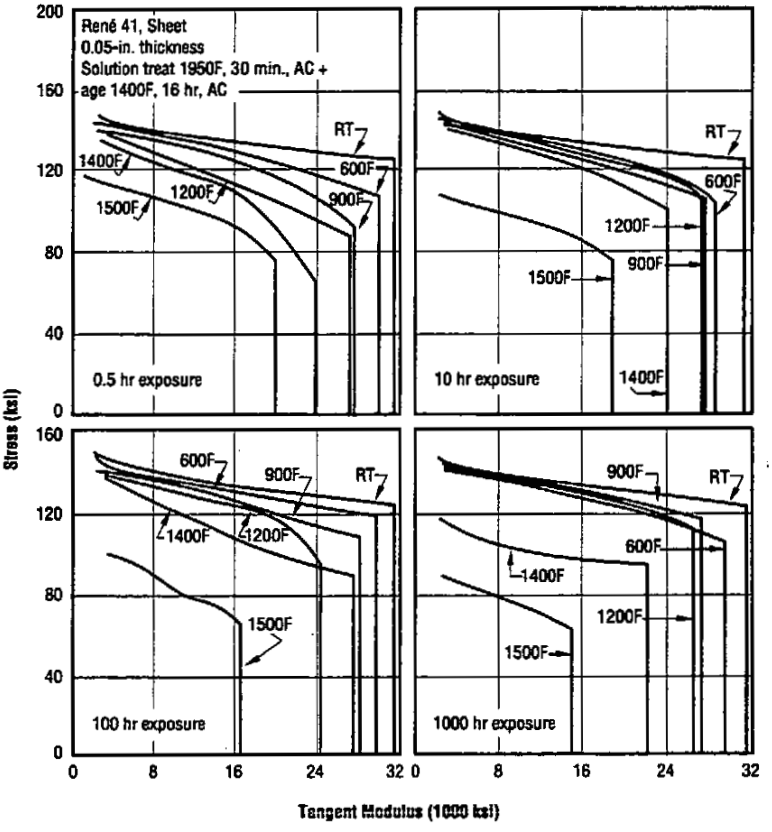

Fig. 3.6.4.1 Tangent modulus curves in compression for various test temperatures and exposure times (Ref. 29)

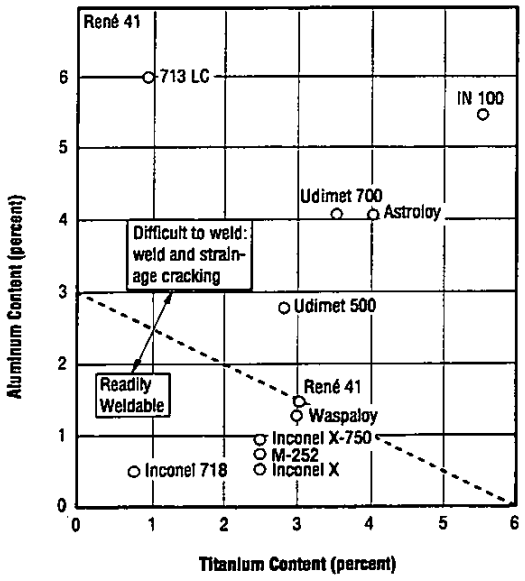

Fig. 4.3.1.1 Weldability of gamma-prime strengthened superalloys (Ref. 133)

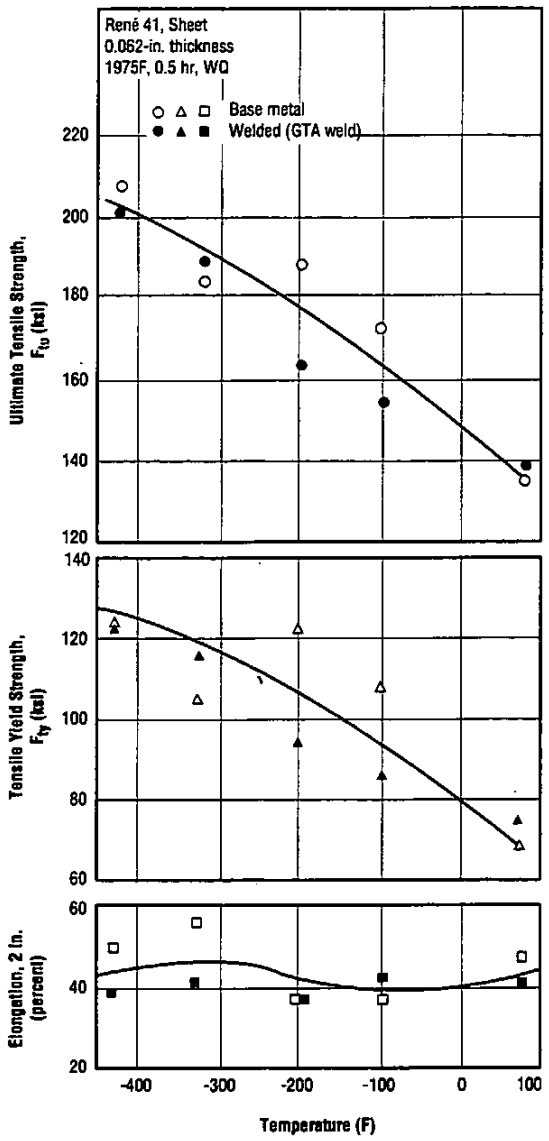

Fig. 4.3.1.2 Tensile properties at room and low temperatureof solution treated sheet with and without GTA weld (Refs. 49, 60)

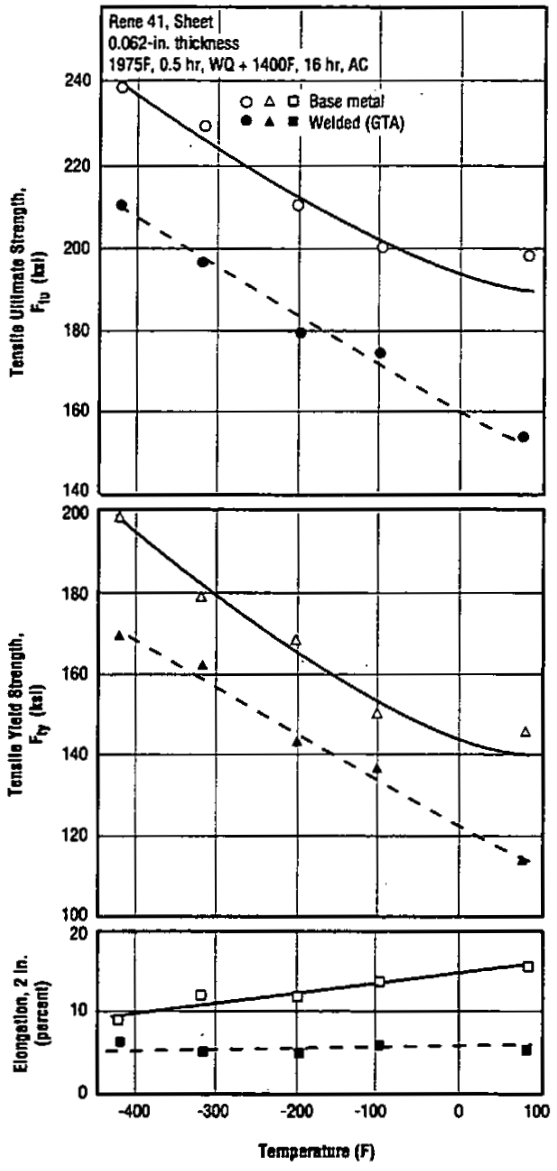

Fig. 4.3.1.3 Tensile properties at room and low temperature of solution treated and aged sheet with and without GTA weld (Ref. 49)

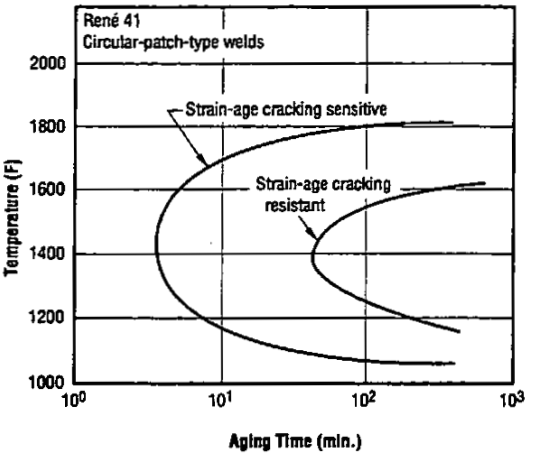

Fig. 4.3.1.4 Time-temperature relationships for isothermal strain-age weld cracking in crack-sensitive and crack-resistant heats of Rene' 41 (Ref. 133)

References

1. AMS 5545C, Society of Automotive Engineers (July 1991).
2. AMS 5712F, Society of Automotive Engineers (July 1989).
3. AMS 5713F, Society of Automotive Engineers (July 1989).
4. AMS 5800D, Society of Automotive Engineers (January 1992).
5. Cannon-Muskegon Corp., "The Alloy Specialist Series, No. 86, X René 41."
6. General Electric Company, "René 41," GE Spec. BS0T44 (January 27, 1958).
7. Pennington, W. J., "Experimental Hardness Results on 1-inch Diameter Bar Stock of René 41," Universal-Cyclops Steel Corp., Research Memo No. 34, Project 504 (May 12, 1958).
8. General Electric Company, "Engineering Data," VM-107, René 41 (May 1958).
9. Utica Metals (1958).
10. Utica Metals (1958).
11. General Electric Company, Data Sheets, A4012220-381 RI (May 6, 1958), A4012220-172 RI (July 16, 1957), A4012220-379 (April 3, 1958), A4012220-380 (April 4, 1958), A4012220-450 (September 30, 1958), A4012220-449 (September 30, 1958).
12. General Electric Company, Data Sheets, A4012220-393 (April 10, 1958), A4012220-392 (April 10, 1958), A4012220-394 (April 17, 1958), A4012220-388 (April 9, 1958), A4012220-389 (April 9, 1958), A4012220-390 RI (July 23, 1958), A4012220-391 (April 9, 1958).
13. General Electric Company, Data Sheet, A4012220-418 (May 10, 1958).
14. Stewart, D. A., "Evaluation of Practical Machinability Limits of René 41," Technical Information Series No. R58ACT212, General Electric Company (June 16, 1958).
15. Wyman-Gordon Company, Data Sheet (January 19, 1959).
16. North American Aviation Inc., "Thermal Conductivity and Surface Emissivity of the René 41 Sandwich Used for Engine Shrouds," Report No. Na-60-1451 of Compilation of NAA Inc. Unpublished Materials Data Phase I (December 1960).
17. Northrop Corporation, Norair Division, "The Determination of Spectral Emissivities, Reflectivities, and Absorptivities of Materials and Coatings," Report No. Nor-61-589 (August 3, 1961).
18. Haynes Stellite Company, "Sales Alloy Manual, Haynes Alloy No. R-41, Vacuum - Melted," (February 22, 1961).
19. Fieldhouse, H. B., and Long, J. I., "Measurement of Thermal Properties," WADD-TR-60-904 (July 1961).
20. General Dynamics, "Properties of R-41 Sheet, 'A Vacuum Melted Nickel Base Alloy'," Report MRG-164 of Report AE 62-0138-3 Compilation of Materials Research Data, 4th Quarterly Progress Report - Phase I (March 1962).
21. Republic Aviation Corporation, "Mechanical Properties of René 41 from Compilation of Unpublished Materials Information," 2nd Quarterly Report (October 1961).
22. Republic Aviation Corporation, "Mechanical Properties of René 41 from Compilation of Unpublished Materials Information," 4th Quarterly Report (March 1962).
23. McDonnell Aircraft Corporation, "Unpublished Materials Research and Development Programs," 1st Quarterly Progress Report, Report 8743, Volume V (April 10, 1962).
24. Bell Aerosystem Company, "Mechanical Properties of René 41 Sheet Materials," Report No. BLR 61-21 (M) (June 29, 1962).
25. The Marquardt Corporation, "Tensile and Creep Properties of 0.010 and 0.050 Inch René 41 Alloy Sheet from Room Temperature to 2000F," Report PR 281-1Q-1 (September 12, 1962).
26. McBride, J. G.; Milhern, B.; and Widmer, R., "Creep Rupture Properties of Six Elevated Temperature Alloys," WADD-TR-61-199 (August 1962).
27. Espey, G. B.; Bubsey, R. T.; and Brown, W. F., Jr., "A Preliminary Report of the NASA Sheet Alloy Screening Program for Mach III Transport Skins," *Proc ASTM*, Volume 62, pp. 837-868 (1962).
28. Southern Research Institute, "An Investigation of the Crack Propagation Resistance of High Strength Alloys and Heat-Resistant Alloys," (November 23, 1961).
29 Lemcoe, M. M., and Trevins, A. Jr., "Determination of the Effects of Elevated Temperature Materials Properties of Several High Temperature Alloys," ASD-TDR-61-529 (June 1962).
30. American Iron and Steel Institute, "High Temperature High Strength Alloys," (February 1963).
31. Lund, C. H., "Physical Metallurgy of Nickel Base Superalloys," DMIC Report 153 (May 5, 1961).
32. Jacobs, F., "Mechanical Properties of Materials Fabricated by Shear Forming," ASD-TDR-67-830 (February 1963).

33. Lepkowski, W. J., and Monroe, R. E., "The Welding and Brazing of Certain Cobalt Containing Alloys," Cobalt Information Center - Cobalt (June 1963).

34. "The Welding of Wrought Age-Hardenable Nickel Base Alloys for Service at Elevated Temperatures," DMIC Memo-38 (November 25, 1959).

35. Busbane, A. W., "The Investigation of the Effects of Loading Rate and Stress Concentration Factors on the Notch Properties of Three Sheet Alloys at Subzero Temperatures," ASD-TDR-62-930 (March 1963).

36. Dioguardo, P. R., and Lloyd, R. D., "Investigation of the Effects of Rapid Loading and Elevated Temperatures on the Mechanical Properties of Compressive and Column Members," ASD-TR-62-199 (January 1962).

37. Strohecker, D. E.; Bryrer, T. G.; Gerds, A. F.; Gehrke, J. H.; and Boulger, F. W., "Deformation Processing of Nickel Base and Cobalt Base Alloys," NASA TMX-53439 (April 18, 1966).

38. Wood, W. W., et al, "Final Report on Sheet Metal Forming Technology," Volumes I and II (Chance Vought) ASD-TDR-637-871 (July, 1963).

39. Wood, W. W., et al, "Theoretical Formability," Volumes I and II, ASD-TR-61-191 (August 1961).

40. Norwood, D. L., "Sheet Formability at Ambient Temperatures," *ASM Metals Engineering Quarterly*, Volume 5, No. 1, pp. 41-51 (February 1965).

41. Wood, W. W., et al, "Final Report on Advanced Theoretical Formability Manufacturing Technology," Volumes I and II, AFML-TR-64-411 (January 1965).

42. Figge, I. E., "Residual Static Strength of Several Titanium and Stainless Steel Alloys and One Superalloy at -109F, 70F and 550F," NASA TN D-2045 (December 1963).

43. Greene, A.; Sieber, H.; Wells, D.; and Wolfe, T., "Research Investigation to Determine Mechanical Properties of Nickel and Cobalt Base Alloys for Inclusion in Military Handbook-5," Volume I, ML-TDR-64-116 (October 1964),

44. Schweikert, W. H., "Properties and Characteristics of a New High Strength, Nickel Base Alloy," *Foundry* Volume 82, No. 3, pp. 128-230 (December 1961).

45. Kura, J. G., et al, "The Making of Nickel and Nickel-Base Alloy Shapes by Casting, Powder Metallurgy, Electroforming, Chemical Vapor Deposition, and Metal Spraying," NASA TMX-53430 (October 1965).

46. Stroup, J. P., and Pugliese, L. A., "How Low Carbon Contents Affect Superalloys," *Metal Progress*, pp. 96-100 (February 1968).

47. Slunder, C. J., and Hall, A. M., "Thermal and Mechanical Treatments for Nickel and Selected Nickel Base Alloys and Their Effect on Mechanical Properties," NASA TMX-53443 (April 1966).

48. *Metals Handbook*, "Heat Treating on Heat Resisting Alloys," Volume II, pp. 257-268.

49. Stratton, W. K., et al, "Advances in the Materials Technology Resulting from X-20 Program," AFML-TR-64-396 (March 1965).

50. Lacy, C. C., and Albertin, L., "How to Heat Treat Space Age Materials," *Metals Progress*, Volume 83, pp. 69-95 (1963).

51. Union Carbide Corporation, Stellite Division, "Haynes Alloy René 41," (July 1960).

52. Dreshfield, R. L., "The Effect of Refractory Elements on the Stability of Complex Carbides in Nickel Base Alloys," *ASM Trans Quarterly*, Volume 61, No. 2, pp. 352, 353 (June 1968)

53. Douglas Aircraft Company, "Notch Resistance and Fracture Toughness Characteristics of High Strength Metals," ASD-TDR-63-494 (September 1963).

54. Raring, R. H.; Freeman, J. W.; Schultz, J. W.; and Voorhess, H. R., "Progress Report of the NASA Special Committee on Materials Research for Supersonic Transports," NASA TN D1798 (May 1963).

55. Schwartzberg, F. R.; Osgood, S. H.; Keys, R. D.; and Kieffer, T. F., "Cryogenic Materials Data Handbook," Air Force Materials Laboratory Report ML-TDR-64-280 (August 1964).

56. Warren, K. A., and Reed, R. P., "Tensile and Impact Properties of Selected Materials from 20 to 300 degrees K," *Monograph 63, NBS* (June 1963).

57. Christian, J. L., and Hurlick, A., "Physical and Mechanical Properties of Pressure Vessel Materials for Application in Cryogenic Environment," ASD-TDR-62-258, Part II, General Dynamics/Astronautics (April 1963).

58. Watson, J. F., and Christian, J. L., "Low Temperature Properties of K-Monel, Inconel X, René 41, Haynes 25, and Hastalloy B Sheet Alloys," Paper 61-WA-12 ASME (1962).

59. Miller, P. C., "Low Temperature Mechanical Properties of René 41 Alloy and its Weldments," IN-P and VE-M-62-6, Marshall Space Flight Center, NASA (1962).

60. Martin, H. L.; Imgram, A. G.; and Lyman, W. S., "Effects of Low Temperatures on Structural Metals," NASA SP-5012 (December 1964).

61. Collins, H. E., and Quigg, R. J., "Carbide and Intermetallic Instability in Advanced Nickel Base Alloys," paper presented at ASM National Meeting, Cleveland, OH (October 1967).

62. Brownfield, C. D., and Apodaca, D. R., "Effects of Severe Thermal Stress Histories on Material Strength Rate Process Theory Approach, AISI 301 Extra Hard, PH 15-7 Mo RH, René 41 7075-T6," ASD-TR-61-194 (January 1962).

63. Thompson, O. N., and Jones, R. L., "Intermittent Creep and Stability of Materials for SST Application," AFML-TR-66-407.

64. Mehra, V.; Mogul, J.; and Slepitis, J., "Low Cycle Fatigue of Advanced Engine Materials," SAE Preprint No. 670336 (April 1967).

65. Schultz, J. W.; Cullen, T. M.; and Freeman, J. W., "Influence of Notch Acuity on the Notch Strength of René 41, Waspaloy, and D979," University of Michigan Report No. 04368-7-T (March 1963).

66. Douglas Aircraft Company, "Chloride Stress Corrosion Susceptibility of High Strength Stainless Steel, Titanium Alloy, and Superalloy Sheet," ML-TDR-64-44, Volume II (May 1964).

67. Espey, G. B.; Bubsey, R. T.; and Brown, W. F., Jr., "A Preliminary Report on the NASA Sheet Alloy Screening Programs for Mach III Transport Skins," *Proc ASTM*, Volume 62, pp. 837-869 (1962).

68. Honeycutt, J. O., and Wilhelm, A. C., "Effect of Protective Coatings on the Stress Corrosion Properties of Supersonic Transport Skin Materials," Twelfth Quarterly Status Report to NASA on Contract No. NASr-117, by Southern Research Institute (September 1, 1965 to November 30, 1965).

69. Cullen, T. M., and Freeman, J. W., "The Mechanical Properties at 800, 1000 and 1200F of Two Superalloys Under Consideration for Use in the Supersonic Transport," NASA CR-92 (September 1964).

70. Christensen, R. H., and Denke, P. H., "Crack Strength and Crack Propagation Characteristics of High Strength Metals," ASD-TR-61-207 (January 1962).

71. Rowe, J. P., and Freeman, J. W., "Evaluation of Effects of Aging on Room Temperature Tensile Properties of Cold Worked René 41, A286, D979 and Waspaloy," University of Michigan Report No. 3 on Screening Programs on Superalloys for Trisonic Transport (June 30, 1962).

72. Wasielewski, G. E., "Nickel Base Superalloy Oxidation," AFML-TR-67-30 (January 1967).

73. Goldhoff, R. M., and Hahn, G. J., "Correlation and Extrapolation of Creep Rupture Data of Several Steels and Superalloys Using Time-Temperature Parameters." "Time-Temperature Parameters for Creep-Rupture Analysis," ASM Publication D8-100.

74. Groves, M. T., and Gerkin, J. M., "Evaluation of Electron Beam Welds in Thick Materials," AFML-TR-66-22 (February 1966).

75. Prager, M., and Thompson, E. G., "A Study of the Mechanical Properties and Strain Age Cracking of René 41 for F-1 Rocket Engine Application," Rocketdyne Report R-7111 (September 1967).

76. Hughes, W. P.; Berry, T. F.; and Yount, R. E., "A Study of the Strain-Age Cracking Sensitivity of René 41," AFML-TR-66-324, Part II (March 1968).

77. AMS 5399, Society of Automotive Engineers (July 1983).

78. Thompson, E. G.; Nunez, S.; and Prager, M., "Practical Solutions to Strain-Age Cracking of René 41," Welding Research Supplement, pp. 299S-313S (1968).

79. Douglas Aircraft Company, Aircraft Division, Long Beach, CA, "Chloride Stress Corrosion Susceptibility of High Strength Stainless Steel Titanium Alloy and Superalloy Sheet," ML-TDR-64-44 (March 1964).

80. Moon, D. P.; Simon, R. C.; and Favor, R. J., "The Elevated-Temperature Properties of Selected Superalloys," ASTM Data Series DS 7 - S1 (Supplement to DS 7, formerly STP 160).

81. Blatherwick, A. A., and Cers, A. E., "Fatigue, Creep, and Stress-Rupture Properties of Several Super Alloys," AFML-TR-69-12 (January 1969).

82. Rizzardi, J. A., "Processing of Superalloy Multifilament Yarn," contained in Report ASD-TDR-62-964, pp. 127-140, ("Symposium on Fibrous Materials," complied by Jack H. Ross) (January 1963).

83. Newton, E. H.; Johnson, D. E.; and Sienczyk, J. L., "Metal Filaments for High-Temperature Fabrics," Contained in Report ASD-TDR-62-964, pp. 143-181 ("Symposium on Fibrous Materials," compiled by Jack H. Ross) (January 1963).

84. Wassil, G. N.; Makepeace, D. E.; et al, "Form-Rolling Close Tolerance Shapes of Superalloys," A. F. Contract AF33(615)-3545 (June 1969).

85. Micillo, C., "Advanced Chemical Milling Processes," AFML-TR-68-237 (August 1968).

86. Malik, R. K., and Stetson, A. R., "Evaluation of Superalloys for Hypersonic Vehicle Honeycomb Heat Shields," AFML-TR-68-292 (October 1968).

87. Kafesjian, R., "Melt Spinning of Superalloys," AFML-TR-68-397 (January 1969).

88. Cammett, J. T., "Elevated Temperature Low Cycle Fatigue Behavior of René 41," G. E. Report No. R69 AEG-332 (July 1969).

89. Aarnes, M., "The Effect of Various Machining Techniques on the Mechanical Properties of René 41 at 1000F," Boeing Report D2-81284, Prepared under contract AF 33(615)-1624 (1965).

90. Gumto, K. H., and Weiss, B., "Creep-Rupture Tests of Internally Pressurized René 41 Tubes," NASA TMX-2505 (February 1972).

91. Young, S. G., and Johnston, J. R., "Accelerated Cavitation Damage of Steels and Superalloys in Liquid Metals," NASA TN D-3426 (May 1966).

92. Lherbier, L. W., and Koffler, R. W., "High Temperature Sheet Alloys - Properties, Problems and Potential," *Space Shuttle Materials*, Vol. 3, Society of Aerospace Materials and Process Engineers, Azusa, CA, pp. 169-182 (1971).

93. Davis, J. W., "Effect of Multiple Entry on the Properties of Superalloys," *Space Shuttle Materials*, Vol. 3, Society of Aerospace Materials and Process Engineers, Azusa, CA, pp. 335-345 (1971).

94. Walter, R. J., and Chandler, W. T., "Effects of High Pressure Hydrogen on Metals," Presented at 1968 Materials Engineering Exposition & Congress (ASM) Detriot, MI.

95. Cataldo, C. E., "Compatibility of Metals with Hydrogen," NASA TMX-53807 (December 26, 1968).

96. Davidson, T. E., and Nolan, C. J., "The Relationship Between Pressure Effects Upon Fracture Mechanisms and Ductility, and its Practical Implications," Watervliet Arsenal Report.

97. Young, S. G., and Freche, J. C., "A Review of NASA Research to Determine the Resistance of Materials to Cavitation Damage in Liquid Metal Environments," NASA TMX-52956 (January 1971).

98. Young, S. G., and Leonard, L., "Effect of Ultrasonic Vibration on Precipitation Hardening of Steels and Superalloys," NASA TN D-5131 (March 1969).

99. Witzel, W. E., and Kerr, "Metallic Materials Evaluation: Fracture and Gleeble Studies," General Dynamics Corporation Report GDC-ERR-1477 (December 1969).

100. Heyer, B. A., "Manufacturing Process for Superalloy Cast Parts, Phase I - Fundamentals," Interim Engineering Progress Report IR-8-297 (VIII), Metals Processing Branch, Manufacturing Technology, AFML (June 15, 1968).

101. Gaw, W. D., and Starr, G. L., "Plasma Arc Welding Process Development Program," Volume I, AFML-TR-68-379 (April 1969).

102. Okamura, K.; Nakajima, N.; Des Ruisseaux, N.; Lemon, J.; Brown, D.; Gerhardt, J.; and Snoeys, R., "Study of Grinding Process as Applied to High-Strength and Thermal-Resistant Alloys," AFML-TR-68-309 (October 1968).

103. Mullin, G. C., and Wetherby, R. E., "Development of Improved Grinding Process," AFML-TR-68-291 (September 1968).

104. Bhat, G. K., and Tobias, J. B., "A Manufacturing Process Development for the Electroslag Melting and Casting of Materials," Part II - Phase I Progress Report IR-9-161, Contract No. AF33(615)-5430 (February 1969).

105. Wiodek, S. T., "The Oxidation of René 41 and Udimet 700," *Trans AIME*, Volume 230, pp. 1078-1090 (August 1964).

106. Clark, A. F.; Childs, G. E.; and Wallace, G. H., "Electrical Resistivity of Some Engineering Alloys at Low Temperatures," *Cryogenics*, pp. 295-305 (August 1970).

107. Gurklis, J. A., "Electrochemical Machining of Heat-Resistant Alloys," *Cobalt 39*, pp. 81-87 (June 1968).

108. D'Annessa, A. T., and Owens, J. S., "Procedures for Avoiding Heat-Treat Cracking in Nickel-Base Superalloy Weldments," AFML-TR-70-224 (July 1970).

109. Collins, H. E., "Relative Long-Time Stability of Carbide and Intermetallic Phases in Nickel-Base Superalloys," *Trans ASM*, Volume 62, No. 1 (March 1969).

110. Imig, L. A., "Effect of Strain-Gage Attachment by Spot-welding and Bonding on Fatigue Behavior of Ti-6Al-4V, René 41 and Inconel X," NASA TN D-5973 (October 1970).

111. "Allvac René 41 (High-Strength, Precipitation-Hardening Alloy)," *Alloy Digest*, Ni-392 (February 1991).

112. Sczerzenie, F., and Maurer, G. E., "Developments in Disc Materials," *Materials Science and Technology*, Vol. 3, No. 9, pp. 733-742 (September 1987).

113. Hack, H. P., "Mechanical, Corrosion, and Fatigue Properties of 15-5 PH, Inconel 718, and René 41 Weldments," NSRDC-4528, Naval Ship Research and Development Center (May 1975).

114. *Metals Handbook*, 10th Edition, Vol. 4, American Society for Metals, p. 812 (1991).

115. *Metals Handbook*, 10th Edition, Vol. 1, American Society for Metals, pp. 955-956 (1990).

116. Machlin, E. S., and Shao, L., "SIGMA-SAFE—Phase Diagram Approach to the Sigma Phase Problem in Ni-Base Superalloys," *Metallurgical Transactions A*, Vol. 9A, No. 4, pp. 561-568 (April 1978).

117. Holt, R. T., and Wallace, W., "Impurities and Trace Elements in Ni-Base Superalloys," *International Metallurgical Reviews*, Vol. 21, pp. 1-24 (March 1976).

118. Wallace, W., "Prediction of Sigma Phase Formation in Nickel-Base Superalloys," *Metal Science Journal*, Vol. 9, No. 12, pp. 547-551 (December 1975).

119. Danford, M. D., "Hydrogen Trapping and the Interaction of Hydrogen With Metals," NASA TP-2744 (July 1987).

120. Nelson, E. E., "The Effect of Hot Salt on the Mechanical Properties of Several Superalloys," NASA TMX-64701, NASA Marshall Space Flight Center (October 1972).

121. Paton, N. E., and Robertson, W. M., "High Temperature Behavior of Superalloys Exposed to Sodium Chloride: I. Mechanical Properties," *Metallurgical Transactions*, Vol. 4, No. 1, pp. 317-320 (January 1973).

122. Mansfeld, F.; Paton, N. E.; and Robertson, W., "The High Temperature Behavior of Superalloys Exposed to Sodium Chloride: II. Corrosion," *Metallurgical Transactions*, Vol. 4, No. 1, pp. 321-327 (January 1973).

123. Chandler, W. T., "The Effect of Hydrazine Decomposition Products on the Mechanical Properties of High-Temperature Alloys," Ri/RD77-143, Rockwell International, Rocketdyne Division, Canoga Park, CA (March 1978).

124. Forman, R. G., "A Fracture Mechanics Study of the Turbine Wheel in the Space Shuttle Auxiliary Power Unit," *Theoretical Applications of Fracture Mechanics*, Vol. 3, No. 2, pp. 71-84 (May 1985).

125. Chandler, W. T., and Walter, R. J., "Testing to Determine the Effect of High-Pressure Hydrogen Environments on the Mechanical Properties of Metals," Presented at Seventy-Fifth Annual Meeting of the American Society for Testing and Materials, held at Los Angeles, CA, June 25-30, 1972, American Society for Testing and Materials (1972).

126. Gray, H. R., "Embrittlement of Nickel-, Cobalt-, and Iron-Base Superalloys by Exposure to Hydrogen," NASA TN D-7805, NASA Lewis Research Center (January 1975).

127. Barrett, C. A., "10,000 Hour Cyclic Oxidation Behavior at 815C (1500F) of 33 High-Temperature Alloys," NASA TM-7307, NASA Lewis Research Center (1977).

128. Zaplatynshy, I., "Volatization of Oxides During Oxidation of Some Superalloys at 1200C," *Oxidation of Metals*, Vol. 11, No. 6, pp. 289-305 (December 1977).

129. McDonald, G., and Hendricks, R. C., "Effect of Thermal Cycling on ZrO_2-Y_2O_3 Thermal Barrier Coatings," *Thin Solid Films*, Vol. 73, No. 2, pp. 491-496 (November 1980).

130. Royster, D. M., and Lisagor, W. B., "Effect of High-Temperature Creep and Oxidation on Residual Room-Temperature Properties for Several Thin-Sheet Superalloys," NASA TN D-6893, NASA Langley Research Center (November 1972).

131. Koster, W. P., "Effect of Residual Stress on Fatigue of Structural Alloys," Conference on Practical Applications of Residual Stress Technology, held at Indianapolis, IN, May 15-17, 1991, ASM International, pp. 1-9 (1991).

132. Kelly, T. J., "Welding Metallurgy of Investment Cast Nickel-Based Superalloys," Conference on Weldability of Materials, held at Detriot, MI, October 10-12, 1990, ASM International, pp. 151-157 (1990).

133. Yeniscavich, W., "Joining (of Superalloys)," *Superalloys II - High Temperature Materials for Aerospace and Industrial Power*, Wiley-Interscience, John Wiley and Sons, pp. 495-516 (1987).

134. Thamburaj, R.; Goldak, J. A.; and Wallace, W., "The Influence of Chemical Composition on Post-Weld Heat Treatment Cracking in René 41," *SAMPE Quarterly*, Vol. 10, No. 4, pp. 6-12 (July 1979).

135. *Metals Handbook*, 9th Edition, Vol. 6, p. 358 (1983).

136. D'Annessa, A. T., and Owens, J. S., "Effects of Furnace Atmosphere on Heat Treat Cracking of René 41 Weldments," *Welding Journal*, Vol. 52, No. 12, pp. 568s-575s (December 1973).

137. Arnquist, J. L., and Hepler, A. K., "Development of Brazed René 41 Honeycomb Structure," *Proceedings of Structural Dynamics and Materials Conference*, AIAA, New York, pp. 132-146 (1978).

138. Hepler, A. K.; Arnquist, J.; Koetje, E. L.; Esposito, J. J.; Lindsay, V. E. J.; and Swegle, A. R., "Design Data for Brazed René 41 Honeycomb Sandwich," NASA CR-3382, Boeing Aerospace Company (1981).

139. Hill, V. L., and Humphreys, V. E., "Thermal Fatigue and Oxidation Data for Alloy/Braze Combinations," NASA CR-135299, IIT Research Institute (June 1977).

140. Schwartz, M. M., "Brazing in a Vacuum," Bulletin No. 224, Welding Research Council, New York (1978).

141. Papadakis, E. P., "Tabulation of the Coefficients of a Quadratic Function for the Thermal Expansion of Various Alloys and Other Engineering Materials," *Materials Science and Engineering*, Vol. 10, pp. 195-203 (1972).

142. Compton, E. C., "Evaluation of a Standard Test Method for Total Hemispherical Emittance of Surfaces from 293K to 1673K," NASA TM-87681, NASA Langley Research Center (January 1986).

143. DeWitt, D. P.; Ono, A.; Taylor, R. E.; and James, H. M., "High-Temperature Spectral Emissivity of Conducting and Nonconducting Materials," *Proceedings of Eighth Symposium on Thermophysical Properties, Vol. 2, Thermophysical Properties of Solids and of Selected Fluids for Energy Technology*, held in Gaithersburg, MD, June 15-18, 1981, American Society of Mechanical Engineers, pp. 122-126 (1982).

144. *Metals Handbook*, 10th Edition, Vol. 4, ASM International, p. 909 (1991).

145. *ibid*, p. 809.

146. *Metals Handbook*, 10th Edition, Vol. 1, ASM International, p. 982 (1990).

This page is blank.